

Development of Oligonucleotide, Small Molecule, and Protein Assays using Square-wave Voltammetry with Electrode-bound Nucleic Acid Nanostructures

by

Subramaniam Somasundaram

A dissertation submitted to the Graduate Faculty of
Auburn University
in partial fulfillment of the
requirements for the Degree of
Doctor of Philosophy

Auburn, Alabama
May 5, 2018

Keywords: Electrochemistry, Analytical Chemistry

Copyright 2018 by Subramaniam Somasundaram

Approved by

Christopher J. Easley, Chair, Knowles Associate Professor of Chemistry and Biochemistry
Curtis Shannon, Andrew T. Hunt Professor and Chairman of Chemistry and Biochemistry
Vince Cammarata, Associate Professor of Chemistry and Biochemistry
Jeffrey Fergus, Associate Dean for Assessment and Graduate Studies, Professor of Materials
Engineering

Abstract

Biomarker analysis plays a decisive role in health care. This role is not only limited to disease diagnosis, but it also involves understanding of biological and physiological functions in order to monitor health, observe the efficiency of treatment, etc. This calls for a need of better methods for clinical analysis in several non-clinical point-of-care (POC) settings, including analysis for patients at home. On the focus of biomarker detection, many sensitive methods are being developed. However, only the methods which are inexpensive, sensitive, automated, and rapid pass as POC systems, which can serve to speed up health improvements, especially in developing countries. One standout among these methods is the electrochemical sensor. Due to its inexpensive instrumentation with well-developed miniaturization strategies, electrochemistry has proven to be ideal for POC settings. This dissertation focuses on the development of DNA-based electrochemical methods toward an effective drop-and-read quantification of multiple classes of biomarkers, namely small molecules, oligonucleotides, and proteins.

In Chapter 1 we discuss conventional electrochemical DNA-based biomarker detection methods and related developments for POC and real-time systems.

In Chapter 2, the electrochemical proximity assay (ECPA), a sensitive protein detection and potential POC method developed in our lab is discussed. We have completed studies that can support the development and quick expansion to quantify biologically relevant molecules. ECPA was applied to leptin and insulin quantification, and insulin was successfully detected in the presence of undiluted, un-spiked human serum. We further highlight the importance of understanding that ECPA sensing complex is made of six components undergoing non-covalent binding (DNA hybridization and antigen-antibody interactions) on the surface of the electrode, which is kinetically and thermodynamically different from complex formation in solution. In addition to that, square-wave voltammetry (SWV), a relatively complicated but very sensitive

electrochemical technique is employed.

Chapter 3 focuses on the understanding of surface hybridization, and its effects on electrochemical kinetics by way of the distance between the redox moiety and the electrode. Most importantly, we offer a different outlook on interpreting SWV signal and the efficiency of SWV frequency, which is useful for any electrochemical DNA-based sensor.

In Chapter 4, we developed an electrochemical oligonucleotide quantification method, specifically designed for short length nucleotides (~ 20 nt) in hopes of developing a mix-and-read quantification for micro-RNA (miRNA). We have developed a system for fine tuning or optimizing electrochemical DNA sensor by carefully controlling hybridization energies, SWV frequency, and temperature. In addition to this, we used polydimethylsiloxane (PDMS) electrochemical cells fabricated from 3D-printed polylactic acid molds to reduce the volume of our sample and reagents (10 μL).

Chapter 5 depicts the development of a generalizable drop-and-read quantification method which is interchangeable between protein and small molecule. A change in the rate of diffusion in the redox moiety is used for quantification, and protein is used as an anchor (large molecule weight) which measurably slows diffusion. By exploiting enzymatic DNA ligation, a DNA nanostructure was built on the surface of the electrode, providing control over the orientation of various tags. In this work, we placed the redox moiety in close proximity to an anchor recognition unit, which helps in aiding signal change by the anchor. As a proof of concept, streptavidin and biotin were quantified. Digoxigenin and anti-digoxigenin antibody complexes also show promising results.

Finally, Chapter 6 summarizes this dissertation and provides an insight on future projects stemming from this work. Concepts toward the development of fully surface-confined, real-time electrochemical sensors of a wide range of analytes are proposed, and proposals to improve the sensitivity of our nanostructure are also outlined.

Acknowledgments

I would like to thank Dr. Easley, my research advisor, for mentoring me during my time here at Auburn. Beyond research and science, I learned the qualities of a confident, unbiased ethical leader from you. Thank you to my committee members: Dr. Shannon, Dr. Cammarata, and Dr. Fergus. Dr. Shannons and Dr. Cammaratas classes helped me in attaining an in-depth understanding of electrochemistry and surface chemistry. Their insightful discussions in my oral examination encouraged and directed me in a right direction. Dr. Kim, thanks for your time in explaining various perspectives in my research and helping me in solving many issues. Jessica, thanks for all of your help; your energy and enthusiasm organized Dr. Easleys students. Mark, Kat, Juan, and Li, after we all moved into the lab in room 254, you became my family. When I joined Auburn, international students were warned in English class not to misunderstand the politeness of Americans as friendship. Jessica, Mark, and Kat, you showed me that these theories and statistics were wrong. Mark, I was amazed by your skills in electronics. Discussions with you improved my knowledge in instrumentation. Kat, thank you for helping me in all the tough times that I had. Your eagerness to learn things amazed me. Juan and Li, your timely help supported me a lot. I want all of you to be successful in bioanalytical research. Bailey, a former undergraduate student, thank you for helping me in research, and I wish you good luck with your future in medicine.

When I came to Auburn for my Ph.D. studies, I didnt have any friends or acquaintances from India. I would like to thank Gerald (Civil Engineering graduate student), Kavitha Reddy (Chemistry graduate student, Livant lab), and Divya Prakash (Chemistry graduate student, Duin lab). Thanks for helping me to understand the American system and traditions.

Finally, I would like to thank my family, Dr. S. Somasundaram (Father), Mrs. S. Chidambarasundari, M.A., B.Ed. (Mother), and S.S. Subashni (younger sister). Thanks for being

supportive, understanding, patient, and motivating. You were the hidden driving force, and without you I would not have accomplished this.

Table of Contents

Abstract	ii
Acknowledgments	v
1 Introduction: Electrochemical Detection of Biological Analytes	1
1.1 Analysis of clinically relevant molecules	1
1.2 Biotransducing elements	3
1.2.1 Antibodies	3
1.2.2 Aptamers	3
1.2.3 Nucleic acids	4
1.3 Conventional technique	4
1.3.1 ELISA	4
1.3.2 Digital ELISA	6
1.3.3 AlphaLISA	7
1.4 DNA driven assay	9
1.4.1 Optical detection	10
1.4.2 Electrochemical detection	12
1.5 Electrochemical Biosensing	13
1.5.1 Typically used voltammetry techniques	14
1.6 Protein, small molecule and oligonucleotide quantification through electrochem- istry	16
1.6.1 Quantification through structure switching capturing probe	16

1.6.2	Quantification through non-structure switching capture probe	23
1.7	Conclusion remarks	25
2	Electrochemical Proximity Assay and its Advancement	28
2.1	Introduction	28
2.2	Reagent and Materials	30
2.3	Experimental Methods	30
2.3.1	Preparation of gold electrode and DNA monolayer assembly	30
2.3.2	Antibody-oligomer conjugation	32
2.3.3	Steps involved in ECPA	33
2.3.4	Reusable ECPA	34
2.3.5	Insulin measurement	35
2.3.6	Optimizing SWV frequency and pulse height	36
2.3.7	Leptin ECPA	36
2.3.8	Optimizing DNA probe density	37
2.3.9	SWV signal processing	38
2.3.10	Thermal Scanning ECPA	39
2.3.11	Surface confined ECPA	40
2.4	Result and discussion	41
2.4.1	Optimizing SWV frequency and pulse height	41
2.4.2	Quantification of Leptin by ECPA	43
2.4.3	Probe density	43
2.4.4	Insulin quantification in murine serum with reusable ECPA	44
2.4.5	tsECPA for insulin measurement in undiluted human serum without spiking	45
2.4.6	Refined instrument parameters for SWV	47
2.4.7	tsECPA of insulin with modified parameters	52

2.4.8	Surface confined ECPA	53
2.5	Conclusion	54
3	Diffusion layer and Double layer in Electrochemical DNA Assays	56
3.1	Introduction	56
3.2	Regent and materials	58
3.3	Experimental methods	59
3.3.1	Electrode preparation and DNA SAM	59
3.3.2	Distance of methylene blue redox moiety	60
3.3.3	Electrochemical kinetics calculation	60
3.3.4	Hybridization kinetics on the electrode surface	61
3.3.5	DNA Strand displacement on surface	61
3.4	Result and discussion	61
3.4.1	Understanding SWV signal from measuring layer perspective	61
3.4.2	Electrochemical rate change due to distance	66
3.4.3	Diffusion layer effect	67
3.4.4	Double layer effect and hybridization Kinetics	68
3.5	Conclusion	73
4	Temperature Dependence of SWV Signal and Branched Assay for ssDNA Quantification	75
4.1	Introduction	75
4.2	Reagents and materials	76
4.3	Experimental methods	79
4.3.1	Preparation of gold electrode and PDMS electrochemical cell	79
4.3.2	PDMS electrochemical cell	80
4.3.3	DNA monolayer assembly	80

4.3.4	Square-wave voltammetry frequency study of DNA melting	81
4.3.5	Single branched DNA model	82
4.3.6	DNA quantification	83
4.3.7	Data analysis	84
4.4	Result and discussion	86
4.4.1	Signal comparisons with varying complex stability	86
4.4.2	Temperature dependence of electrochemical kinetics	88
4.4.3	Characterizing signal and background	90
4.4.4	Oligonucleotide quantification	94
4.5	Conclusion	97
5	DNA Nanostructure for Electrochemical Detection of Broad Range of Analytes . . .	99
5.1	Introduction	99
5.2	Reagents and materials	100
5.3	Experimental methods	102
5.4	Electrode preparation and DNA SAM	102
5.4.1	On-electrode DNA nanostructure assembly using through T4 DNA ligase	103
5.4.2	Electrochemical measurement	104
5.4.3	Data analysis	105
5.4.4	Quantification protocol	105
5.4.5	Biotin quantification	105
5.5	Result and discussion	106
5.5.1	DNA monolayer formation and its stability	106
5.5.2	Proof of concept for DNA nanostructure signal suppression by high molecular weight anchor	108
5.5.3	Streptavidin and biotin	111
5.5.4	Anti-digoxigenin and digoxigenin	111

5.6	Conclusion	113
6	Summary and future work	115
6.1	Summary	115
6.2	Future directions	115
6.2.1	Bistable switch DNA quantification model	115
6.2.2	Insulin Quantification	116
6.2.3	Optimizing the DNA nanostructure	117
6.2.4	Real time measurement	118
6.2.5	Impact of this work on future systems	119
	References	120

List of Figures

1.1	Clinically relevant molecules	2
1.2	Sandwich ELISA	5
1.3	DigitalELISA	7
1.4	AlphaLISA	8
1.5	Proximity effect	10
1.6	Proximity ligation assay	11
1.7	Pincer assay	12
1.8	Ratiometric electrochemical proximity assay	13
1.9	Pulse voltammetry	15
1.10	Potential wave form for square wave voltammetry	16
1.11	Electrochemical DNA/aptamer sensor	17
1.12	SWV response for DNA switch	19
1.13	Small molecule quantification by E-aptamer	21
1.14	Microfluidic electrochemical detector for in vivo continuous monitoring (MEDIC)	23
1.15	Electrocatalytic reporter system	24
1.16	Steric hindrance assay	26
2.1	ECPA	28
2.2	Mechanical cleaning of electrodes	31
2.3	Mercapto-hexanol on surface	32
2.4	Solulink antibody-oligomer conjugation	33
2.5	ECPA Protocol	35

2.6	Enzymatic regeneration of thiolated-DNA on surface	36
2.7	SWV baseline subtraction	39
2.8	Thermal scanning setup with electrochemical cell	40
2.9	Surface Confined ECPA model	41
2.10	Optimization of square-wave voltammetry frequency and peak height	43
2.11	Leptin ECPA	44
2.12	Optimal probe density of thiolated DNA	45
2.13	ECPA standard addition measurement in murine serum	45
2.14	Thermal Scanning ECPA of insulin sample and undiluted human serum	46
2.15	Circuit of Reference 600 instrument	48
2.16	Resolution change in potentiostat	49
2.17	Applied pulse height and frequency	50
2.18	Peak height and resolution after fixing the instrument	51
2.19	Thermal scanning ECPA with new setup	52
2.20	scECPA signal output	54
3.1	Random walk model	57
3.2	SWV signal from measuring distance perspective	62
3.3	Peak height change due to distance of redox moiety	64
3.4	Peak height shift at lower frequencies	64
3.5	Electrochemical kinetics change by distance of methylene blue	66
3.6	Diffusion layer and SWV response	67
3.7	Hybridization on the surface of electrode	69
3.8	Double layer effect on average hybridization lifetime	70
3.9	Toe hold strand displacement on surface	71
3.10	Upper toe hold and lower toe hold strand displacement kinetics	72
4.1	AZ photomask model used for GoG preparation	79

4.2	3D-CAD and PLA mold for electrochemical cell	81
4.3	Single branched DNA quantification structure	82
4.4	Third order polynomial calculated baseline subtraction	84
4.5	Peak height as a function of SWV frequency increase	86
4.6	Heat map comparing peak height, temperature and SWV frequency of signal and background of all 25 complex	87
4.7	Heat map showing the shift in electrochemical critical time with temperature . .	88
4.8	I_p/f_{SWV} vs $1/f_{SWV}$ of temperature	89
4.9	Shift in the diffusion layer shown by peak height response	90
4.10	Heat map of background signal subtracted from signal	91
4.11	Heat map of signal over background of all complexes	92
4.12	SWV frequency and temperature response of selected complexes	94
4.13	Single and two step quantification of the selected complexes	96
4.14	Limit of detection comparison	97
5.1	DNA scaffold architecture for electrochemical detection of protein-small molecule interaction	100
5.2	Schematic view of DNA nanostructure anchor model for quantification of small molecule and large protein	101
5.3	Electrode photomask used for DNA nanostructure quantification	103
5.4	3D-CAD and PLA mold for 2 mm diameter electrode	104
5.5	DNA nanostructure formation on gold electrode	107
5.6	DNA nanostructure stability	108
5.7	DNA nanostructure formation and stability by DNA melting analysis	109
5.8	Proof-of-concept of signal suppression and comparison of various distance . . .	110
5.9	Streptavidin and biotin detection	112
5.10	Anti-digoxigenin and digoxigenin detection	113
6.1	Bistable switch DNA quantification model	116

6.2	DNA nanostructure for insulin quantification	117
6.3	Optimizing the DNA nanostructure	118
6.4	Real time measurement of small molecules using DNA nanostructure model . .	119

List of Tables

2.1	DNA sequence used for insulin ECPA	37
2.2	SWV parameters for insulin ECPA	38
2.3	SWV parameters for optimizing SWV frequency and pulse height	38
2.4	SWV parameters for Leptin ECPA	39
2.5	DNA sequence used for scECPA	42
3.1	DNA sequence used for distance dependence and salt concentration study	59
3.2	SWV parameters for diffusion and double layer study	60
4.1	Sequences of DNAs used in single-branched electrochemical oligonucleotide quantification study	78
4.2	SWV parameters for single branched DNA quantification study	82
5.1	Sequence of DNAs used in anchor model quantification	102
5.2	SWV parameter used in DNA nanostructure quantification	104

List of Abbreviations

3D-CAD	3D computer animated design
AB	Antibody
Apt	Aptamer
ATP	Adenosine triphosphate
bp	Base pair
CV	Cyclic voltammetry
DPV	Differential pulse voltammetry
E-Apt	Electrochemical aptamer sensor
ECPA	Electrochemical proximity assay
E-DNA	Electrochemical DNA sensor
ELISA	Enzyme-linked immunosorbent assay
Fc	Ferrocene
f_{sw}	Square-wave voltammetry frequency
GoG	Gold on Glass
HEPES	(4-(2-hydroxyethyl)-1-piperazineethanesulfonic acid)
HRP	Horseradish peroxidase
i_{diff}	Differential current in Square-wave voltammetry
i_f	Forward current in Square-wave voltammetry
i_p	Square-wave voltammetry peak height
i_r	reverse current in Square-wave voltammetry
LOD	Lower detection limit
MB	Methylene blue
MCH	6-Mercapto-1-hexanol
nt	Nucleotide
PDMS	Polydimethylsiloxane
PLA	Polylactic acid

POC	Point-Of-Care
SAM	Self-assembled monolayer
SWV	Square-wave voltammetry
TCEP	(tris(2-carboxyethyl)phosphine)
T_m	DNA melt temperature
V_f	Forward voltage in SWV
V_r	Reverse voltage in SWV

Chapter 1

Introduction: Electrochemical Detection of Biological Analytes

1.1 Analysis of clinically relevant molecules

The overall approach to analysis and treatment of disease is moving towards a multiparameter measurement in the blood [1]. This measurement includes detecting wide ranges of analytes from single atomic ions like sodium or potassium to large proteins which are involved in carrying out various biological activities [2]. It has also been shown that for an efficient treatment, drugs or biomarkers should be quantified regularly to enable personalized medicine, since pharmacokinetics differs between individuals [1, 3]. Kelly et al. divided the clinically relevant molecules into three subdivisions: small molecules, nucleic acids, and proteins. Some of the analytes which are considered clinically relevant as of now are separated according to this subdivision and shown in Figure: 1.1 [2].

Metabolites, vitamins, neurotransmitters, and amino acids fall under the small molecule category. The intermediates or final products of metabolism are termed as metabolites. Quantifying metabolites will be helpful in diagnostics for metabolic disorders. In many biological functions in the body, a limited amount of organic compounds or vital nutrients are required. These compounds are called vitamins. Maintaining the right amount of these micronutrients in the body is essential, which explains the need for monitoring. Neurons, or nerve cells, communicate with another neurons and cells through chemical messengers known as neurotransmitters. An imbalance in the amounts of neurotransmitters is associated with many diseases and mental disorders.

Small molecule analytes	Nucleic Acid analytes	Protein analytes	
Metabolites urea lactate UA hypoxanthine cholesterol Xanthine glucose creatinine		Tumor Markers EGFR Ferritin Tg VEGF NSE AFP p53 CD105 VEGFR Ct CD146 PDGF-BB SCCA HER2 PAcP CEA HER3	Cardiac Markers Mb H-FABP cTnT GPBB CK-MB sLOX-1 cTnI NT-proBNP ApoB-100
Vitamins 25(OH)D ascorbic acid riboflavine biotin pyridoxine	cfDNA Bacterial NAs Viral NAs miRNAs	Inflammatory Markers Hp CRP TTR TSF	
Neurotransmitters 5-HT Ep ACh NE DA			
Amino acids			
			Other small molecules heparin glutathione ATP

Figure 1.1: **Clinically relevant molecules:** Several small molecules, nucleic acids, and protein analytes are considered as clinically relevant due to their contribution in metabolism and its nature as biomarker [2].

Viral and bacterial infections can be diagnosed by analyzing the presence of their nucleic acids. In addition to this, the formation and growth of cancer cells can be determined by quantification of specific nucleic acids. A correlation has even been discovered between circulating free nucleic acids and trauma patients [4]. Patient with myocardial infarction exhibit ten times higher plasma DNA concentrations [5]. Analyzing cell-free nucleic acids (cfNAs) opened a new path in clinical diagnosis of early stage noninvasive tumors for detection and characterization [6].

Proteins are macromolecules with one or more long chain of amino acid residues found circulating in the body and within cells of all tissues. They execute a wide range of functions

within organisms, like catalyzing metabolism, contributing to signaling pathways, DNA replication, transporting molecules, etc. Diseases, pathogens, metabolic imbalances, mental disorders, tumor cells, cardiac issues, etc. have effects on the concentrations of proteins involved in these process [7]. Clinically relevant protein molecules fall under three main categories: tumor, cardiac, and inflammatory markers. In addition, protein quantification plays a critical role in research focused on understanding metabolism, cell signaling, etc.

1.2 Biotransducing elements

Biotransducers are biological units which act as target recognition units and also impart a physicochemical change in the presence of their target. This physicochemical change is used for analysis, and biotransducer capture is of central importance in biosensing. Due to evolutionary adaptation, these biological units often provide high sensitivity and selectivity toward their targets. These elements are either found in living systems or synthetically prepared. Antibodies, enzymes, aptamers, nucleic acids, etc. are some of the most widely used transducing elements.

1.2.1 Antibodies

Antibodies are Y-shaped proteins produced in the immune system to counteract the antigens. They possess two antigen recognition sites, called fragment antigen-binding (Fab sites, which selectively interact with antigen through noncovalent binding. This binding has very high affinity and selectivity, which has been exploited in biosensors to selectively analyze targeted antigens.

1.2.2 Aptamers

Aptamers are synthetic nucleic acid which compete with antibodies as a biotransducing element. Through intramolecular DNA binding, aptamers form a three dimensional structure

with binding pockets and clefts, which contributes for a selective and tight binding to certain targets [8]. Aptamers are isolated from library screening of oligonucleotides by a method termed systemic evolution of ligands by exponential enrichments (SELEX) process [9]. Since the aptamers are synthesized and screened in-vitro, their affinities and selectivities can be tailored, which cannot be done in the case of antibodies. Allosteric aptamers have also been developed [10]. In addition to that, by comparison aptamers are more stable than antibodies, which makes them convenient for long term storage and testing in non-typical environments. Finally, customized aptamer structures can be carefully designed, controlled, and synthesized with nanometer resolution based on the well-known base-pairing interactions and their ease of synthesis—a feature that is exploited often within this dissertation work.

1.2.3 Nucleic acids

For effective analysis of oligonucleotides, nucleic-acids are used as a biotransducing elements. This recognition utilizes the sequence specific non-covalent binding between the target and transducer. Nucleic acids as the transducer captures the central importance in the diagnosis of genetic diseases [11].

1.3 Conventional technique

1.3.1 ELISA

ELISA was developed in 1971 by two research groups simultaneously [12, 13], by modifying the radioimmunoassay (RIA) method. In the past fifty years, by this method peptides, proteins, hormones, vitamins, drugs of very-low concentration were selectively quantified [14, 15]. Enzyme-linked immunosorbent assay (ELISA) is the current gold standard used by clinicians around the world for diagnosing and monitoring diseases that inflict biological system (Aydin, 2015). Figure: 1.2 shows the commonly used heterogeneous sandwich ELISA. In this method the capture antibody is immobilized on the surface of the well, then the sample is introduced to the well and incubated. Usually, only the target of interest binds to the capture antibody due to

its excellent selectivity. After a rinse step to remove other components and unbounded sample molecules, the secondary antibody with horseradish peroxidase (HRP, typically used) tag is introduced to bind with the target molecule. Then the plate is rinsed to remove non-bounded secondary antibody, and substrate is introduced. HRP reacts with the substrate to generate color. In about twenty minutes, the stop solution is added to quench the HRP-substrate reaction. By absorbance reading of the enzyme amplified substrate signal, the concentration of target can be calculated. The usage of dual antibody binding increases the specificity of the assay, and enzyme amplification helps in lowering the LOD of the assay. As long as the target has at least 2 antibodies binding to two separate epitopes, the target can be quantified by ELISA [16].

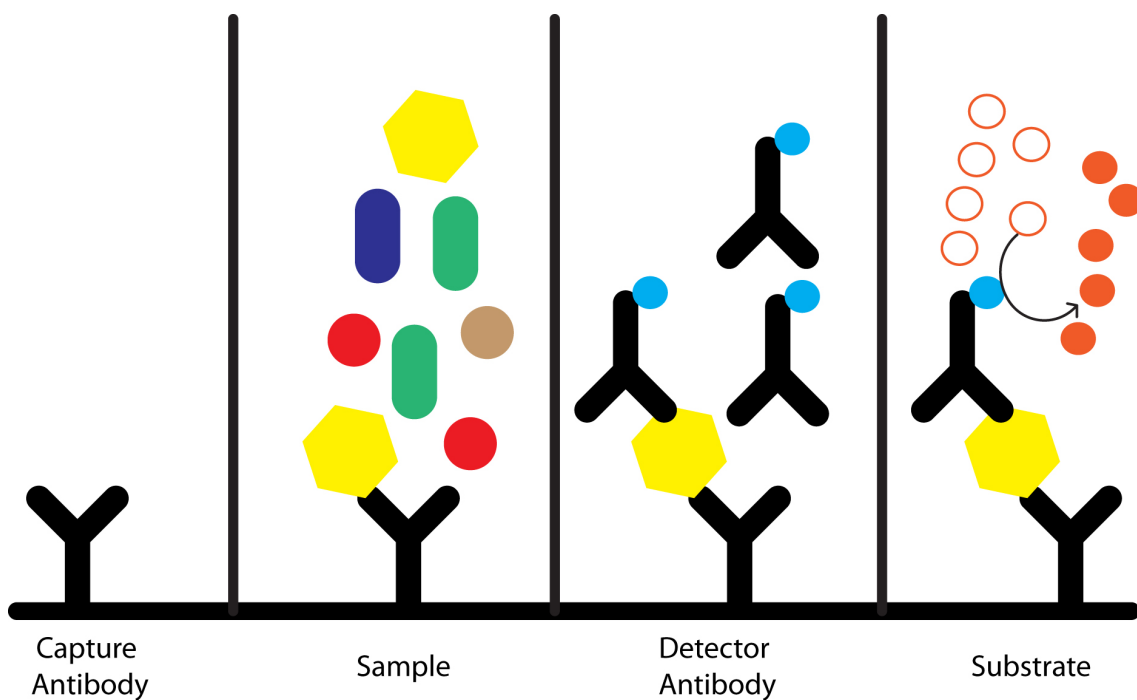


Figure 1.2: Sandwich ELISA: To the capture antibody, when the sample is incubated, only the target of interest is attached. Following the wash step, the detector antibody is incubated. Later, non-specific binding and excess detector antibody is removed by washing, and substrate is introduced. This enzyme reaction facilitates an observable color change. The stop solution inhibits the enzyme reaction, and an absorbance measurement is made.

Even though ELISA is very selective and sensitive, it is not a Point-of-Care (POC) assay. The method demands a well-trained clinical technician to operate correctly. In addition to that,

ELISA comes in 96-well format, and the reagent should be used in a single sitting. An ELISA plate cost an average of \$500, which represents about \$5 for each well. Moreover, there is a need for doing measurement with standards to calibrate the instrument and duplicate or triplicate measurement is a must to eliminate handling error, which adds up to about \$40 per sample. Typical turnaround time for the ELISA workflow is ~ 6 to 8 hours which makes another drawback from the POC perspective. Clearly, this shows that there is a need for further development in ELISA or other methods for POC assay.

1.3.2 Digital ELISA

ELISA is successful in quantifying proteins of concentration above 10^{-12} M [17]. However, there is a need for very sensitive quantification methods for diagnosis in cancer [18, 19], neurological disorders, etc. In the process of developing a sensitive assay, Walt, et al. developed a single-molecule enzyme-linked immunosorbent assay [20–23], which is an extension of ELISA where the enzyme amplification is done in a micro-well of 50 fL volume. Since the output is digital, it is called as digital-ELISA. Figure: 1.3 shows the protocol and components used in digitalELISA. In case of digitalELISA, the capture antibody is immobilized on the magnetic beads, and the secondary antibody is biotinylated, and an enzyme is tagged with streptavidin. In the presence of target, the complex shown in Figure: 1.3a. The magnetic beads are washed with buffer to remove all the non-specific binding. Then the beads are introduced into an array of micro-well, the size of array is only 2 mm wide. The device has $\sim 50,000$ wells with 4.5 μm diameter and 3.25 μm depth. The dimension of the well is so small that only one bead can be confined into it. Once the beads are introduced, the enzyme substrate is introduced and closed quickly with a silicone gasket. The bead with the target therefore has the enzyme, which generates fluorescent products quickly within the fL volume wells. Figure: 1.3d, shows the fluorescent turned on wells, and the concentration of the target can be calculated digitally using the Poisson distribution.

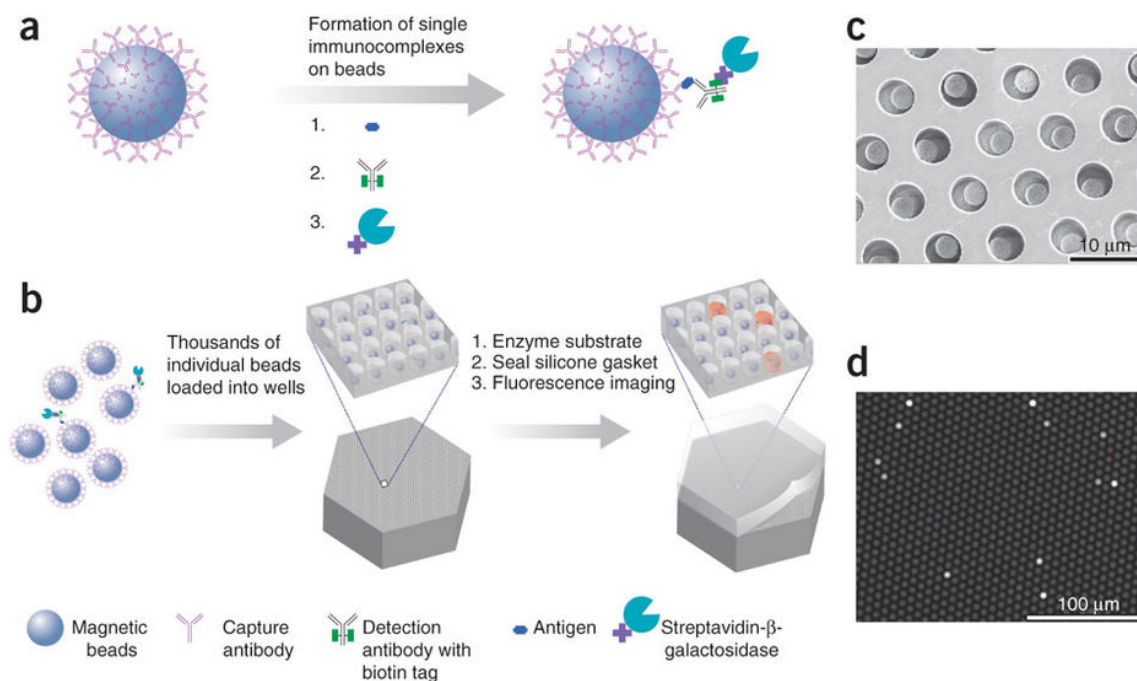


Figure 1.3: **DigitalELISA**: Using standard ELISA reagents single protein molecules are captured with enzyme label (a). then the beads are loaded into the femtoliter-volume well in which only one bead can fit in a well, then the substrate is introduced and wells are sealed with silicone gasket and ready for fluorescence imaging (b). SEM of femtoliter well (c). The bead with the protein generate signal enzymatically (d). [20]

Reprinted with permission Copyright ©(2010) Nature Publishing Group

In digitalELISA, the sensitivity is improved, and the volume of the sample and other substrate is decreased due to its micro-well nature. Quanterix Corporation, Lexington, MA, sells a fully automated digitalELISA analyzer, which helps in eliminating the need for clinical technicians. Technically, this positions the instrument as feasible for clinical POC. However, the need for expensive (above \$ 100,000) sophisticated instrument make it as not suitable for most other POC formats or do-it-yourself (DIY) measurements.

1.3.3 AlphaLISA

AlphaLISA is a homogeneous mix-and-read assay, which was also developed from the sandwich ELISA format [24]. It uses luminescent oxygen channeling for amplification of signal [25, 26]. In this method, two beads are used; one is a photosensitizer, and the other is chemiluminescent. If these particles are in close proximity (~ 200 nm), and the photosensitizer

(donor bead) is excited by 680 nm, it releases more than 60,000 singlet oxygens ($^1\text{O}_2$). This singlet oxygen can travel to the chemiluminescent bead (acceptor bead) to react only if it is in close proximity to the donor bead due to target presence, and this produces luminescence at 615 nm. Figure: 1.4 shows the protocol of AlphaLISA. The acceptor beads, which are immobilized with capture antibody, are incubated with sample and biotinylated secondary antibody. Later, donor beads with streptavidin are introduced, which in the presence of target makes the complex shown in Figure: 1.4B. This makes the acceptor and donor beads in close proximity, which helps the $^1\text{O}_2$ to transfer effectively. Reduction of background interference by luminescent signal and amplification by bulk $^1\text{O}_2$ production makes this method sensitive and easily generalizable compared to ELISA.

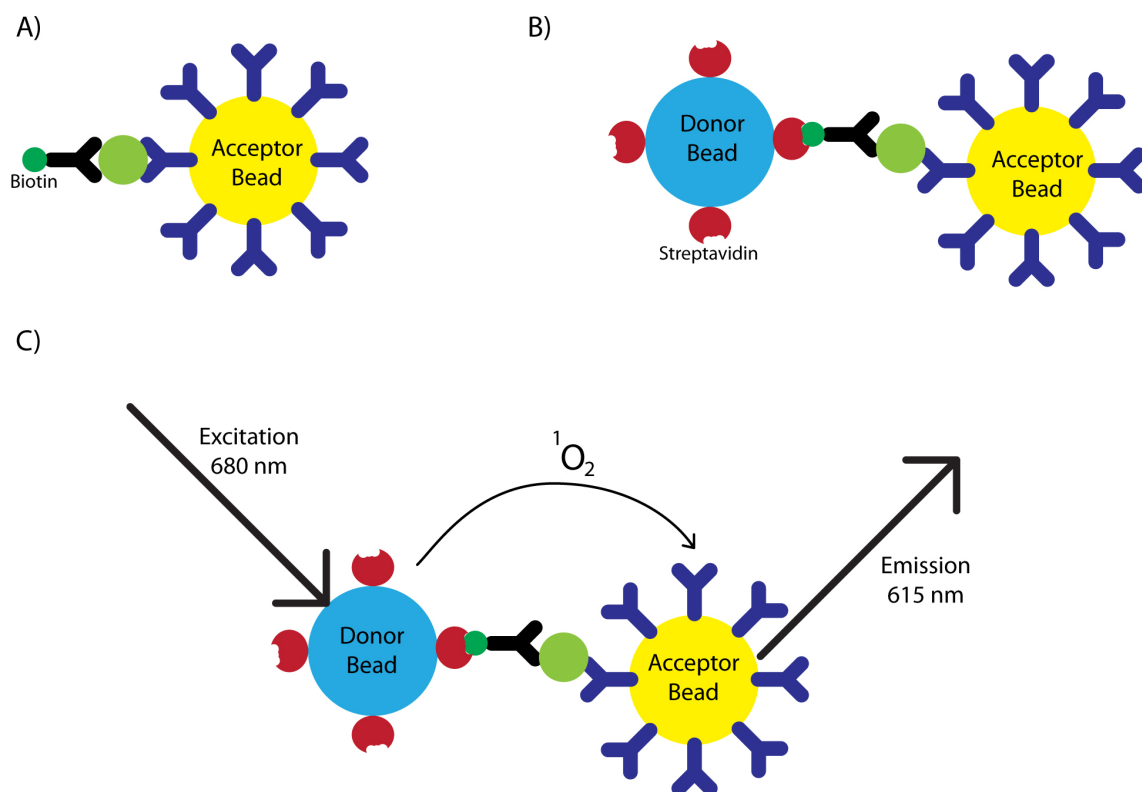


Figure 1.4: AlphaLISA: A) antibody immobilize acceptor bead forms the sandwich with biotinylated secondary antibody in the presence of target. B) streptavidin coated donor bead is introduced which binds with biotinylated antibody placing the acceptor and donor in close proximity. C) 680 nm excites the donor bead to generate singlet oxygen molecules, this singlet molecule reaches the acceptor bead and generate series of chemical reactions resulting in emission of 615 nm light [24].

Although AlphaLISA is a highly innovative, no wash, mix-and-read homogeneous immunoassay that is more sensitive than ELISA, there is a need for a specialized instrument. Specifically, optics to permit excitation at 680 nm and emission at 615 nm (higher energy) is not available on typical fluorescence systems. Again, this issue limits the technology and prevents its use as a POC assay.

1.4 DNA driven assay

In the past decade, ultrasensitive protein detection has been achieved through target-induced DNA assembly, called the proximity effect [27–29]. Chris Le, et al. in their review article *Assembling DNA through affinity binding to achieve ultrasensitive protein detection* [30] theoretically explained the proximity effect by a change in local DNA concentration and comparison of inter and intramolecular DNA hybridization. Figure: 1.5 shows their depiction of the proximity effect, in which target molecules stabilize the weak DNA hybridization. When a weak DNA pair (6 base pair) tagged to two antibodies which specifically binds to a target in separate epitope is diluted in same buffer to 1 nM, the distance between two DNA will be ~ 1500 nm, and the volume confining the two DNA will be 1.7 fL. When the target is introduced, the antibodies bound to it force the DNA close to each other. Now the DNAs are only 20 nm away within volume of only 4.2 zL. If we calculate the concentration of DNA, we arrive at ~ 400 μ M, which is a 400,000-fold increase compared to in the absence of target. At such high concentrations, even weak hybridization interactions become strong and are spontaneous at room temperature. Figure: B shows the stability by comparing the melt temperature (T_m) of inter- and intra-molecular hybridization. The intermolecular T_m of the 6 bp DNA at 1 nM (in 1 mM Mg^{2+} and 50 mM Na^+) is only 10 $^{\circ}C$ (calculated using IDT Oligo Analyzer). If the same 6 bp is in the ends of a single strand making an intramolecular hairpin DNA binding, the T_m is much higher at 53 $^{\circ}C$. The proximity complex with and without target can be conceptually compared to intra- and inter-molecular binding, respectively.

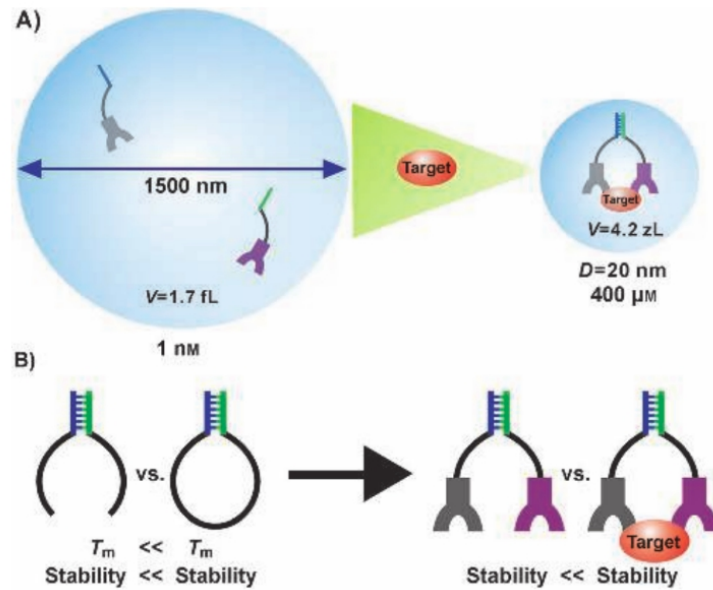


Figure 1.5: **Proximity effect:** A) When two antibody conjugated with weakly hybridizing complimentary DNA is in a solution with 1 nM concentration, the distance between them will be 1500 nm and 1.7 fL as local volume. On introduction of target the distance drops to 20 nm making local volume as 4.2 zL and 400 μM as local concentration. B) Proximity hybridization in the presence and absence of target can be seen as intra and inter DNA hybridization, with intra being very strong than inter [30]
 Reprinted with permission Copyright ©(2013) John Wiley and Sons

1.4.1 Optical detection

Proximity Ligation Assay (PLA)

Exploiting the proximity effect with T4 DNA ligation and DNA amplification by PCR, Fredriksson, et al. developed a sensitive homogeneous protein detection method termed the proximity ligation assay (PLA) [31, 32]. Figure: 1.6 shows the schematic view of aptamer based PLA; when two aptamers bind with the protein target, the binding of connector DNA (black) with these two aptamers becomes stronger due to the proximity effect. The 5' end of one aptamer is phosphorylated, and upon connector DNA binding this phosphorylated 5' is placed closer to the 3' and in double stranded state, where the two strands can be effectively ligated by T4 DNA ligase enzyme. With this ligated DNA, the Taqman probe (Green) can bind strongly. The primer binding sites are shown in boxes, which upon polymerase-chain-reaction the DNA can be amplified, which attracts more Taqman probe to bind. At the same time, the DNA polymerase exonuclease activity digests the dsDNA while amplifying. This separates the fluorophore from

the quencher, resulting in fluorescence signal increases. In the absence of protein, this ligation reaction will not happen, and binding between the Taqman probe and the aptamers is weaker, giving very little fluorescence signal.

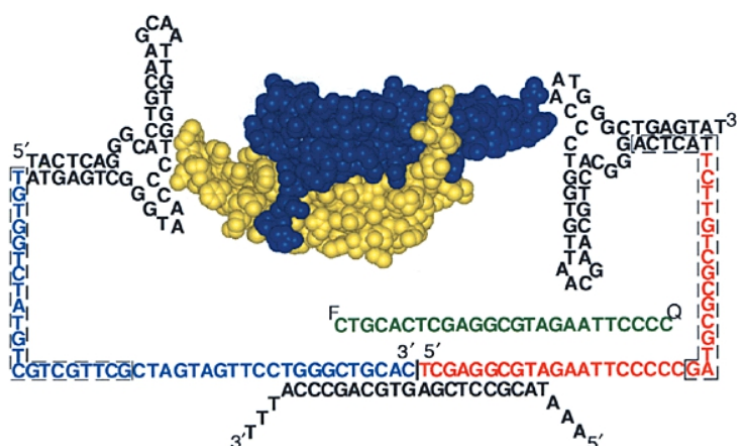


Figure 1.6: Proximity ligation assay: The aptamer region shown in black, when it binds with the protein brings the tails to close proximity, which can strongly bind with connector. Upon enzymatic ligation the tails acts as a single DNA which can be amplified by real time PCR. The primers are shown in boxes and taqman probe is shown in green [31].

Reprinted with permission Copyright ©(2002) Nature Publishing Group

Pincer assay

Also exploiting the proximity effect, Heyduk, et al. developed a fluorescence assay called the pincer assay [27, 33, 34]. This is a homogeneous, mix-and-read assay in which an aptamer pair or antibody pair can be used as the recognizing unit. Figure: 1.7 shows the schematic view of antibody based pincer assay. In the presence of target, the DNA hybridization happens by the proximity effect, which brings fluorophores closer together, enabling fluorescence resonance energy transfer (FRET). Figure: 1.7C shows the emission spectrum, where only in the presence of target emission at 670 nm occurs, and in the absence of target there is very little FRET.

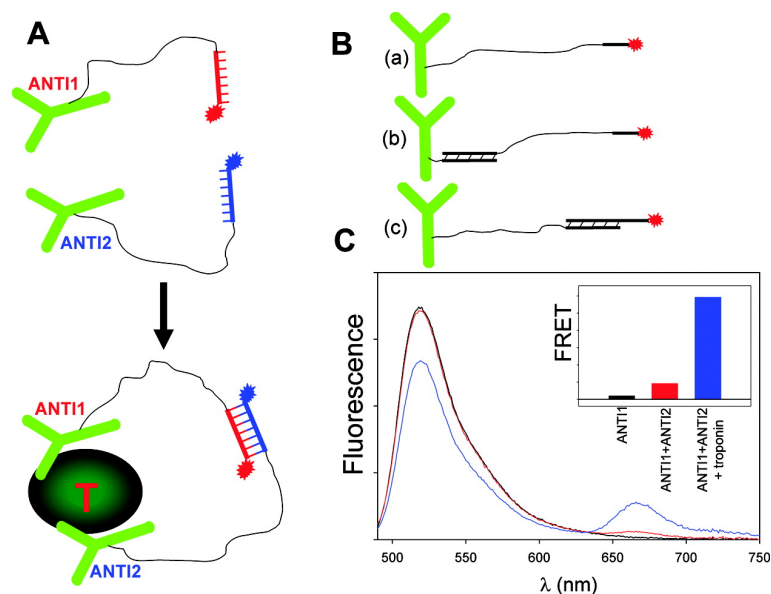


Figure 1.7: **Pincer assay:** A) Upon target (T) binding the hybridization energy between two DNA with FRET pair becomes stronger due to proximity effect; B) Different model of DNA conjugate used; C) The FRET signal is observed only in the presence of target. [34]

Reprinted with permission Copyright ©(2008) American Chemical Society

1.4.2 Electrochemical detection

The proximity effect has also been used in electrochemical detection of protein. Easley, et al. developed an electrochemical detection method in which DNA assembly happens on the electrode surface in the presence of the target protein [35, 36]. This methodology, along with its optimization and further development are discussed in Chapter 2. As an improvement to this method, Ren, et al. developed a ratiometric electrochemical proximity assay shown in Figure: 1.8 [37]. DNA tagged to antibody 1 is also tagged with methylene blue, an electrochemical redox molecule. This antibody–DNA complex is bounded to capture DNA on the electrode surface, this DNA is bound to the electrode covalently due to its thiol-modification. The other end of the surface bound DNA is tagged with ferrocene, another electrochemical redox molecule. Initially there will be signal from methylene blue but not from ferrocene. When target is introduced with antibody 2, due to the proximity effect, the antibody 1 is removed from the surface, the thiolated DNA forms a loop placing the ferrocene at the place of methylene blue. The target introduction results in an increase and decrease of ferrocene and methylene blue signals, respectively, making a ratiometric sensor. Zhang, et al. also used dual aptamers in a different configuration and quantified platelet-derived growth factor protein (PDGF) through

electrochemical detection of proximity dependent complex on electrode surface [38, 39]. More details of electrochemical detection and sensor are presented in following sections.

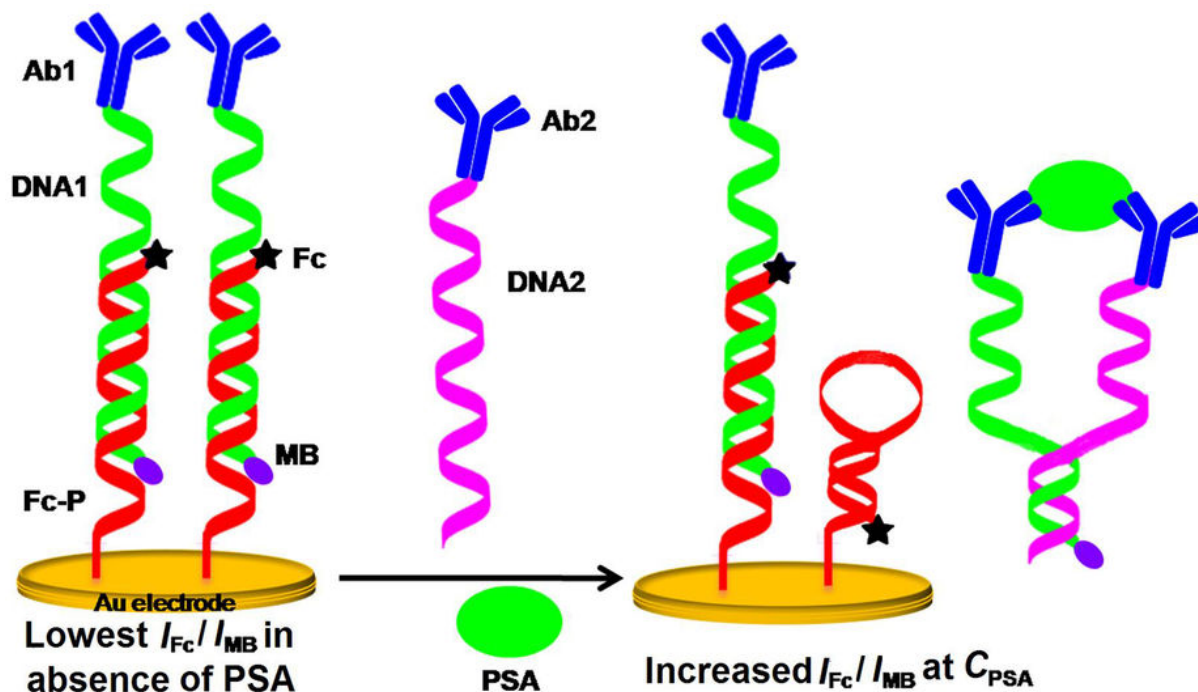


Figure 1.8: Ratiometric electrochemical proximity assay: Initially since methylene blue (MB) is closer to the surface and ferrocene (Fc) being far, the I_{Fc} / I_{MB} is lower. On introducing the target due to proximity effect the DNA tagged with MB is removed from surface and Fc is brought closer which increases I_{Fc} / I_{MB} , by which protein can be quantified ratio-metrically [37].

Reprinted with permission Copyright ©(2014) Nature Publishing Group

1.5 Electrochemical Biosensing

In this section we focus on strategies used in amplification-free electrochemical biosensing of clinically relevant molecule using oligonucleotides immobilized on electrodes. The amplification-free electrochemical sensors have versatile applications in dip-and-read, point-of-care quantification.

1.5.1 Typically used voltammetry techniques

Cyclic, differential pulse and square-wave voltammetry are suitable for these sensors [40]. Cyclic voltammetry (CV) is the method most commonly used in electrochemistry. In this method the voltage is gradually swept between two points while current is measured. The voltammetry is plotted as applied voltage vs current. CV is suitable for quantification of biological molecules if the target is electrochemically active and the biological concentration is higher. Schmidt, et al., for example, used carbon nanotube yarn and detected neurotransmitters in live brain tissue [41]. The limitation of the cyclic voltammetry is the current observed from electrode capacitance, which makes its signal to noise ratio lower compared to the other two methods.

Pulse Voltammetry

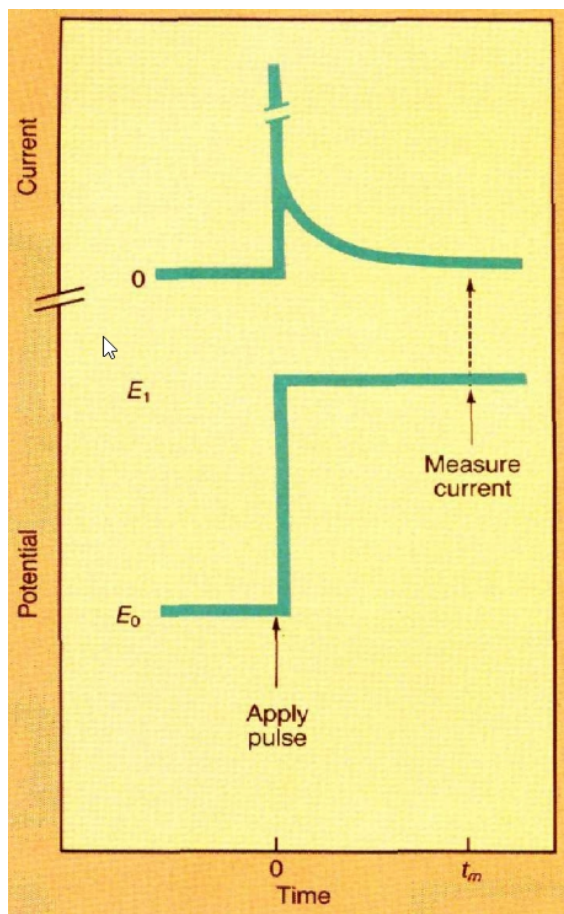


Figure 1.9: **Pulse voltammetry:** Current response to the pulse, initially there is a huge current which is not been measured, while measurement is done the signal to noise ratio is higher. [42]

Reprinted with permission Copyright ©(1985) American Chemical Society

To improve the signal to noise ratio, pulse voltammetry is introduced. Figure: 1.9 shows the potential pulse and current response. Unlike cyclic voltammetry or chronoamperometry, pulse voltammetry is not a continuous measurement. The current is measured after a certain time period (shown in figure). By this approach, the signal-to-noise ratio is improved as the large amount of capacitance current decays in some situations much faster than the current due to the electrochemical reaction (faradaic), so while measuring the contribution from non-faradic current is reduced to give a high signal-to-noise ratio [43]. There are various waveforms of pulses actually used in pulse voltammetry. Normal, differential, staircase, and square-wave, are examples; among these, square-wave voltammetry (SWV) is the most sensitive one [42]. Selection of the measuring technique is determined by the faradic and non-faradic current in the particular experiment.

Square-wave voltammetry

SWV is a sensitive voltammetry technique. In this method, not only the capacitance is reduced but also the signal is increased due to its differential output. Figure: 1.10 shows the SWV pulse wave format and measuring pattern. It is a combination of a staircase and a square wave,

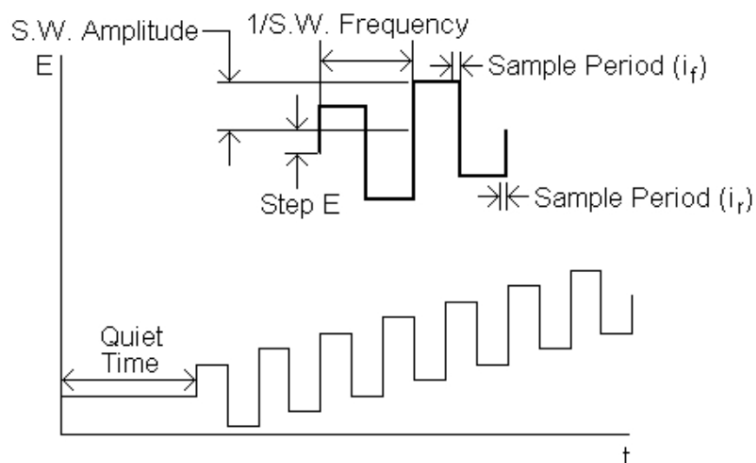


Figure 1.10: *Potential wave form for square wave voltammetry*
<https://www.basinc.com/manuals/EC-epsilon/Techniques/Pulse/pulse>

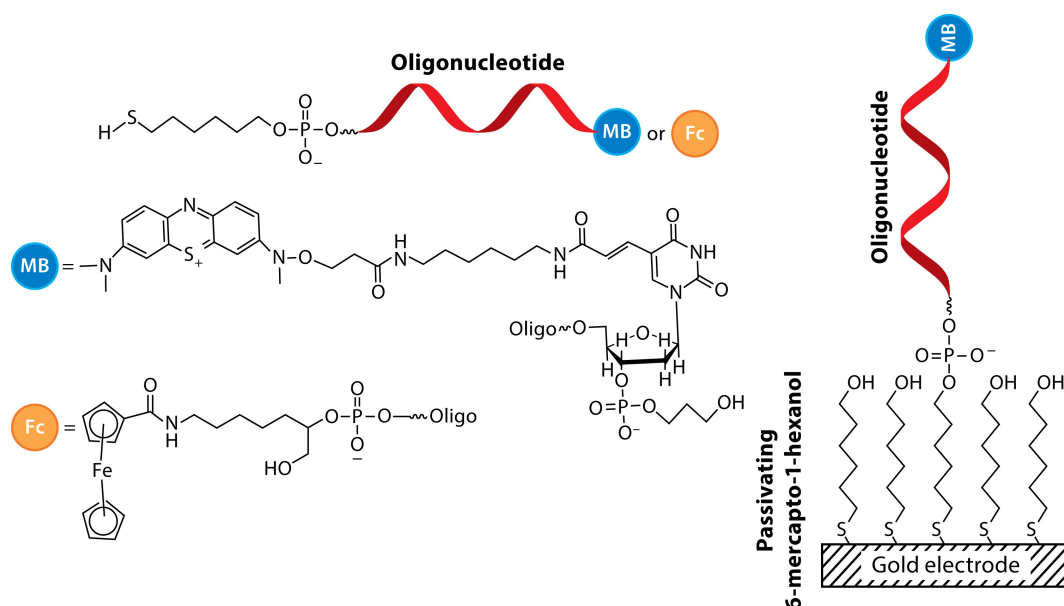
since each square-wave cycle has a minute increment in the potential controlled by a step size input. The frequency input determines the timing of one cycle ($1/\tau$), which also determines the measuring time since measurement is done at the end of each half-cycle, i.e. before the next pulse. The scan rate in SWV is controlled by both step size and frequency. The output signal is $\Delta i = i_f - i_r$. By doing this in case of reversible redox molecule both oxidation and reduction are measured, and the difference signal is essentially doubled, which helps in increasing the sensitivity. Finally, due to the SWV pulse pattern being phase- and frequency-locked with the detection trigger, SWV operates as a lock-in-detection method. As such, a large amount of measurement noise in this technique is reduced, which also improves signal-to-noise ratio.

1.6 Protein, small molecule and oligonucleotide quantification through electrochemistry

1.6.1 Quantification through structure switching capturing probe

In the past decade, the development of target-induced structure switching oligonucleotides on the electrode surface were successful in analyzing in a wide range sample matrices [40]. Plaxco and coworkers introduced the method of using target capturing DNA, which undergoes the change in electron transfer rate between redox molecule tagged to capture DNA and the electrode, for quantification [44, 45]. This is an electrochemical equivalent of aptamer or

oligonucleotide beacon which alters the distance between FRET pair on target binding [46]. Figure: 1.11 shows the overview of typical oligonucleotide self-assembled monolayer used in this method. Methylene blue and ferrocene are the most commonly used redox tags, and 6-mercapto-1-hexanol is used as a spacer and passivating layer. The capturing oligomer binds with the target in high specificity, and the spacer helps in eliminating the nonspecific binding on the surface. These features result in a sensitive and selective assay. Even though the LOD is not as low as the gold standard (ELISA), the less sophisticated and non-expensive instrumentation and the ability of miniaturization for POC makes this as an exciting platform for diagnosis.




 Schoukroun-Barnes LR, et al. 2016.
Annu. Rev. Anal. Chem. 9:163–81

Figure 1.11: Electrochemical DNA/aptamer sensor: Typically oligonucleotide is thiolated in one end and tagged with either methylene blue (MB) or ferrocene (Fc). 6-mercapto-1-hexanol is used as a spacer [40].

Permission Not Required for republishing in Dissertation Annual Reviews

Electrochemical distinction of signal from baseline in target induced structure switching DNA

The change in the structure of DNA by target affects the electron transfer rate between the redox moiety and the electrode. This change in electron transfer is mainly due to the change in the

dimension of redox moiety on the surface which alters the distance traveled by it to interrogate with surface. SWV is the most predominantly used voltammetric technique for quantification. As we saw earlier in SWV, continuous current measurement is avoided to have a high signal-to-noise ratio (faradic to capacitance current), and in this situation it is helpful in discriminating signal from baseline. In addition to the discrimination of signal and baseline, the direction of percentage change, degree of signal change, and sensor sensitivity are all controlled by SWV frequency [47–49], which controls the measuring time after the pulse. Figure: 1.12 shows the change in faradaic current responses following the pulse for linear-DNA probe before and after the target is bound. As an approximation, the unbound sensor has the electron transfer rate of capture DNA at 100 s^{-1} , which has a higher measurable current at 100 Hz. As the result of target binding (complementary DNA), the electron transfer rate becomes about 6 s^{-1} , which permits 5 Hz to have higher signal [49]. This guides to switching the direction of signal change (signal-on to signal-off) by a simple SWV frequency change. The input frequency can be optimized to give a sensitive sensor, and this is one of the important measures for these types of sensors.

Ion and small molecule quantification

Radi and OSullivan used a guanine-rich DNA aptamer attached to the gold electrode for recognition of potassium (K^+) ion [50]. In the presence of K^+ the DNA undergoes structure switching, making the ferrocene redox moiety closer to the electrode surface, which is otherwise far away (Figure: 1.13A). In this work they used impedance for measurement. Baker et al., developed an electrochemical aptamer sensor for rapid quantification of cocaine [51]. This sensor is capable of quantifying cocaine even in unadulterated samples and biological fluids (Figure: 1.13C). They were successful in detecting the target rapidly within seconds. In addition to this, the sensor is reusable with an aqueous wash at room temperature. Zuo et al., with the ATP aptamer hybridized with complementary sequence on the surface, quantified ATP [52]. The ATP displaces the complementary sequence and coils the aptamer around it placing the ferrocene redox molecule closer to the electrode surface (Figure: 1.13B). Ferapontova et al., quantified

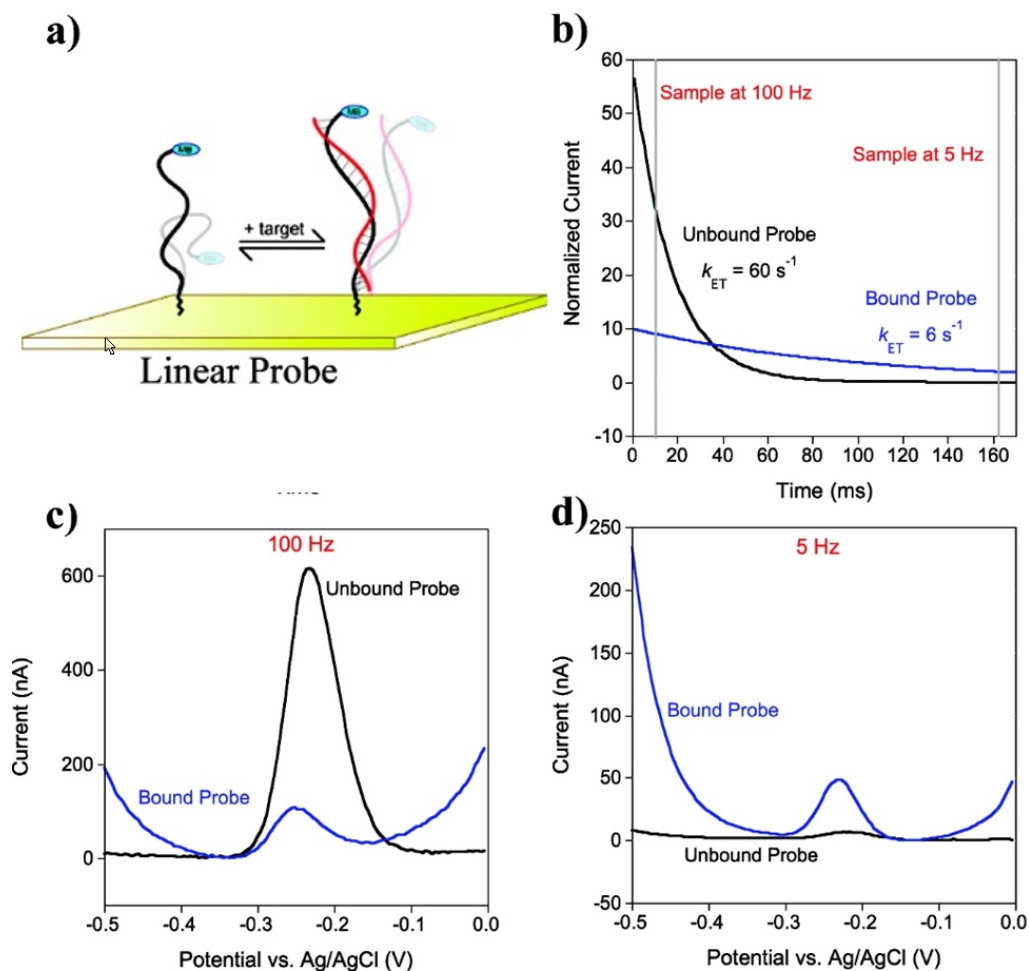


Figure 1.12: SWV response for DNA switch: a) shows the probe model, when DNA target binds with the capture probe the electron transfer rate is altered due to change in mobility. b) Faradaic current response for target unbound and bounded probe. Due to high mobility the redox moiety reaches the surface quickly to give signal resulting more signal at low measuring time and very less signal at later time no molecule is left to give signal. In case of bound probe the faradaic current is lower initially and gradually dropping, resulting in having higher signal in larger measuring time compared to unbound probe. (c,d) SWV response at 100 Hz and 5 Hz, higher signal is observed by unbound probe at 100 Hz and bound probe at 5 Hz. This shows that just by switching the frequency the percentage change dimension can be shifted. [49]

Reprinted with permission Copyright ©(2010) American Chemical Society

theophylline with an RNA aptamer on the surface of the electrode [53]. The target introduction induces a positional change placing the redox moiety in close proximity to the surface (Figure: 1.13D).

Protein and antibody quantification

Proteins and antibodies are also analyzed successfully through electrochemical aptamer sensors. In addition to the signal change by positional change of aptamer by target, the property of these larger targets hindering the flexibility also contributes to the signal change (usually signal suppression). Plaxco and Heeger developed a label-free, amplification-free thrombin aptamer sensor, which undergoes signal suppression by thrombin binding [45]. They were successful in using the sensor in blood serum. Later they improved the sensor to signal-ON by adding complimentary DNA to the aptamer, which increases the sensitivity of sensor and gives 3 nM as the LOD [45]. In the same collaboration, picomolar level platelet-derived growth factor was detected in blood serum [54]. In following years, the Plaxco group has quantified antibodies using bioelectrochemical switches [55] and tagged peptide epitope recognition units in surface DNA [56]. In their latest work, protein-protein interactions on the surface were studied, which is promising in development of various protein sensor that lack a sensitive aptamer [57]. The Revzin group accomplished simultaneous electrochemical detection of tumor necrosis factor alpha, interferon gamma, and transforming growth factor by incorporating electrochemical aptamer sensors into microfluidics [58–60]. This method provides near real time quantification, achieved by the quick reproducibility of the sensors, which makes this method as a rapid, multiplexable, sensitive, and selective approach. These advantages of this technology and simple instrumentation projects as a good alternative to traditional method in (ELISA), in spite of typically higher LOD.

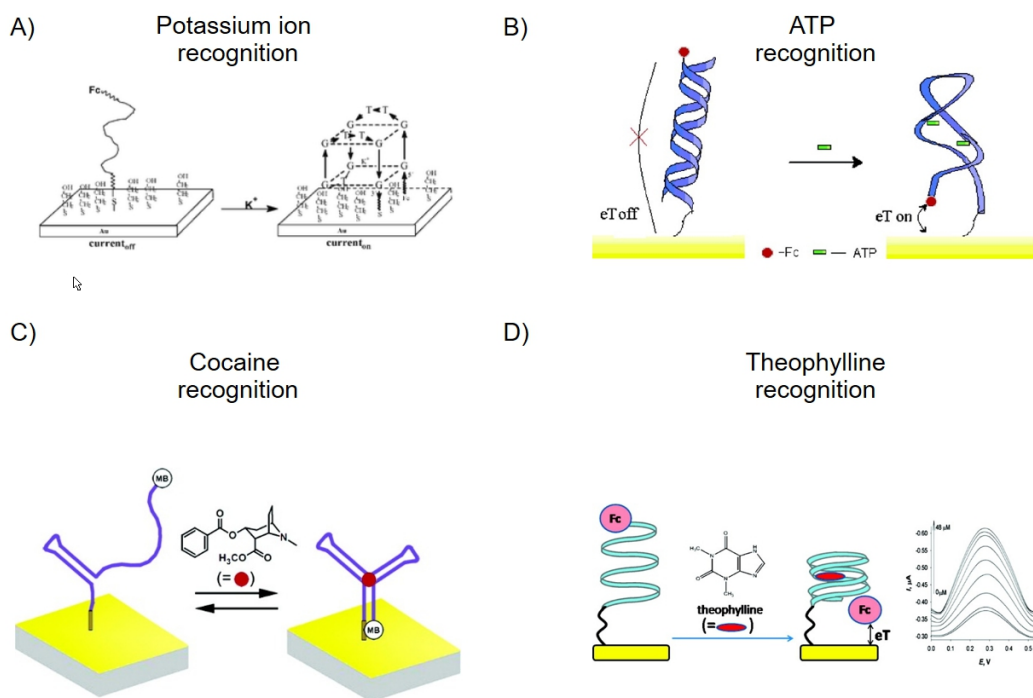


Figure 1.13: Small molecule quantification by E-aptamer: A) Potassium ion recognition by structural transition of G-rich aptamer to form G-quadruplex [50]; B) ATP quantified by displacement of complementary strand DNA [52]; C) DNA switch by cocaine placing the MB closer to surface [51]; D) RNA aptamer for electrochemical detection of theophylline [53].

Reprinted with permission Copyright ©(2006,2007,2008) American Chemical Society (2006) Royal Society of Chemistry

Oligonucleotide quantification

Anne, et al. interrogated the flexibility of short DNA on electrode surface through cyclic voltammetry [61]. 3-ferrocene labeled DNA is immobilized on the electrode, and upon hybridization signal suppression is observed. Around the same time period, the Heeger and Plaxco groups, using methylene blue tagged hairpin-loop DNA on the surface, quantified complementary DNA using cyclic voltammetry [44]. Later, linear DNA probes were used to check the electrochemical signal change by hybridization, and testing and regeneration of probes were done both in buffer and blood serum [47]. For increasing the sensitivity of the sensor, Idili, et al. used a clamp-switch signal-on E-DNA sensor which upon target (DNA) binding formed a triple helix DNA structure [62]. On comparing the mismatched target, the clamp-switch discriminates the false positive effectively. Wang, et al. used TCEP for enzymeless electrochemical signal amplification for sensitive quantification of micro-RNA (miRNA-122) [63]. The sensor is very sensitive with LOD of 0.1 fM, which selectively discriminates miR-122-3p present in serum. This quick readout of target makes the possibility of development of analytical systems capable of in-home, POC or DIY applications.

Real time and calibration free measurement using structure switching capturing probe

Plaxco and White have also worked on re-engineering the aptamers [48, 64, 65], understanding the SWV frequency responses [49], and altering probe packing [66]. In addition to this, in collaboration with the Soh lab, aptamer-based real-time tracking of circulating therapeutic agents in living animals has been accomplished recently [67]. Figure: 1.14 shows the microfluidic setup for real-time electrochemical quantification. The doxorubicin specific aptamer acts as a signal-OFF sensor at lower frequency (>30 Hz) and a signal-ON in higher frequency, which gives a dual conformation of the drug concentration drift. Later a closed loop feedback control for doxorubicin was developed [3]. Arroyo-Curras, et al. measured four drugs (doxorubicin, kanamycin, gentamicin, and tobramycin) with the temporal resolution of 3 s in the bloodstream of live animals [68]. For calibration free real-time quantification and to counter the signal drift

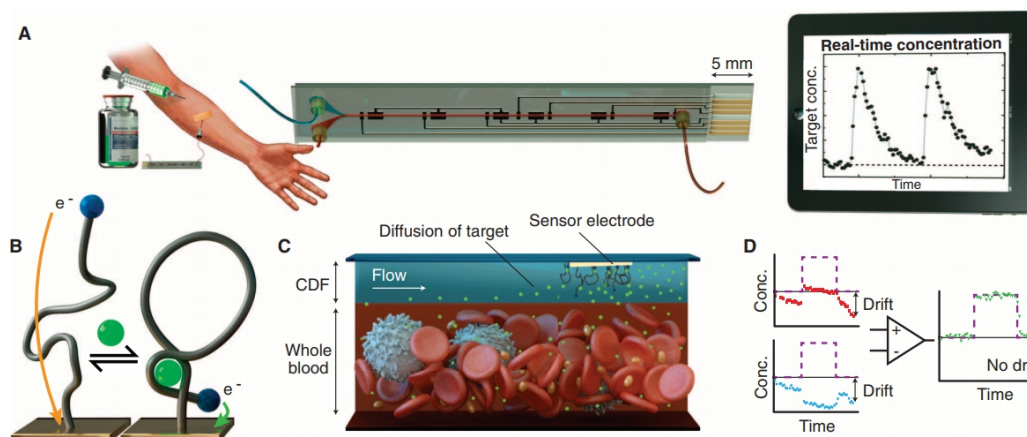


Figure 1.14: Microfluidic electrochemical detector for in vivo continuous monitoring (MEDIC):A) MEDIC chip connected to patients bloodstream to measure pharmacokinetics; B) Aptamer model used in the sensor, conformational change happens by target; C) Through microfluidics the laminar flow of buffer and blood is achieved; D) Simultaneously both signal-off (blue) using lower SWV frequency and signal-on (red) is measured which helps in minimizing the drift [67].

Reprinted with permission Copyright ©(2013) The American Association for the Advancement of Science

due to time and microfluidic flow, dual-reporter can be used [69]. In addition to this, the advantage of the structure switching capturing probe is that they have a frequency dependent signal change. This makes some threshold frequency having signal unaltered due to target, and the signal in these frequencies can be used as a reference for ratio-metric quantification [70].

1.6.2 Quantification through non-structure switching capture probe

The electrochemical quantification by change in electron transfer kinetics is successful for a wide range of analytes. However the need of an aptamer, specifically a structure switching aptamer, is a hindrance in extension of this approach for versatile development [71]. So, the exploration in using non-covalently (on the surface) attached redox reporters for bio-molecular quantification is done by the Kelley [72], Vallee-Belisle [73], and Easley [35] groups. Lu, et al. immobilized the thrombin aptamer and hybridized with the complementary sequence, which was tagged with ferrocene. The thrombin displaced the complementary sequence, resulting in signal loss [71]. Chen, et al. used anti-lysozyme DNA aptamers with which ruthenium hexamine ($[\text{Ru}(\text{NH}_3)_6]^{3+}$) was bound electrostatically [74]. The lysozyme pushed away the $[\text{Ru}(\text{NH}_3)_6]^{3+}$, which was reflected in the signal for quantification. Das, et al. by using

nanostructured gold electrode achieved ultrasensitive read out of CA-125 (cancer biomarker) in serum and whole blood [72]. In this method, antibodies upon interaction with protein blocked the redox molecules ($[\text{Fe}(\text{CN})_6]^{3-/4-}$) from the bulk solution from reaching the electrode and signaling. Later, they developed an oligonucleotide quantifying sensor using the nanostructured gold electrode [75–78]. In this method, $[\text{Ru}(\text{NH}_3)_6]^{3+}$ complex electrostatically adsorbed to the DNA, and the signal for this complex was amplified by an electrocatalytic reporter system in which $[\text{Ru}(\text{NH}_3)_6]^{3+}$ was regenerated by chemical oxidation of Ru(II) by Fe^{3+} of $[\text{Fe}(\text{CN})_6]^{3-}$ in the bulk solution [77]. Figure: 1.15 shows this electrochemical readout pattern. Circulating tumor DNA analysis was successful by using this method. The wild type were blocked using a DNA clutch probe, which made the sensor more sensitive to the mutant type [76].

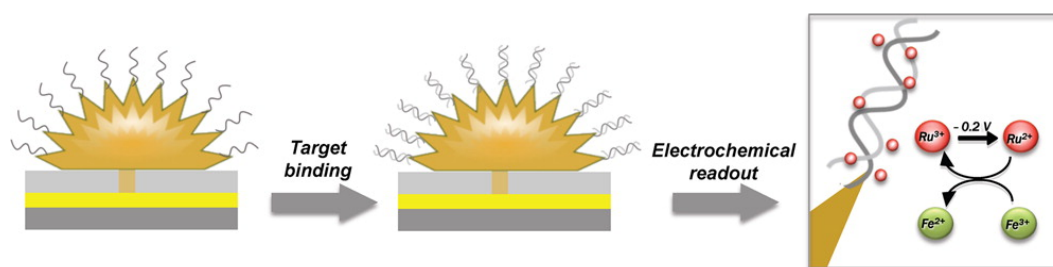


*Figure 1.15: **Electrocatalytic reporter system:** The $[\text{Ru}(\text{NH}_3)_6]^{3+}$ adsorbs on the negatively charged nucleic acid on surface. Ru^{3+} is electrochemically reduced, is been regenerated by Fe^{3+} ($[\text{Fe}(\text{CN})_6]^{3-}$) [77]*

Reprinted with permission Copyright ©(2013) American Chemical Society

Quantification by steric-hindrance on the surface

White, et al. showed that the probe density plays a crucial role in the sensitivity of the sensor [66]. For every new sensor strategy the probe packing should be optimized, as higher packing leads to loss of sensitivity due to steric hindrance. Mahshid, et al. developed a strategy of exploiting the steric hindrance for quantification [73]. To show the effect of steric hindrance, they compared the SWV signal from various molecules ranging from 0.2 to 150 kDa. These molecules were tagged to a DNA, which has methylene blue tag on other end. This DNA hybridized with the surface DNA via 16 bp. Since hybridization energy was the same, the drop

in the signal as due to the effect of steric hindrance. With this knowledge, indirect quantification of larger proteins was developed. The signaling DNA (which has redox moiety) is tagged to target recognizing unit (Biotin and digoxigenin for quantification of streptavidin and anti-digoxigenin respectively). If the target is present in the sample, the signaling DNA binds with the target, which due to steric hindrance is unable to bind with the capturing probe. In the absence of target, the signal is generated due to lack of hindrance. By this method, larger proteins can be indirectly quantified, and the system worked in whole blood (Sahar Sadat Mahshid et al., 2015). This method was extended to indirectly quantifying small molecules [79], then the sensitivity was improved developed using nanostructured electrodes [80]. This work has recently been followed by an application of detecting signaling factors in stem cell cultures [81].

1.7 Conclusion remarks

Quantification of clinically relevant molecules is becoming very crucial not only in POC diagnosis but also in research for better understanding of living systems. We have seen that sensitive methods often required sophisticated, expensive instruments. Aptamer-based electrochemical methods overcome the instrumentation burden, but they are hindered by the lack of versatility to be applied toward a wide range of targets. One of the drawbacks in generalizing these sensors is aptamer selection. In most of these sensors, the aptamer, upon target binding, should undergo a drastic change in the structure to give an observable signal change. We have also seen methods like steric hindrance assays which ignore the dependence of conformational change and have been successful in extending the quantification to both small molecules and large proteins. The drawback in this method is the usage of multiple components in the buffer which eliminate it from being drop-and-read.

Within this dissertation, the main goal is to develop a method for quantification of small molecules and large proteins which is suitable for dip-and-read and POC diagnoses. Chapter 2 focuses on the electrochemical proximity assay (ECPA) and its optimization. This work evaluates DNA fabrication on the electrodes, instrumentation issues, and attempts to make ECPA

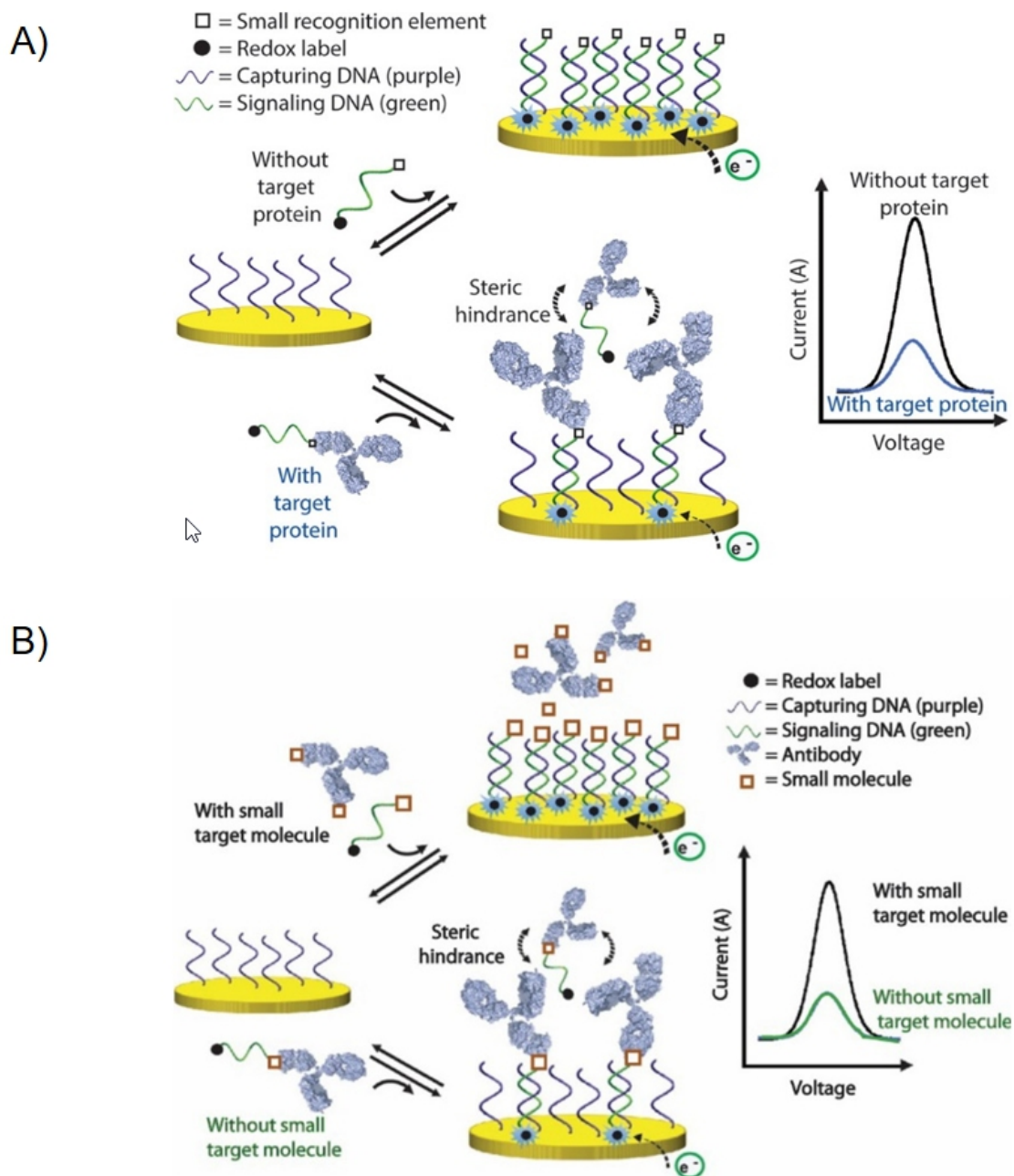


Figure 1.16: **Steric hindrance assay:** A) Detection of larger proteins, in the presence of larger protein the signaling DNA binds with it, so unavailable for surface hybridization due to steric hindrance. With target has lower signal [73]. B) Strategy for small molecular quantification, in the presence of small molecule, the target will block the region in the large protein. So signaling molecules can bind with large protein ending in surface hybridization and generating signal. With target has higher signal [79]. Reprinted with permission Copyright ©(2015, 2017) American Chemical Society

as a dip-and-read measurement. Chapter 3 focuses on improving our understanding of the surface hybridization, the distance dependence of redox moiety in hybridized mode, the effects of double layer on the surface hybridization, and finally on better understanding diffusion layer effects in DNA-driven SWV assays. In Chapter 4, a simple oligonucleotide quantification approach is developed by exploiting the role of measuring temperature in signal and background. From the experience and knowledge of our work and literature survey we developed, a strategy which uses a DNA nanostructure on the electrode surface for quantification of large proteins and small molecules is explained in Chapter 5. This method, in the future, should provide a generalizable platform for quantifying multiple proteins, peptides, or small molecules by a dip-and-read workflow, and this should promote future real time measurements, as discussed in Chapter 6 (Future work).

Chapter 2

Electrochemical Proximity Assay and its Advancement

2.1 Introduction

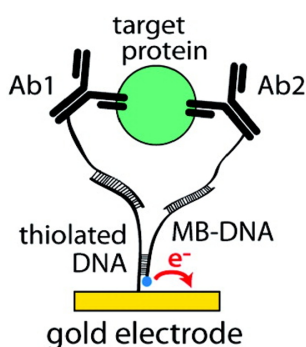


Figure 2.1: ECAPA: Pictorial description of complete complex of ECAPA which has six component including target [35].

Reprinted with permission Copyright ©(2012) American Chemical Society

On Chapter 1, I have introduced various quantitative and qualitative methods used to analyze clinically relevant molecules. Even with these developments, there remains a need for improved quantification techniques from the perspectives of cost, sensitivity, and POC detection. Most of the methods address the issue of sensitivity, but due to instrument sophistication and the need for expert technicians, there is still a need for better technology to address the other two issues. To address these, some point-of-care methods have been developed for selected analytes, those that are highly specialized to a particular target molecule [82, 83]. For future point-of-care testing, in addition to high sensitivity and do-it-yourself workflows, more flexible methods are needed that can function with a variety of targets

using the same platform.

For protein quantification in clinical and research laboratories, sandwich enzyme-linked immunosorbent assays (ELISA) have emerged as the method of choice due to its high sensitivity and—perhaps more importantly—its effective flexibility to a wide range of targets. However, this method requires expert technicians to accomplish its multiple, tedious steps, instrument management, and data analysis. In addition to that, a typical ELISA takes 6–8 hours

for quantification. These limitations make ELISA unsuitable for POC detection. Dr. Easley's and Dr. Shannon's groups from Auburn University built from the sandwich ELISA concept and developed a generalizable protein assay within an electrochemical detection platform that exploits the proximity effect, termed the Electrochemical Proximity Assay (ECPA) [35]. Like sandwich ELISA, ECPA is also flexible and can be extended to any protein target with two antibody or aptamer probes. Figure : 2.1 shows a cartoon depiction of ECPA, where the protein target has two antibodies targeting different epitopes. The hybridization between methylene blue tagged DNA (MB-DNA) and thiolated DNA (thio-DNA) is made stronger in the presence of the target protein by the proximity effect. The electrochemical signal from the methylene blue is thus proportional to the concentration of target protein. Thrombin and insulin were successfully quantified with aptamer and antibody-oligo pairs respectively, with LODs of 50 pM for thrombin and 130 fM for insulin. Later, a reusable form of ECPA was developed, in which the electrodes after each use was enzymatically regenerated to the initial state and could be used again [36]. Thus, the ECPA platform represents an important step forward in developing generalizable, point-of-care analysis systems with high sensitivity and selectivity.

While ECPA has shown great promise, a number of questions remain concerning the fundamental signaling mechanism, particularly with respect to the frequency-dependence and temperature-dependence of signal generation in square-wave voltammetry (SWV). In order to move beyond the proof-of-concept stage with the technology, it is important to carefully evaluate the signal changes accompanying the relatively complex molecular assembly shown in Figure : 2.1. This chapter gives an in-depth explanation of ECPA and provides new insight into the roles of SWV parameters on signal and background. In addition to that, we have devised several advancement of ECPA technology. The present chapter and the following chapters will be helpful in understanding various factor influencing electrochemical, DNA-based protein and small molecule sensors. This information should be useful not only in optimizing ECPA but also with many DNA-based electrochemical platforms for detecting clinically relevant molecules.

2.2 Reagent and Materials

All solutions were prepared with deionized, ultra-filtered water (Fisher Scientific). The following reagents were used as received: insulin antibodies (clones 3A6 and 8E2; Fitzgerald Industries), 4-(2-hydroxyethyl)-1-piperazineethanesulfonic acid (HEPES) and sodium perchlorate (NaClO_4) from Alfa Aesar, tris-(2-carboxyethyl) phosphine hydrochloride (TCEP), 6-mercapto-1-hexanol (MCH) and insulin from Sigma-Aldrich St.Louis, MO. Insulin antibodies (clones 3A6 and 8E2) are brought from Fitzgerald Industries. Methylene blue-conjugated DNA (MB-DNA) was purchased from Biosearch Technologies(Novato, CA), purified by RP-HPLC. All other oligonucleotides were obtained from Integrated DNA Technologies (IDT; Coralville, Iowa). All measurements were performed using Reference 600 Potentiostat (Gamry Instruments Inc, Warminster, PA).

2.3 Experimental Methods

2.3.1 Preparation of gold electrode and DNA monolayer assembly

ECPA and all other experiments were done with commercially available gold electrodes (CH Instruments, diameter = 2 mm). As the first step in sensor fabrication, a gold electrode was cleaned and polished. Freshly prepared piranha solution ($\text{H}_2\text{SO}_4:\text{H}_2\text{O}_2$, 3:1) was dropped onto the electrode and left for 5 minutes. (*Caution: piranha solution is dangerous to human health and should be used with extreme caution and handled only in small quantities.*) Piranha solution is a strong oxidizing agent and freshly prepared has a temperature of 85 °C, a combination which removes impurities on the surface of gold electrode. Following this step, the electrode was thoroughly rinsed with deionized water, followed by careful polishing to a mirror-like surface with deagglomerated alumina suspension (0.05 micrometer; Allied High Tech Products, Inc. Rancho Dominguez, CA). The suspension had been dropped on a polishing mat MicroFloc (Buehler, Lake Bluff, IL), and the electrode was held perpendicularly while a spinning motion was done as shown in Figure: 2.2 for 10 minutes. Mark Holtan, another graduate student in our group, built a robot to do this polishing (shown in Figure: 2.2), which was helpful in automating

the process and eliminating human errors or person-to-person polishing discrepancies. Then the electrode was rinsed and sonicated in an ethanol and water mixture (1:1) for five minutes to remove alumina particles effectively. The gold electrode was further cleaned electrochemically by 5 cycles of cyclic-voltammetry (CV) in 0.5 M H₂SO₄ with a three electrode system (Ag/AgCl as reference, platinum as counter). The CV scans were from -0.35 to +1.5 V at a scan rate of 0.1 V s⁻¹. The electrochemically cleaned electrode was finally rinsed with deionized water, and it was ready for introduction of the DNA self-assembled monolayer (SAM).

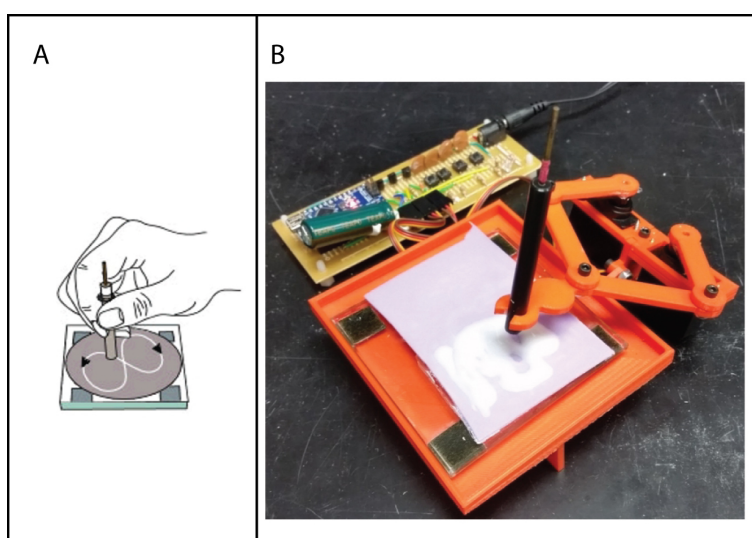


Figure 2.2: Mechanical cleaning of electrodes :A) shows the procedure for mechanical cleaning, where electrode is held perpendicular and polished by patterning the motion as 8; B) shows the Arduino controlled robot build our lab which replicates the mechanical cleaning by hand

Thiol tagged DNA were shipped as disulfides, thus they required chemical reduction by dithiothreitol or TCEP. We used TCEP for reduction, where 1 μL of 200 μM thio-DNA and 3 μL of 10 mM TCEP were mixed in a 200 μL PCR tube and placed in the dark for 1 hour at room temperature. The solution was then diluted with HEPES buffer (10 mM HEPES and 0.5 M NaClO₄, pH 7.0) to a concentration of 1.25 μM and a volume of 300 μL for an electrode in a 15 mL shell vial. The electrode was dipped in this solution (making sure the electrode was not hitting the surface) and incubated at room temperature for another 1 hour in the dark (for some experiments a 16-hour incubation was used). This thio-DNA concentration (1.25 μM) was concluded after an optimization experiment, which will be explained in Section: 2.4.3.

After 1 hour of incubation, the electrode was removed and rinsed with deionized water for 30 seconds (water should be carefully passed on the side and flown over the gold area; no forceful ejection of water should be applied to the gold). Then the electrode was dipped into 300 μL of 3 mM MCH for 1 hour in the dark at room temperature. The MCH solution should be freshly prepared, and since MCH has a foul smell, it is advised to do all these processes in a fume hood. MCH acts as a spacer molecule between covalently bounded thio-DNA, which is helpful in reducing the capacitance current in electrochemical measurements. In addition to that, it also helps to remove non-specific binding between DNA or proteins and the gold surface, and it contributes toward effective orientation of the thio-DNAs on the gold surface (Figure: 2.3). Once this incubation was done, the electrode was rinsed with deionized water and transferred to HEPES buffer. This SAM electrode was ready to be used and could be stored at 4 $^{\circ}\text{C}$ for about a week.

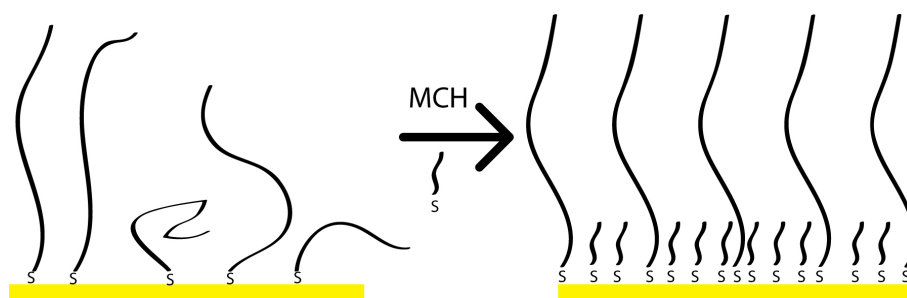


Figure 2.3: Mercapto-hexanol on surface: MCH acts not only as a filler but also helps in orientation of thio-DNA on gold surface

2.3.2 Antibody-oligomer conjugation

In ECPA, the insulin antibodies (clones 3A6 and 8E2) were conjugated with the amine tagged DNA Ab1 and Ab2 respectively using Antibody-Oligonucleotide All-In-One Conjugation Kit (Solulink), and the manufacturers instructions were carefully followed. Figure : 2.4 explains the chemistry behind the conjugation, and the experimental steps are described on the right side. Briefly, the antibodies and amine-tagged DNAs were separately activated with S-HyNic and S-4FB. Later, the activated molecules were mixed, and excess of DNA oligos were used to make sure all the antibodies were tagged with one or more DNAs. After a two hour incubation

at room temperature, conjugated antibodies were separated from the excess oligonucleotides by magnetic affinity beads. The final concentrations of the conjugates were determined by the Bradford protein assay. In some project herein, customized antibody-oligonucleotides were synthesized and purified by Mediomics, LLC.

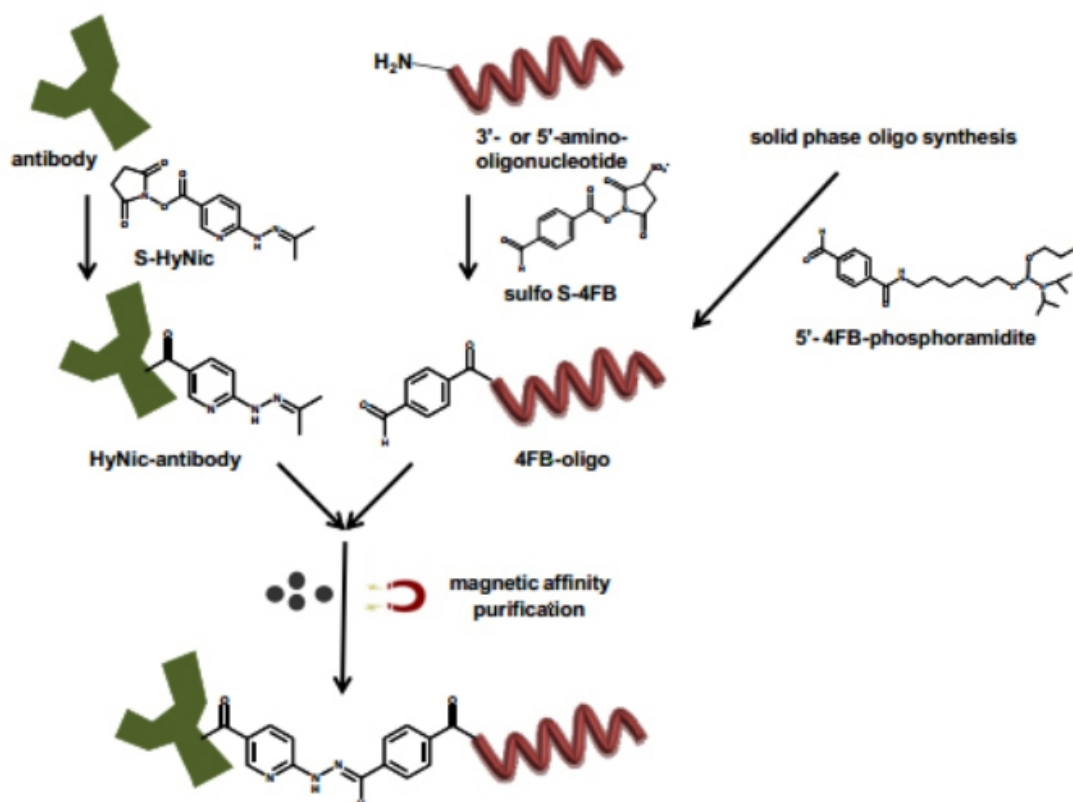


Figure 2.4: *Solulink antibody-oligomer conjugation*: Amine tagged DNA was attached to amine of the antibody through the bioconjugation reaction shown in the figure

2.3.3 Steps involved in ECPA

Reusable ECPA is a fast protein quantification method which can take less than 15 minutes for a cycle of measurement and regenerating the probe surface. The theory behind the regeneration is explained in Section: 2.3.4. ECPA workflow can be operated as homogeneous or heterogeneous. As a homogeneous assay, the sample is mixed with antibodies-oligomers/aptamers and the signaling MB-DNA. The electrode with SAM is dipped into the mixture, and SWV

measurement is done after 1 hour [35]. The heterogeneous method is preferred for measurements in biological matrices and cell secretion measurements [36]. For that, a multi-step procedure is followed. Once the gold electrode is ready with the thiolated-DNA, first 10 μL antibody-oligomer/aptamer is introduced, which has nucleotide sequences complimentary to the thiolated-DNA. The number of base pairs in this binding should be at least 15 so that the equilibrium strongly favors binding at room temperature. After three minutes of incubation, the antibody-oligomer/aptamer is removed, and the electrode is rinsed in HEPES buffer for 30 sec. Later, the electrode is dipped into the sample ($\sim 200 \mu\text{L}$) and incubated for 3 min at room temperature. Following a buffer rinse for 30 s, the second antibody-oligomer/aptamer (10 μL) is incubated for 3 min. This forms a complex where the target is sandwiched between two antibodies/aptamers. This complex on the surface is then introduced into the MB-DNA solution (500 μL), and SWV measurement is done after 3 minutes. This MB-DNA was complimentary to the oligomer in the second antibody/aptamer and binds with it strongly. In the presence of target, due to the proximity effect, the other end of MB-DNA binds with the thiolated-DNA strongly and forms the complex as shown in Figure 2.5. In the absence of the target, there will be no second antibody-oligomer/aptamer, and the binding between the MB-DNA and thiolated-DNA is very weak by design, making the background complex formation negligible. The SAM was enzymatically regenerated, as discussed further in the next section, to prepare the electrode for further cycles.

2.3.4 Reusable ECPA

In the presence of target protein, the ECPA complex has five components bound together, (thiolated-DNA) (AB1/Apt-1) target (AB2/Apt-2) (MB-DNA). Thiolated-DNA was bound to AB1 and MB-DNA. To effectively remove the complex and regenerate the thiolated-DNA, deoxy-Uracil RNA nucleotides were incorporated into the sequence of AB1-oligomer and MB-DNA. Using uracil-DNA excision mix, which is a mixture of HK-UNG and Endonuclease IV, the HK-UNG enzyme specifically cleaves the uracil nucleotide out of the DNA backbone, then Endonuclease IV cleaves the nucleotide-less backbone. This makes the binding between the

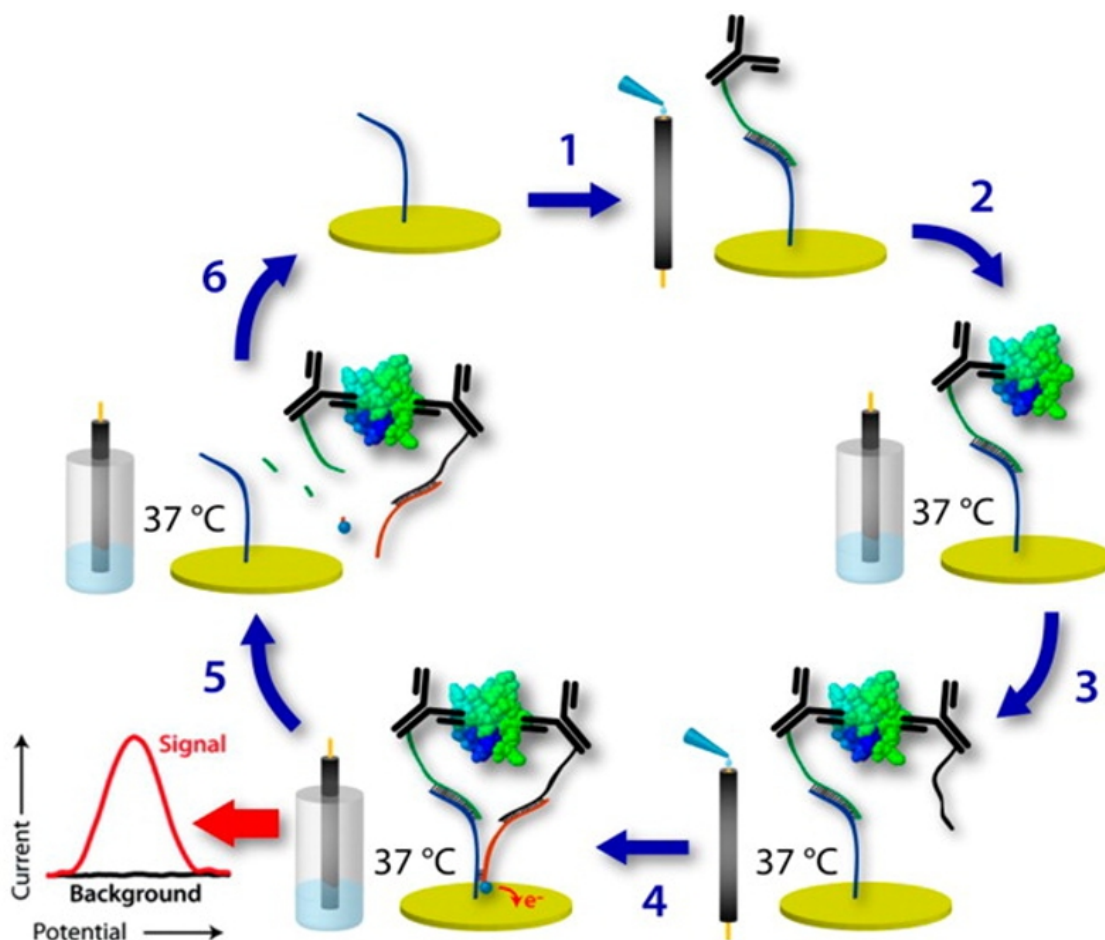


Figure 2.5: ECPC Protocol: Figure shows the ECPC cycle, where the complex is built in steps and after measurement it is been removed by exonuclease enzyme reaction [36]. Reprinted with permission Copyright ©(2014) American Chemical Society

AB1 and thiolated-DNA much weaker and promotes dissociation. Cleaving the MB-DNA destabilizes the proximity effect. This was done by dipping the electrode with complex into the enzyme mixture for 7 min at 37 °C [36]. Following a water rinse, the thiolated-DNA was ready for the next cycle. Figure 2.6 depicts the steps involved in regeneration of the thiolated-DNA SAM.

2.3.5 Insulin measurement

The DNA sequences used for insulin ECPC are shown in Table 2.1. Special modifications are shown in bold, and the deoxy-uracil RNA nucleotides are shown in blue color in the sequences.

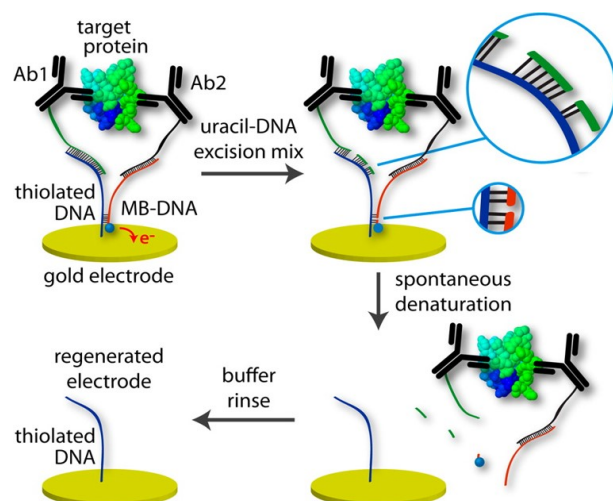


Figure 2.6: Enzymatic regeneration of thiolated-DNA on surface: The uracil DNA excision mix removes the complex from thiolated-DNA, which can be reused [36]. Reprinted with permission Copyright ©(2014) American Chemical Society

The G5-thio, G7-thio, and G10-thio hybridize with MB-DNA with 5,7, and 10 base pairs. Insulin antibody clones 3A6 and 8E2 were conjugated with AB1 and AB2 respectively using a Solulink kit (explained in Section: 2.3.2). Electrode preparation and protocols explained in Section: 2.3.3 and 2.3.3 were followed with 16 hrs thiolated-DNA incubation. SWV parameters used for insulin ECPA measurements were detailed in Table 2.2.

2.3.6 Optimizing SWV frequency and pulse height

Square-wave voltammetry frequency plays a vital role in electrochemical-DNA sensors [49]. For elucidating optimal SWV frequency, following one hour incubation in 100 nM MB-DNA, SWV measurements were done using the parameters mentioned in Table 2.3

2.3.7 Leptin ECPA

Quantification of leptin through ECPA was done by preparing the electrode using the protocol explained in Section 2.3.1 & 2.3.3, with G7-thio of concentration 2 μ M and 16 hours incubation. The sample volume was 20 μ L. SWV parameters mentioned in Table 2.4 were used for

Sequence Name	Abbreviation	DNA Sequence listed 5'-3'
ECPA-Gold-5	G5-thio	/5ThioMC6-D/GCA TGA ATT TTC GTT CGT TAG GGT TCA AAT CCG CG
ECPA-Gold-7	G7-thio	/5ThioMC6-D/GCA TGG TAT TTT TCG TTC GTT AGG GTT CAA ATC CGC G
ECPA-Gold-10	G10-thio	/5ThioMC6-D/GCA TGG TGA CAT TTT TCG TTC GTT AGG GTT CAA ATC CGC G
ECPA-MB	MB-DNA	CCA CCC TCC TCC TTT TCC TAT CTC TCC CTC GUC ACC AUG C/MB-C7/
ECPA DNA-loop	loop	TAG GAA AAG GAG GAG GGT GGC CCA CTT AAA CCT CAA TCC ACC CAC TTA AAC CTC AAT CCA CGC GGA UUU GAA CCC UAA
Antiboby-1	AB1	/5AmMC6//iSp18/CCC ACT TAA ACCTCA ATC CAC GCG GAU UUG AAC CCU AAC G
Antibody-2	AB2	TAG GAA AAG GAG GAG GGT GGC CCA CTT AAA CCT CAA TCC A/iSp18//3AmMO/

Table 2.1: DNA sequence used for insulin ECPA

/5ThioMC6-D/ = Dithiol attachment (IDT), /MB-C7/= Methylene Blue (Biosearch), /3AmMO/ and /5AmMC6/ = Amine (IDT), /iSp18/= PEG spacer (IDT)

measurement.

2.3.8 Optimizing DNA probe density

For optimizing the probe density, we used G7-thio DNA. Concentrations between 0.5 μM to 2 μM were used for incubation. The thiolated-DNA was incubated for 1 hour followed by 1 hour incubation of MCH (3 mM). Later, the electrode was introduced into 100 nM of MB-DNA, and SWV measurements with parameters shown in Table 2.4 was done at the 30 minutes time point.

Parameter Name	Symbol	Values Used
Initial voltage	V_i	-0.45 V
Final voltage	V_f	0.00 V
Step size	E_s	1 mV
Pulse height	E_p	50 mV
Frequency	SWV-Hz	60 Hz

Table 2.2: SWV parameters for insulin ECPA

Parameter Name	Symbol	Values Used
Initial voltage	V_i	-0.45 V
Final voltage	V_f	0.00 V
Step size	E_s	1 mV
Pulse height	E_p	10 to 90 mV
Frequency	SWV-Hz	10 to 100 Hz

Table 2.3: SWV parameters for optimizing SWV frequency and pulse height

2.3.9 SWV signal processing

The SWV data output has forward voltage (V_f), reverse voltage (V_r), step voltage (V_{step}), forward current (i_f), reverse current (i_r), and difference current (i_{diff}). In these V_f , V_r , i_f , and i_r are measured values, V_{step} is input and i_{diff} is a calculated value. In these, V_{step} and i_{diff} was transferred to Microsoft Excel sheet, followed by baseline subtraction. The data where the methylene blue signal starts and ends were selected (in this case -0.325 to -0.310 V and -0.070 V to 0.055 V), with that slope and intercept were calculated followed by calculation of linear baseline (calculated baseline is plotted with raw data in Figure: 2.7A). This calculated baseline was subtracted from raw data points to get baseline corrected SWV voltammogram (Figure: 2.7B). Following this peak height was extracted from the SWV curve by Excel MAX function. For some experiments integrated signal was calculated by summing all the current data points in signaling region (-0.300 to -0.100 V for methylene blue).

Parameter Name	Symbol	Values Used
Initial voltage	V_i	-0.45 V
Final voltage	V_f	0.00 V
Step size	E_s	1 mV
Pulse height	E_p	90 mV
Frequency	SWV-Hz	75 Hz

Table 2.4: SWV parameters for Leptin ECPA

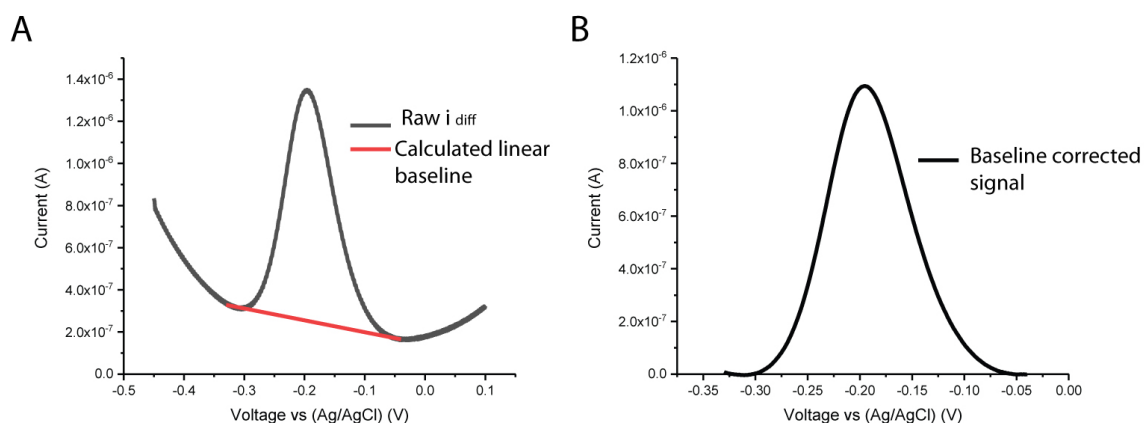


Figure 2.7: SWV baseline subtraction: A) Shows the raw i_{diff} (black) and calculated linear baseline (red), B) Baseline subtracted curve

2.3.10 Thermal Scanning ECPA

Thermal scanning ECPA was carried out using commercially available 2 mm diameter gold disc electrodes or gold electrode of 2 mm x 1 mm made by etching gold sputtered glass electrodes. The procedure of photolithography, gold etching and making of PDMS electrochemical cell will be explained in Chapter 4. The electrode model and the electrochemical cell 3D-CAD is shown in Figure: 4.2.

For 2 mm diameter electrodes in tsECPA experiments, the electrodes were prepared following the protocol explained in Sections 2.3.1, with 2 μ M of thiolated-DNA used for incubation with 16 hours incubation time. The steps explained in Section 2.3.3 were followed, except the incubation time for antibody and sample was 30 min. For insulin detection in human serum, undiluted human serum was used as the sample. Finally, the electrochemical measurement done

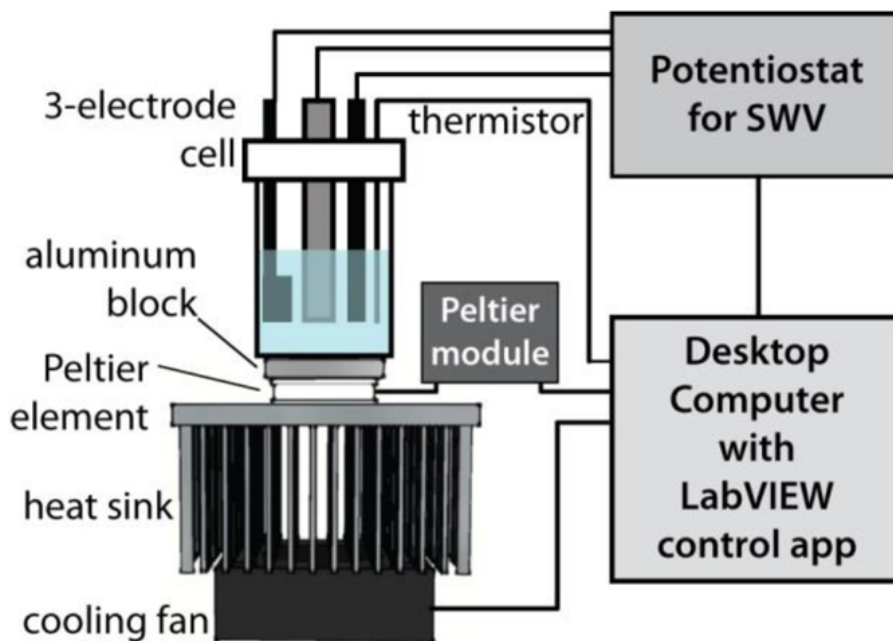


Figure 2.8: *Thermal scanning setup with electrochemical cell*

with parameters listed in Table 2.4.

2.3.11 Surface confined ECPA

In surface confined ECPA (scECPA), two thiolated-DNA were immobilized on the surface of the electrode. One was the typical ECPA thio-DNA (G5, G7, and G10), which binds with the AB1-oligomer with 20 bp. The other one has an intermediate polyethylene glycol, show in Table: 2.5. This PEG-thio binds with both MB-DNA and AB2-oligomer with 10 bp, forming a single branched DNA complex as shown in Figure 2.9. Based on the design, the formation of the complex was possible only in the presence three DNAs, whereas the binding between any two was weaker and could be removed by rinsing, this was to eliminate false positive signal. In the absence of target, the methylene blue is held far from the surface, giving low background. When the target was introduced due to proximity effect, the MB-DNA binds with the thio-DNA (G5, G7, or G10) and makes the methylene blue closer to the surface, which results in increase in signal proportional to target. Since both the antibodies were on the surface, this method should be helpful for real-time measurement of hormone secretion from cells.

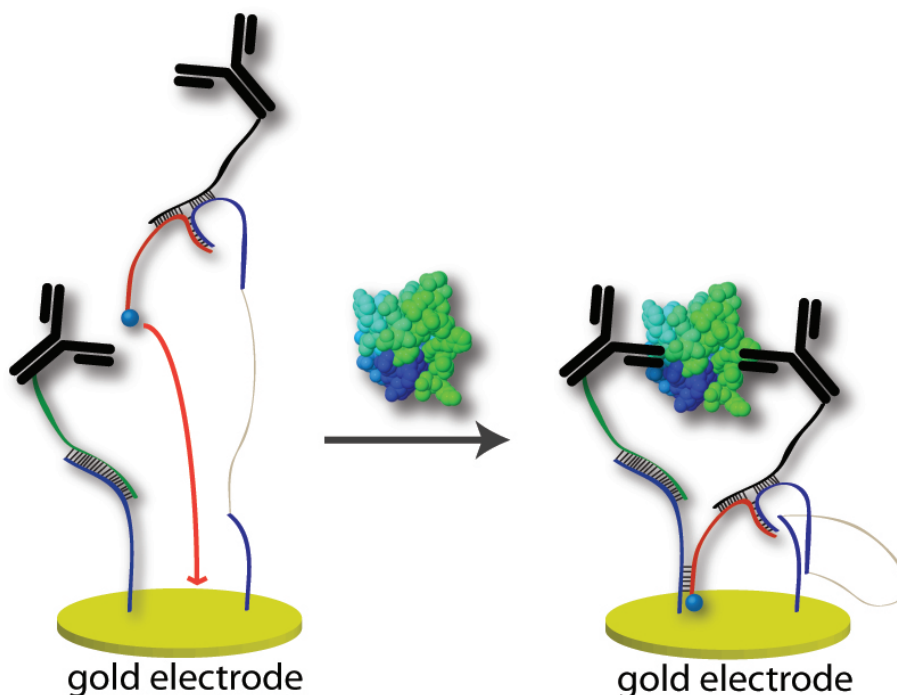


Figure 2.9: *Surface Confined ECPA model: Both the AB are placed on the surface of the electrode through atrong hybridization*

Protocol followed for scECPA experiment

The electrodes were cleaned by the protocol mentioned in Section: 2.3.1. The same immobilization protocol was followed as mentioned in Section: 2.3.1, but in this case two thiolated-DNA (thio-DNA and PEG-DNA) of 1.25 μM was used and incubated for an hour. Once the electrodes were ready, they were incubated overnight in buffer containing 100 nM Ab1, 100 nM Ab2, and 100 nM MB-DNA in room temperature. Later, the electrode was rinsed with water, then the background complex current was measured. Followed by incubation of target for 90 minutes at 37 $^{\circ}\text{C}$, the signal complex measurement was done. The change in the signal was plotted.

2.4 Result and discussion

2.4.1 Optimizing SWV frequency and pulse height

As described in Chapter 1, the SWV measurement process is some what more complicated compared to other types of voltammetry. Since SWV involves a fast transition of voltage and

Sequence Name	Abbreviation	DNA Sequence listed 5'-3'
scECPA-MB	scMB-DNA	TTG UTA TTG UCC TTU TCC UAT CTC TCA CAC GUC ACC AUG C/MB-C7/
PEG-Thio-DNA	PEG-DNA	/5ThioMC6-D/ AAA AAA AAA A /iSp18/iSp18/iSp18/ CCA CCC TCC TAC AAT AAC AA

Table 2.5: DNA sequence used for scECPA
/MB-C7/= Methylene Blue (Biosearch), /iSp18/= PEG spacer (IDT)

measurement, proper instrumental parameters should be carefully evaluated and used. This is explained more elaborately in Section: 2.4.6. In our original optimization of the SWV parameters discussed here, the default instrument setup was used. These default settings included a RC filter for reduction of noise and smoothing of signal. While the noise reduction is certainly effective, this RC filter can cause inconsistencies in the potentiostats function, which will be discussed later in Section: 2.4.6.

From the graph in Figure 2.10, we initially concluded that 75 Hz and 90 mV are optimal parameters for ECPA under these instrument settings, thus these parameters were used in leptin ECPA and initial tsECPA experiments. In the case of frequency optimization (Figure 2.10A), the signal was increasing as frequency increased, and it reached a maximum at 75 Hz, above which the signal decreased. The increase from 40 to 75 Hz can be attributed to the typical SWV response for surface-confined redox reporters ([84]). The decrease toward zero current at frequencies greater than 75 Hz is likely a result of the in-line RC filter smoothing the input voltage pulses, which will be discussed later. The pulse-height dependence in (Figure 2.10B) shows that signal can be increased with pulse heights up to 90 mV, which gives a nearly 40% improvement in current compared to our previous work (50 mV).

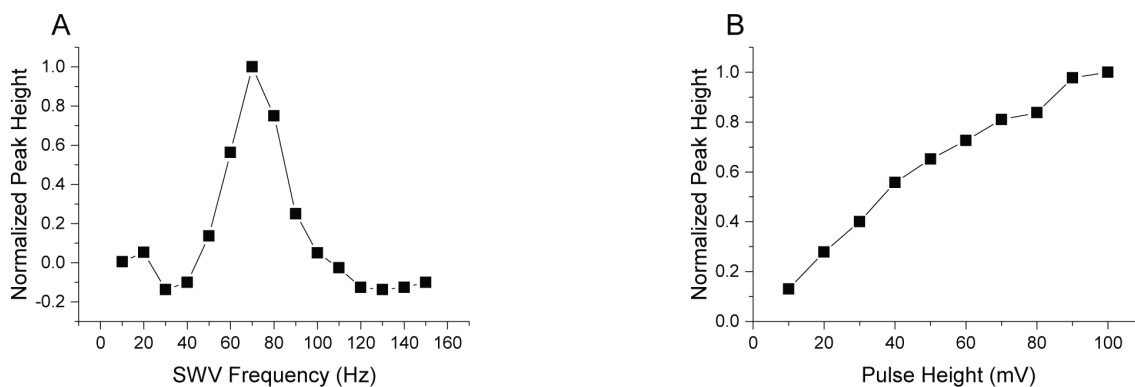


Figure 2.10: **Optimization of SWV frequency and peak height:** A) shows the frequency response; B) Pulse height response.

2.4.2 Quantification of Leptin by ECPA

ECPA is a generalizable assay; if a target molecule has two capturing probes like aptamers or antibodies that bind to two distinct epitopes, it should be quantifiable using ECPA. Earlier research work from our group proved the system functional with thrombin and insulin, each of which have two aptamers or antibodies, respectively. Here, preliminary experiments show that ECPA is also responsive to leptin, a hormone synthesized in adipose tissue which helps in energy regulation and is sometimes referred to as the hunger hormone. Figure 2.11A shows the baseline corrected SWV output of leptin ECPA. A clear increase in signal with concentration was observed, with 125 pM as lowest measured concentration. Figure 2.11B shows the calibration curve of leptin ECPA, in which integrated signal is plotted against the concentration of leptin. The integrated signal has a non-linear response to the concentration, as expected. This result shows an additional application of ECPA, although additional experiments and optimization should be done to determine the LOD and apply to hormone secretion from fat cells.

2.4.3 Probe density

DNA probe density on the surface of the electrode plays a crucial role in electrochemical DNA based sensors [66]. The kinetics of DNA hybridization, protein, and small molecule binding to a DNA/aptamer on the surface of the electrode depends on probe density [85]. Lower probe density can result in lower signal due to lack of capture probes, and larger probe density can

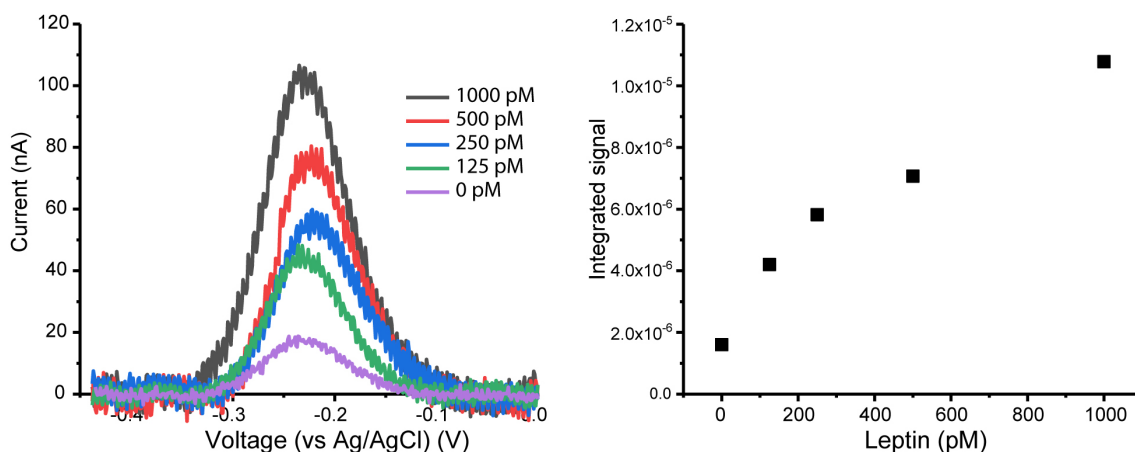


Figure 2.11: **Leptin ECPA**: A) SWV output (baseline corrected) of the different concentration of leptin; B) Calibration curve of leptin

result in steric hindrance [73]. Plaxco, et al. compared their cocaine and thrombin aptamer sensors and the effect of the changing thiolated-DNA concentration, which resulted in differences in capture probe packing density. In addition, they conducted a kinetic study in both these cases, concluded that lower packing density is optimal for cocaine, while for thrombin the intermediate density is preferred [66]. Thus, it can be concluded that optimizing probe density is an essential step in improving assay performance. From the plot of integrated signal versus concentration of thio-DNA (Figure 2.12), we observed an optimal thio-DNA concentration of 1.25 μ M for ECPA electrode preparation.

2.4.4 Insulin quantification in murine serum with reusable ECPA

To verify the suitability of reusable ECPA for clinical measurements, insulin was initially quantified in murine serum using standard addition methodology. Murine serum samples were collected in house, diluted 20-fold, and used as the sample for insulin quantification by reusable ECPA. The samples were kept on ice during the entirety of the experiment to prevent probe degradation from DNases. By using the standard addition method, insulin concentrations were back-calculated as 120 and 140 pM for two different samples, which fell within previously published insulin serum values $113.8 \text{ pM} \pm 31.2 \text{ pM}$. These results show that ECPA is a promising approach for selective insulin quantification in serum, which could be useful for adapting to

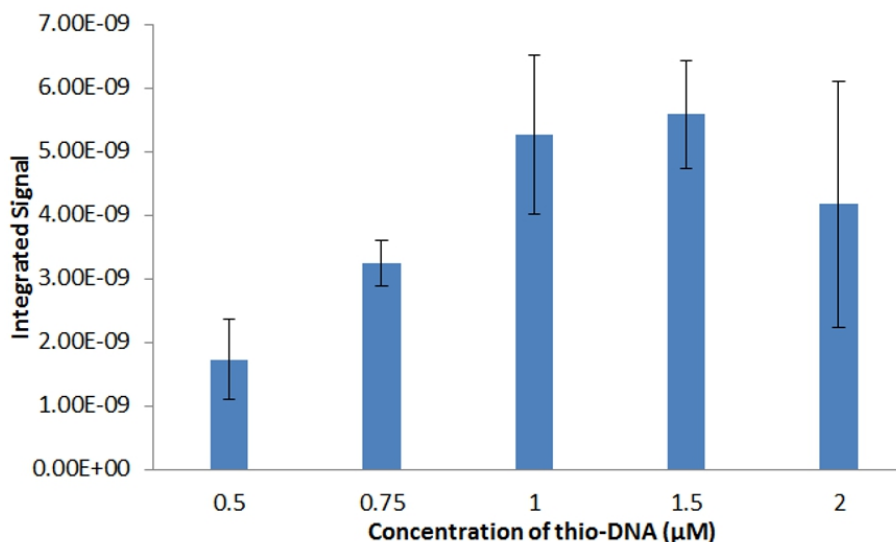


Figure 2.12: **Optimal probe density of thiolated DNA:** As concentration of thiolated DNA increases initially there is an increase in signal followed by decreasing; 1 μM and 1.5 μM have similar signal making as to concluded 1.25 μM as optimal concentration.

diabetic blood monitoring devices such as glucose meters or insulin pumps.

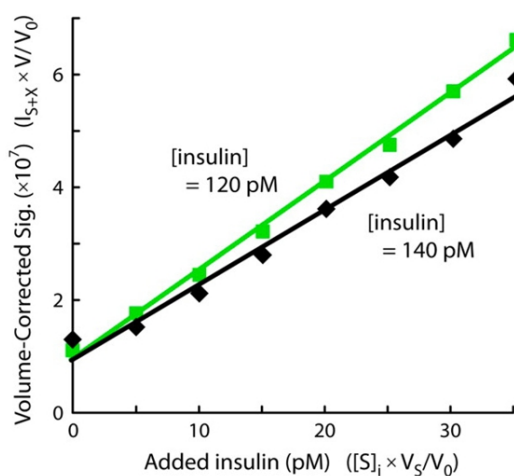


Figure 2.13: **ECPA standard addition measurement in murine serum** Insulin quantification in unspiked serum from two different C57Bl/6 mice was accomplished [36].

Reprinted with permission Copyright ©(2014) American Chemical Society

2.4.5 tsECPA for insulin measurement in undiluted human serum without spiking

Proximity assays were explained in Chapter 1, where the stability of DNA hybridization is increased by the proximity effect in the presence of target molecules. The stability of the DNA

hybridized complex can also be viewed from the perspective of DNA melting. If the DNA hybridization is stronger, additional energy is needed to melt or dissociate the complex, meaning that the target-containing complex should have a higher melting temperature (T_m). If so, when the temperature is increased, the background complex would melt first, followed by the signal complex. To test this hypothesis, we designed a thermal scanning electrochemical cell using Peltier heating/cooling (shown in Figure 2.8). SWV current was measured as the temperature was slowly scanned from 15 °C to 35 °C. In the derivative plots ($-dS/dT$), as predicted, the background and signal melting was clearly distinguished by two separate peaks. Figure 2.14 A shows the measurement of standard insulin solutions of 0, 0.1, and 10 nM concentrations. The 0 nM data only showed the background melting peak at 23 °C, but in the case of 0.1 and 10 nM, the signal melting peak was observed at higher temperature. Moreover, the peak area of the signal melting peak depended on the concentration of the target, which is obvious in comparing the 10 and 0.1 nM data sets.

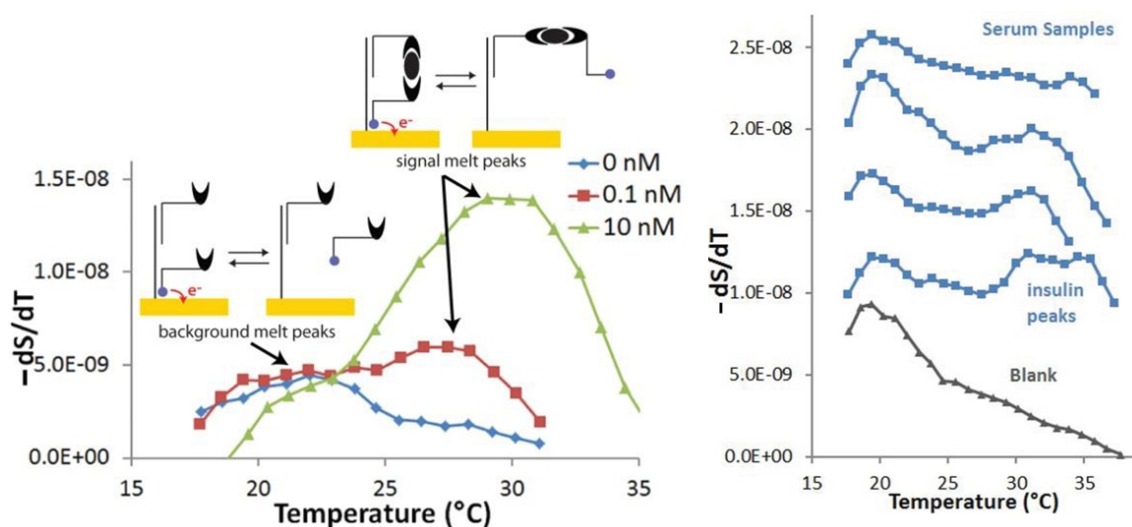


Figure 2.14: Thermal Scanning ECPA of insulin sample and undiluted human serum: A) background and two concentration of insulin differential curves are plotted against temperature, at higher temperature in presence of insulin there is an obvious peak proportional to the concentration of insulin. B) Blank and four different undiluted, unspiked human insulin samples are plotted, all sample shows the peak at higher temperature which prove the stability of the method in serum sample.

To evaluate the capability of tsECPA to measure insulin in serum samples, the method was then applied to undiluted human serum, this time with no spiking of standard insulin. Figure

2.14B shows the derivative curve of four different samples. The signal peak at higher temperature was observed in all four samples, and the peak area as similar to the 0.1 nM curve in the standard insulin measurement. This shows that there is no loss of sensitivity of the method in biological matrix, which is not the case of many DNA driven assay. Not only is the pretreatment step removed, due the sensitivity of the assay the standard addition is also elimination. These add benefic by reduction of the sample volume needed.

In case of many DNA driven assay, the measurement of the target in raw serum is challenging due to the background noise and instability by DNAase. So, the sample should be pretreated, which may result in erroneous quantification due to loss of target. In addition to that pretreatment of samples hinders the methodology form being POC. The above result support that ECPA can be a POC method.

2.4.6 Refined instrument parameters for SWV

As mentioned earlier, in a SWV cycle, the potential is pulsed very fast, and the current measurement is made after a specified time delay (which is decided by the frequency used). This is accomplished during forward and reverse voltage pulses. In one SWV run, hundreds of pulse cycles are done at a fast pace (~500 cycles in a typical experiment here). Needless to say, the potential should be very precisely controlled to accomplish SWV, and commercially available potentiostat designs have provided researchers with exquisite control over voltage to do so. In addition, companies often provide a dummy cell with the potentiostat, which helps in calibrating and cross-checking of the instrument by users.

In case of ECPA or any other measurement leveraging a self-assembled monolayer, we show here that properties of the monolayer can, in fact, influence the input voltages from the potentiostat, especially in case of SWV. As such, users should always be aware of the effects of varying each instrumental parameter for their particular measurement system. Figure 2.15 shows an outline of the circuit model for the Gamry Reference 600 potentiostat used in our

work. With this instrument, other than the obvious SWV parameters (pulse height, frequency, voltage range), there are three other important parameters that must be carefully evaluated. The parameters termed CA speed, Max current (R_m), and IE stability can influence the potentiostats function during SWV. The CA speed parameter defines a capacitor across the counter electrode. The R_m value defines a resistor in the working electrode circuit through which current is measured by operational amplifiers. The IE stability parameter defines a capacitor parallel to R_m .

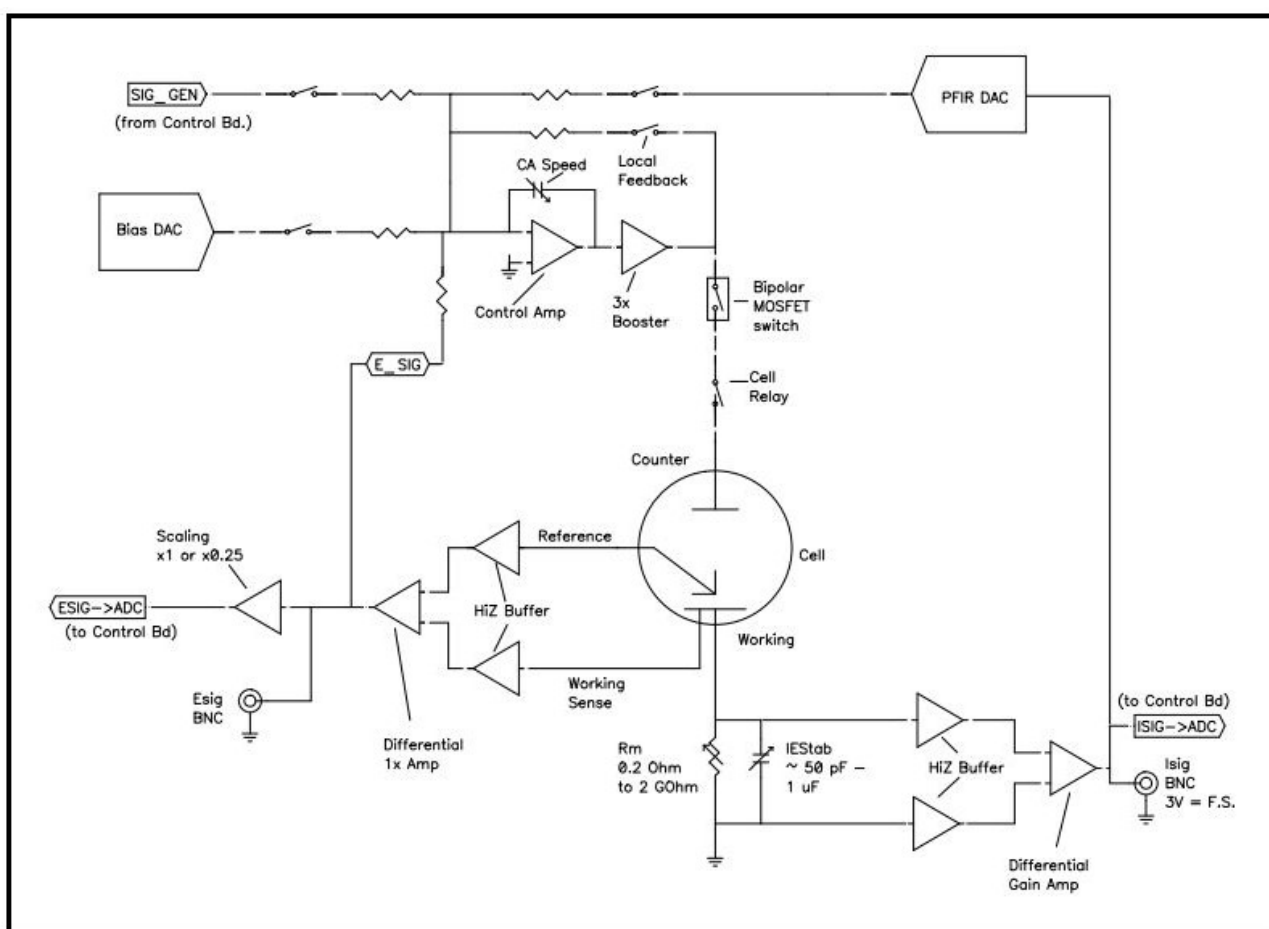


Figure 2.15: *Circuit of Reference 600 instrument*

In the Gamry Reference 600, the R_m value (despite the name) actually defines the maximum measurable current, with units of mA. Since the analog-to-digital converter (ADC) has fixed resolution (16 bits), lowering the maximum current with this parameter will effectively increase the sensitivity of the system such that smaller changes in current can be resolved.

While changes in this setting should not affect the magnitude of Faradaic current measured in a particular system, we noticed inconsistencies when operating under default settings in the instrument. Under the default settings, SWV measurements of MB-DNA bound to thiolated DNA (G10) showed drastic signal changes upon changing the maximum current, which is shown in Figure 2.16. Furthermore, the SWV frequency response was observed to be different; with a 0.001 mA range, 75 Hz showed the highest current, yet under the 0.0001 mA range, 50 Hz showed the highest current response. Clearly, these instrumental settings were creating artifacts in SWV current responses of our surface-confined DNA systems. These artifacts were not observed when using cyclic voltammetry or for SWV across a resistor (dummy cell), which proves that the instrument was functioning correctly. Presumably, these issues were specific to our particular assay system, and further experiments were conducted to determine the source(s) of these errors.

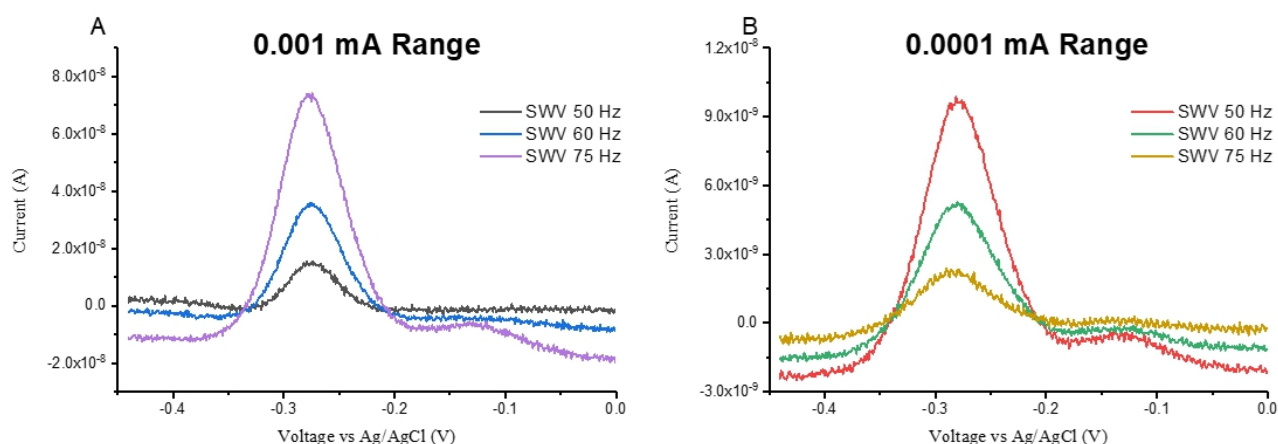


Figure 2.16: Resolution change in potentiostat: Changing the potentiostat resolution should not change the signal, but we observe a drastic change not only in the signal but also on the frequency response. A) The SWV output of 50, 60, and 75 Hz at 0.001 mA range B) Same experiments on A) done with higher resolution 0.0001 mA.

For any analytical system, it is crucial to ensure that software-programmed values are effectively translated into the instrument and the experiment. During an extensive evaluation of the SWV system, we checked whether the input potential and the actual measured potential correlated under default settings. Fortunately, the Gamry Reference 600 provides a readout of

V_{fr} and V_{re} , voltages which the potentiostat is tasked to maintain while the SWV current measurements are made. Here, the difference of $V_{fr}-V_{re}$ was calculated manually to find the pulse height, and this result is plotted against the V_{step} . Figure 2.17A shows the pulse height at different frequencies (5 Hz–125 Hz). Shockingly, the potentiostat-controlled pulse height did not match with the input parameter (50 mV), and there was a drastic change in the pulse height with SWV frequency. In addition to this problem or perhaps one consequence of this problem we observed a shift in pulse height at the redox signaling region for methylene blue (observed only when MB-DNA was present). There was clearly an instability in the potentiostat-controlled potential when SWV measurements were done in the presence of the DNA monolayer under the default SWV settings of the instrument. Figure 2.17B shows the pulse height artifact observed at various frequencies, where the potentiostat was functioning correctly (holding at 50 mV) through 25 Hz but erroneously between 30 and 150 Hz. It is also important to note that this increasing pulse height results in an increase of both faradaic and capacitance currents (see Figure 2.17A), such that our previous interpretation of optimal frequency at 75 Hz (see Figure 2.10A) was likely an artifact of these instrumental settings.

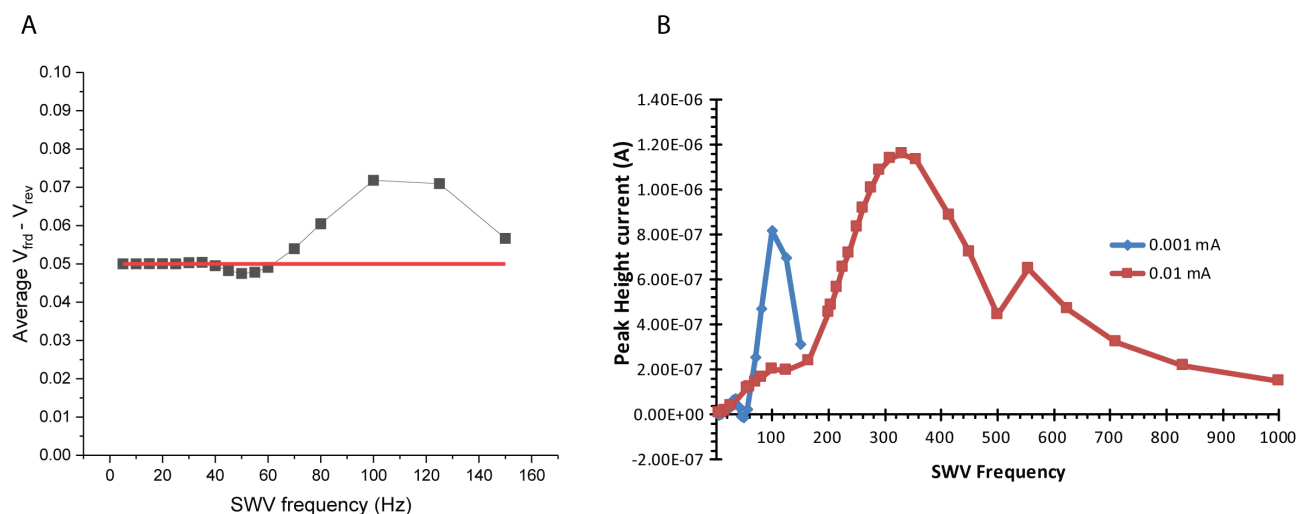


Figure 2.17: **Applied pulse height and frequency:** Pulse height is seen to vary with the frequency, A) On plotting Average $V_{fr}-V_{re}$ vs SWV Hz we can see the peak height is not similar to input, its changing with frequency, and it looks similar to the optimal frequency study in Figure: 2.10 B) Peak height change due to the resolution change is shown.

We hypothesized that the increased capacitance current from the highly charged DNA monolayers was incompatible with the potentiostats default circuit capacitances in SWV mode. Thus, we altered the CA speed and IE stability capacitor values. These capacitors normally help in reducing the environmental noise, such that larger capacitors are preferred and used in default settings for analysis of simpler systems. From our results above, we conclude that SWV measurements for more intricate systems like DNA monolayers obviously should be done using lower capacitor values. Indeed, we observed the potentiostat to function as expected under the fastest CA speed and IE stability settings. The G10 DNA baseline (in the absence of MB-DNA) and its hybridization with MB-DNA (signal) was measured with different pulse heights using SWV frequencies between 20 and 200 Hz. The pulse height was plotted against peak height, as shown in Figure 2.18A. Later we confirmed that the peak height or signal did not change upon varying the measurement range (R_m), as shown in Figure 2.18B. The lesson learned from these results is that SWV experiments with DNA monolayers using the Gamry Reference 600 potentiostat should be done with advanced settings, not under default SWV settings. Obviously, the companys goal was to make a user friendly instrument and to remove interfering and environmental noise effectively. However, with exploratory research, it is of utter importance to be mindful of advanced settings and their impacts on measurements. All the following experiments were done with these new advanced settings.

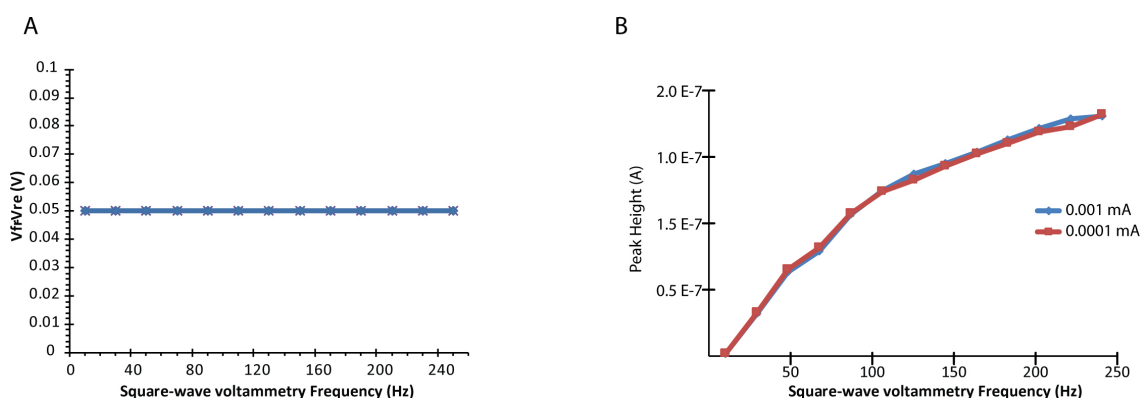


Figure 2.18: **Peak height and resolution after fixing the instrument:** A) Average $V_{fr} - V_{re}$ vs SWV Hz shows the input and output are same; B) there is no change in peak height due to resolution change.

2.4.7 tsECPA of insulin with modified parameters

The new settings with optimized instrumental RC constants were applied to thermal scanning ECPA (tsECPA). In these experiments, tsECPA was done using a gold electrode of 2 mm x 1 mm dimensions, made on microscopic slides sputtered on glass (GoG, gold on glass). The benefit of using GoG is that the glass is placed on the Peltier temperature controller, which allows thermal equilibrium of the electrode to be reached faster and facilitates more efficient scanning for tsECPA. Figure 2.19 shows the SWV response at 100 Hz for four different concentrations of insulin, scanned from 15 to 70 °C.

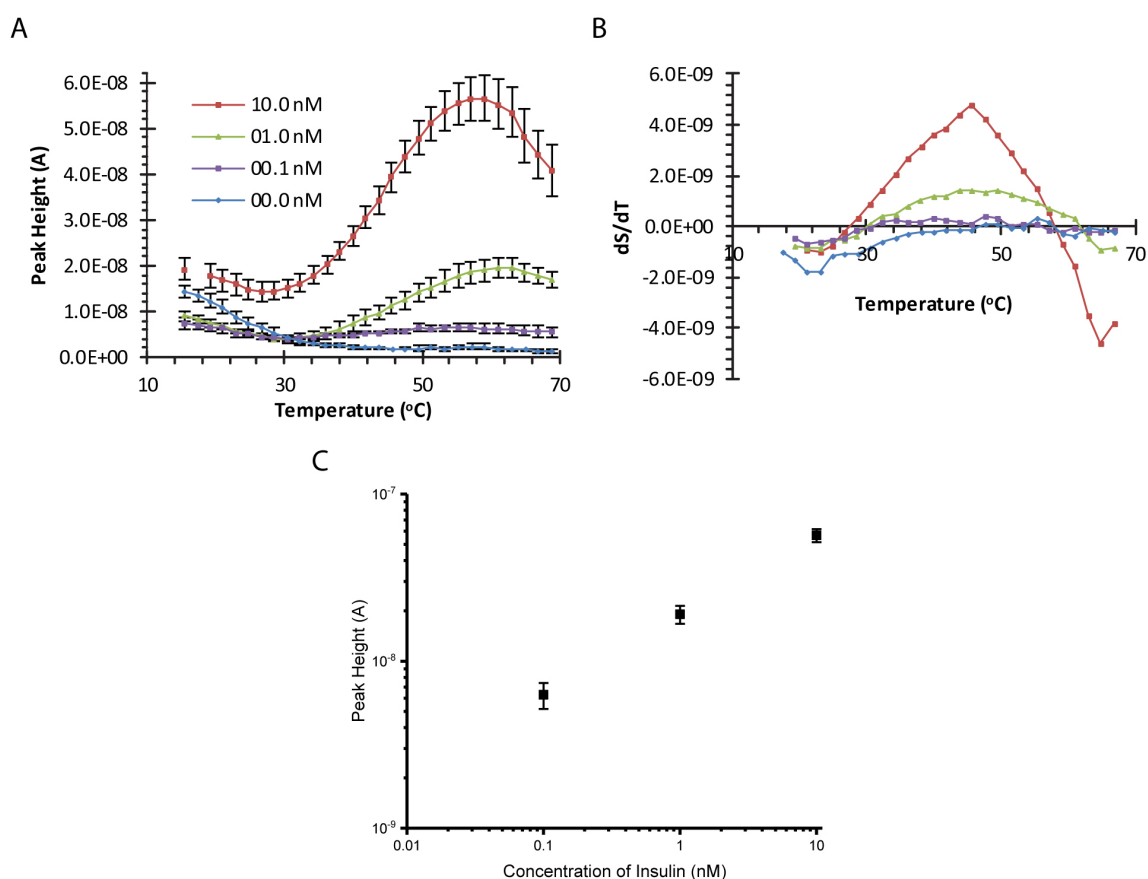


Figure 2.19: Thermal scanning ECPA with new setup: (A) Peak height is plotted against the temperature, initially there is decrease in signal at lower temperature which is considered due to background melting, later there is increase in signal proportional to the concentration of the standard insulin used. (B) the derivative curve of the tsECPA is shown; (C) Calibration of insulin in tsECPA: The Peak height at 56 °C is plotted against the concentration of the insulin in a log-log plot. This proves that tsECPA can be used for quantification of insulin.

As the temperature was increased from 15 °C, a gradual decrease in peak height was observed through 70 °C for the 0 nM control and through 30 °C for insulin samples. The rate of increase after 30 °C was proportional to the concentration of insulin. Between 55 and 60 °C the signal reached the highest point (except for 0 nM) then decreased at higher temperatures. The initial drop in the signal is likely due to background complexes melting, while the later increase in signal is likely due to the temperature enhancement of electrochemical reaction rate. This effect is explained in further detail in Chapters 3, 4, and 5. The error bars in Figure 2.19 represent the standard deviation of measurements on 4 separate electrodes. In Figure 2.19C, the peak height at 56 °C was extracted and plotted against the log of concentration of insulin, showing a proportional response.

This result shows multiple positive signs: 1) tsECPA has improved sensitivity compared to ECPA (comparing peak height to our previous work); 2) by the help of temperature controller the discrepancy between the electrodes are minimized (we can observe slight change in the temperature result in signal change); 3) it also helps in improving signal to background ratio by melting the background complex; 4) in DNA-based electrochemical assay temperature can be used as an amplification factor.

2.4.8 Surface confined ECPA

Our proposed surface confined ECPA (scECPA) is a model system for real time measurement of protein, especially in the study of hormones secreted by tissues. The schematic was shown in Figure 2.9. In this case, both the antibodies were intentionally bound to the surface, with AB2 and methylene blue designed to be distant from each other on average, making the electrochemical signal lower. In theory, the introduction of insulin pulls the AB2-MB-DNA complex closer to the surface, resulting in the binding of thio-DNA and MB-DNA due to the proximity effect. Our hypothesis was that the rate of increase in the signal should be proportional to the concentration of the insulin introduced or flowing over the electrode. By derivation, the insulin

secretion could be effectively studied at higher temporal resolution.

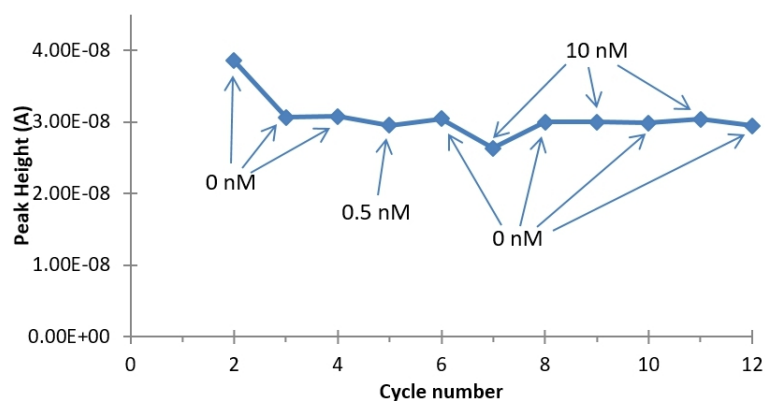


Figure 2.20: scECPA signal output: Cycles of scECPA shows that there is no signal change by insulin.

Figure 2.20 shows the response of the scECPA system, where each cycle represent 20 minutes of incubation time in the sample. Sample concentration is noted through arrows. The response was not as expected, and there was no signal change observed as a function of concentration. At the same time, we observed a significant background current. We believe this is due to two reasons: 1) in the absence of insulin, the methylene blue is not far enough away from the surface, which results in an unwanted proximity effect due to the surface of electrode, and 2) antibodies and MB-DNA are attached to the surface by DNA hybridization, even though it is stronger, it is in equilibrium so any change in buffer results in shifting the equilibrium which may have a false positive effect on the output. Considering these drawbacks and also the improved knowledge in electrochemical signal in the DNA self-assembly platform in Chapter 5, we did not further evaluate the scECPA platform.

2.5 Conclusion

ECPA, a potential POC method, is explained in this chapter and completed studies that can support the versatility of the method. Leptin is shown to have a good response in ECPA, with the sample volume of 20 μ L. Measurement in undiluted human serum without spiking is done, this eliminates the pretreatment of sample in clinical diagnostic, which supports its application for POC. tsECPA results gives as a better understanding in surface confined DNA-driven assay,

which helps in increasing the sensitivity by increase in signal to noise ration. Most importantly, the importance of instrumentation and the effect of DNA-monolayer in the feedback control of the potentiostat is explained.

Chapter 3

Diffusion layer and Double layer in Electrochemical DNA Assays

3.1 Introduction

This chapter focuses on work done in our laboratory to improve our understanding of the distance dependence of square-wave voltammetry (SWV) current from a redox moiety on DNA during its hybridization on the surface of an electrode. Huang and White [86] explained the electrochemical kinetic change by the distance of a surface-tethered redox moiety and developed a random walk mathematical model which was corroborated with cyclic-voltammetric (CV) experimental results. This random-walk model views the surface confined redox moiety as being locked into an imaginary hemisphere, which is shown in the Figure 3.1. The authors altered the length of the tether (5–20 nm) then simulated and measured current at various scan rates. They showed that the electrochemical diffusion layer thickness and the length of the tethered linker play crucial roles in the electron transfer rate of the redox molecule. The general rule is that the redox molecule acts as an adsorbed species until the diffusion layer thickness (Diffusion layer = $(2Dt)^{1/2}$) is approximately 10 times the length of the tether linker. This study showed that SWV frequency is an important parameter in our studies, since the frequency determines the scan rate of the experiment. Similarly, we know that SWV is not a continuous measurement. The Plaxco group [49], in their earlier work with SWV, compared many E-DNA and E-apramer sensors and showed that Signal-OFF sensors can sometimes be changed into Signal-ON sensors by changing the SWV frequency. Generally, an understanding of the frequency response of the sensing complex helps in developing and optimizing any DNA-driven electrochemical sensor.

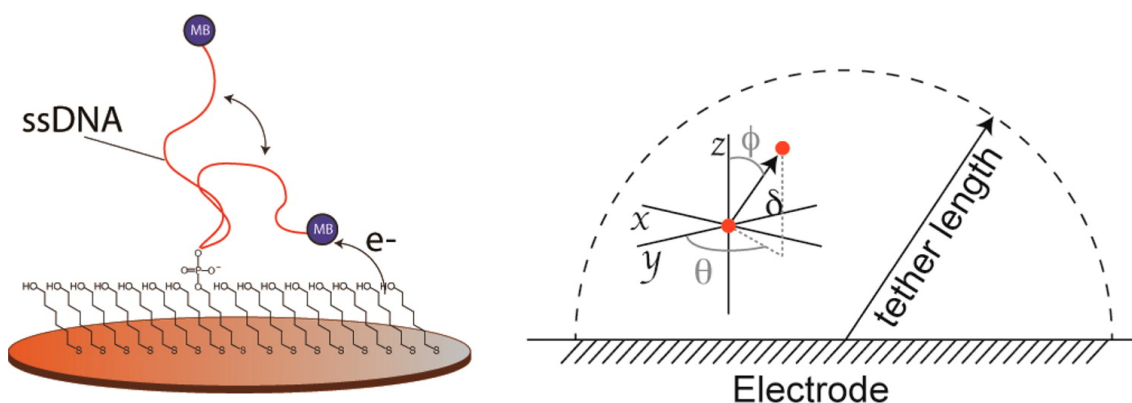


Figure 3.1: Random walk model: Methylene blue tagged to the DNA acts as a tether molecule, with the length of the DNA being the radius of the hemispherical region which is the diffusional region of methylene blue [86]

Reprinted with permission Copyright ©(2013) American Chemical Society.

Like ECPA (see Chapter 2), many DNA-driven electrochemical assays involve DNA hybridization on the electrode surface [44,55,73,76,79–81]. The kinetics and thermodynamics of surface DNA hybridization is different from that of the solution-phase [87], because it involves diffusion of one or more of the reactants to the surface, while another reactant on the surface is highly dense and essentially multivalent. In addition to this, the abundance of surface charges would likely have an effect on hybridization of the DNA due to its negative charge [88]. Understanding the hybridization kinetics is essential for optimizing the sensitivity of such sensors, especially for sensors with lower hybridization energies (≤ 10 bp) as in the case of ECPA [35,36].

The first part of this chapter focuses on a distance-dependent sensing. Our hypothesis is that as the redox moiety is placed far away with respect to the surface of the electrode, there will be a drop in the signal in higher frequency but an increase in lower frequency. The second part of this chapter on the hybridization kinetics in such sensors and the contributions of hybridization location with respect to the electrode surface. Our hypothesis on this part is that the double layer of the surface hinders the hybridization very close to the surface. To validate our hypothesis, we altered the double layer by changing the concentration of the salt and studied the hybridization kinetics. Toehold-mediated DNA strand displacement on the surface is also studied for further support. Overall, the studies in this chapter shed additional light on the

importance of the electrochemical diffusion layer and the ionic double layer in electrochemical assays leveraging DNA hybridization.

3.2 Regent and materials

All solutions were prepared with deionized, ultra-filtered water (Fisher Scientific). The following reagents were used as received: 4-(2-hydroxyethyl)-1-piperazineethanesulfonic acid (HEPES) and sodium perchlorate (NaClO₄) from Alfa Aesar, tris-(2-carboxyethyl) phosphine hydrochloride (TCEP) from Sigma-Aldrich (St.Louis, MO). Methylene blue-conjugated DNA (MB-DNA) was purchased from Biosearch Technologies(Novato, CA), purified by RP-HPLC. All other oligonucleotides were obtained from Integrated DNA Technologies (IDT; Coralville, IA).

Table: 3.2 gives the sequences of all the DNA used in this chapter.

Sequence Name	Abbreviation	DNA Sequence listed 5'-3'
0A-Thiolated DNA	0A	/5ThioMC6-D/GCA TGG TGA CAT TTT TCG TTC GTT AGG GTT CAA ATC CGC G
1A-Thiolated DNA	1A	/5ThioMC6-D/AGC ATG GTG ACA TTT TTC GTT CGT TAG GGT TCA AAT CCG C
2A-Thiolated DNA	2A	/5ThioMC6-D/AAG CAT GGT GAC ATT TTT CGT TCG TTA GGG TTC AAA TCC G
3A-Thiolated DNA	3A	/5ThioMC6-D/AAA GCA TGG TGA CAT TTT TCG TTC GTT AGG GTT CAA ATC C
4A-Thiolated DNA	4A	/5ThioMC6-D/AAA AGC ATG GTG ACA TTT TTC GTT CGT TAG GGT TCA AAT C
5A-Thiolated DNA	5A	/5ThioMC6-D/AAA AAG CAT GGT GAC ATT TTT CGT TCG TTA GGG TTC AAA T
6A-Thiolated DNA	6A	/5ThioMC6-D/AAA AAA GCA TGG TGA CAT TTT TCG TTC GTT AGG GTT CAA A

7A-Thiolated DNA	7A	/5ThioMC6-D/ AAA AAA AGC ATG GTG ACA TTT TTC GTT CGT TAG GGT TCA A
9A-Thiolated DNA	9A	/5ThioMC6-D/ AAA AAA AAA GCA TGG TGA CAT TTT TCG TTC GTT AGG GTT C
11A-Thiolated DNA	11A	/5ThioMC6-D/ AAA AAA AAA AAG CAT GGT GAC ATT TTT CGT TCG TTA GGG T
14A-Thiolated DNA	14A	/5ThioMC6-D/ AAA AAA AAA AAA AAG CAT GGT GAC ATT TTT CGT TCG TTA G
19A-Thiolated DNA	19A	/5ThioMC6-D/ AAA AAA AAA AAA AAA AAA AGC ATG GTG ACA TTT TTC GTT C
MB-10bp DNA	MB10	CCA CCC TCC TCC TTT TCC TAT CTC TCC CTC GUC ACC AUG C/ MB-C7/
MB-40bp DNA	MB40	CGC GGA TTT GAA CCC TAA CGA ACG AAA AAT GTC ACC ATG C/ MB-C7/
Competitor- 33 bp- upper	C-33U	CGC GGA TTT GAA CCC TAA CGA ACG AAA AAT GTC
Competitor- 33 bp- lower	C-33L	TTG AAC CCT AAC GAA CGA AAA ATG TCA CCA TGC

Table 3.1: DNA sequence used for Distance dependence and salt concentration study
/5ThioMC6-D/ = Dithiol attachment (IDT), **/MB-C7/**= Methylene Blue (Biosearch)

3.3 Experimental methods

3.3.1 Electrode preparation and DNA SAM

The electrodes were cleaned mechanically and electrochemically followed by formation of the DNA SAM and filling the unreacted regions with filler mercaptohexanol molecule as explained in Section 2.3.1. All electrochemical measurements were performed using a Gamry

Reference 600 electrochemistry workstation with a standard three-electrode system, composed of Ag/AgCl (3 M KCl) reference electrode (BASi), platinum wire (CH instruments) as the counter electrode, and 2-mm diameter disk gold electrode (CH instruments). Table: 3.2 shows the SWV parameters used.

Parameter Name	Symbol	Values Used
Initial voltage	V_i	-0.45 V
Final voltage	V_f	0.00 V
Step size	E_s	1 mV
Pulse height	E_p	50 mV
Frequency	SWV-Hz	1 to 1000 Hz

Table 3.2: SWV parameters for diffusion and double layer study

3.3.2 Distance of methylene blue redox moiety

One aim was to elucidate the effect of distance on electrochemical signal. Twelve different thiolated DNA were used (0A, 1A, 2A, 3A, 4A, 5A, 6A, 7A, 9A, 11A, 14A, and 19A). The distances are represented in units of nucleotides (adenine to be specific), since DNA synthesis was used to control the length. Once the electrodes were ready, they were each incubated in 500 μ L of 100 nM MB10 DNA in 10 mM HEPES and 0.5 M NaClO₄ buffer overnight (16 hrs). After incubation, the SWV measurement was done in the same solution using nineteen different SWV frequencies between 1 Hz and 1000 Hz.

3.3.3 Electrochemical kinetics calculation

To find the critical reaction time, we followed the procedure explained by Lovric et.al [89]. Briefly, the peak height was divided by the SWV frequency (i_p/f_{SWV}) and normalized to the highest values of this set and plotted against $1/f_{SWV}$. The time which corresponds to the peak point of this data defined the critical electrochemical reaction time. If the value was lower, it

shows the electrochemical rate was faster.

3.3.4 Hybridization kinetics on the electrode surface

Thiolated DNAs 0A, 1A, 2A, 3A, 4A, 5A, 6A, and 7A were used for this study. Once the electrode was ready to use, 500 μL of 100 nM MB10 DNA in HEPES buffer was introduced into the electrochemical cell. The reference and counter electrodes were immersed, and SWV at 100 Hz was very quickly measured as soon as the working electrode was introduced into the solution for the zero time measurement. Following this, SWV was done every 5 minutes for 125 minutes.

3.3.5 DNA Strand displacement on surface

To study the effects of surface double layer on DNA hybridization kinetics, a toehold-mediated DNA strand displacement reaction was measured in cases where the distance of the strand displacement event (toehold location) from the electrode was varied. 4A and 0A thio-DNA was used with the MB40 signaling strand in the presence of C-33U (upper toehold) and C-33L (lower toehold). Once the electrode was ready with the SAM of DNA, it was incubated in 300 μL of HEPES/ NaClO_4 containing 500 nM of either C-33U or C-33L for 24 hours at room temperature. Later, the electrodes were rinsed to remove excess physically adsorbed competitor on the sensor surface and introduced into the electrochemical cell containing 500 μL of HEPES/ NaClO_4 buffer with 100 nM MB40 DNA. The hybridization kinetics study was done as explained above.

3.4 Result and discussion

3.4.1 Understanding SWV signal from measuring layer perspective

SWV is one of the pulse voltammetry techniques which was developed for effective reduction of capacitance current in measurement. So, the high signal-to-noise ratio that is achieved

helps in increasing the sensitivity of the measurement. In electrochemical DNA and aptamer sensors, SWV is used to distinguish the DNA bound to target from unbound DNA. In other words, signal is differentiated from background, in which both signal and background have the same redox moiety. Others have shown that the electron transfer rate is changed due to target binding [49], which results in either gain or loss of signal proportional to the concentration of target. In this work, we controlled the distance between the electrode surface and the redox moiety and explained the electrochemical reaction rate from the perspective of the measuring layer.

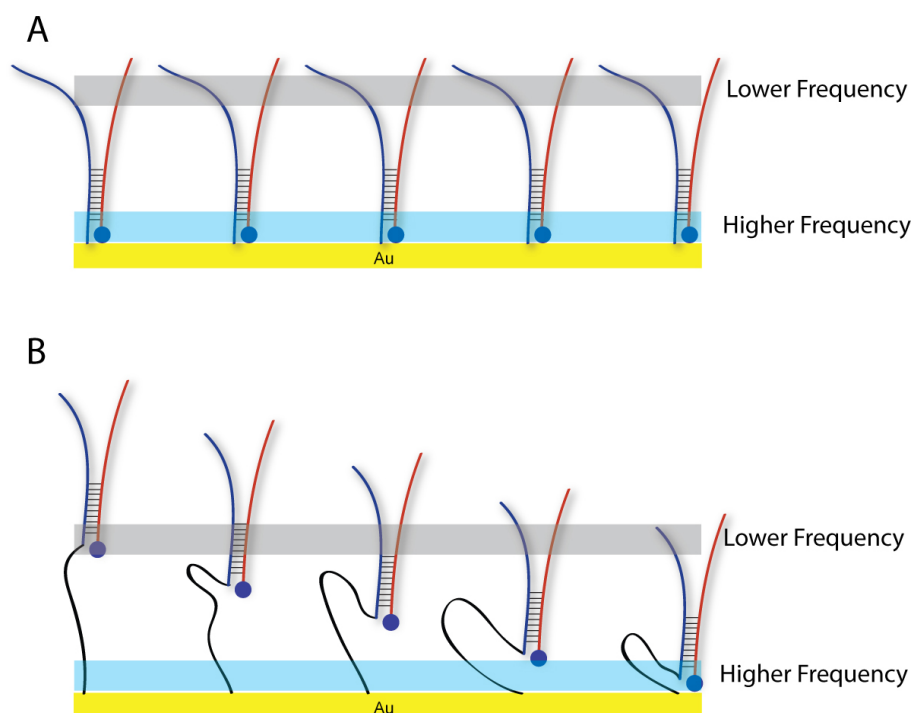


Figure 3.2: SWV signal from measuring distance perspective If the MB is attached closer to the surface the signal at lower frequency is very low due to the absence of MB in that range. In case of MB with long tether the possibility of the MB present at lower frequency range is feasible. This also show why signal is lower at higher frequency in long tethered MB.

Twelve different 40-nucleotide thiolated-DNAs were used in this work, and the same concentration and protocols were used. Due to same length and concentration of thiolated-DNA, similar probe density should be achieved. In all experiments MB10 methylene blue DNA was used, which binds with the thiolated DNAs via 10 base pairs. Since hybridization energy is same, the concentration of MB-DNA hybridized on the surface should be about the same in all

cases, but the distance between the methylene blue redox moiety and the electrode surface was varied. Figure 3.2 shows a simple representation of the measuring distance model. The gray and blue regions show where lower and higher SWV frequencies measure, respectively. Figure 3.2A shows the scenario of MB-DNA hybridized closer to the surface. We can observe that there are no molecules available in the lower frequency region, since at low SWV frequency these molecules have already participated in electron transfer with the electrode prior to current readout. On the contrary, when MB-DNA is hybridized far away from the surface, due to the flexibility of the DNA, the methylene blue diffusion range is extended, and some molecules are still available for electron transfer at the later measurement time (low frequency). This results in lower SWV frequency having measurable signal, as shown in Figure 3.2B. Since the concentration of methylene blue is same in both the case, we are expecting the signal to change as mentioned earlier. This measuring layer depends on the diffusion of the molecule, so in this experiment the final complex molecular weights are similar, and measurement is done at uniform temperature (25°C). The effect of changes in temperature and molecular weight are explained in Chapters 4 and 5, respectively.

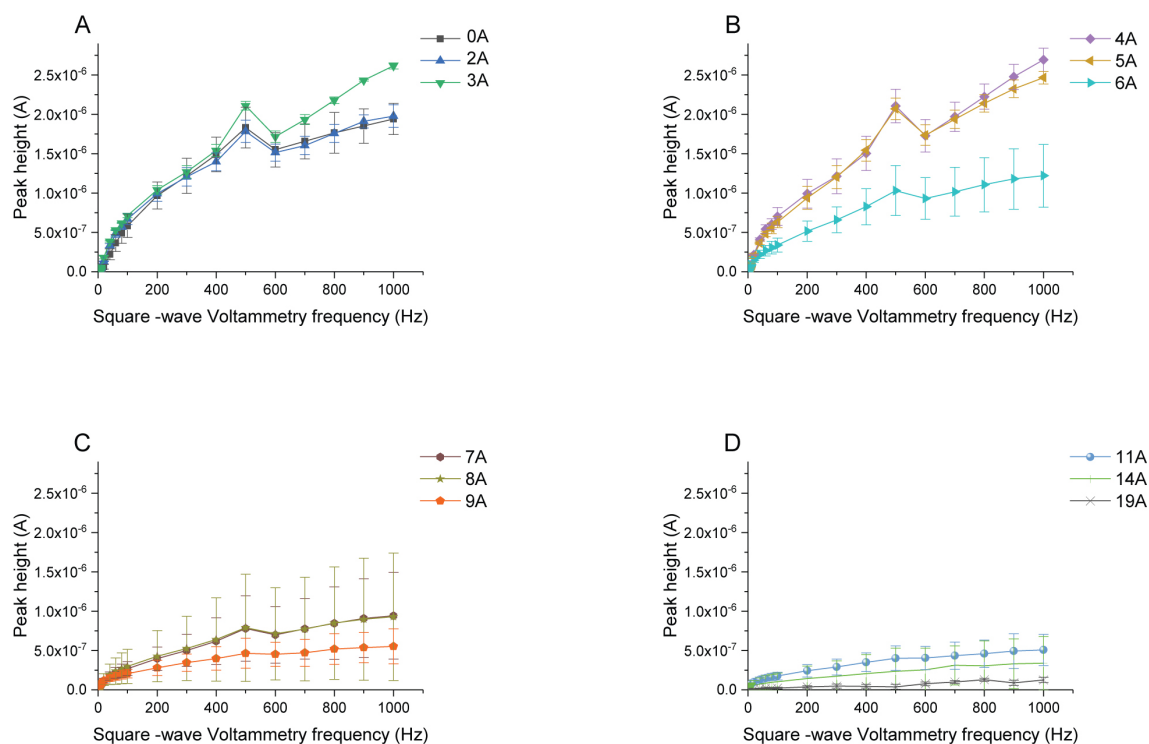


Figure 3.3: Peak height change due to distance of redox moiety: From 0A to 4A the signal is observed to increase shown in A and B, later as distance increases there is a drastic drop in the peak height current in higher frequency.

Figure 3.3 shows the graph of peak height plotted against SWV frequency. Surprisingly, the peak height for higher frequencies increased somewhat as we moved the methylene blue from the surface until the 4A length, which is shown in Figure: 3.3A and B. Later, as we expected, the peak height decreased as we moved the MB further away from the surface, shown in Figure: 3.3 B,C, and D. An excerpt of some thiolated DNA peak heights for small SWV frequencies (1-10 Hz) are shown in Figure: 3.4, and this

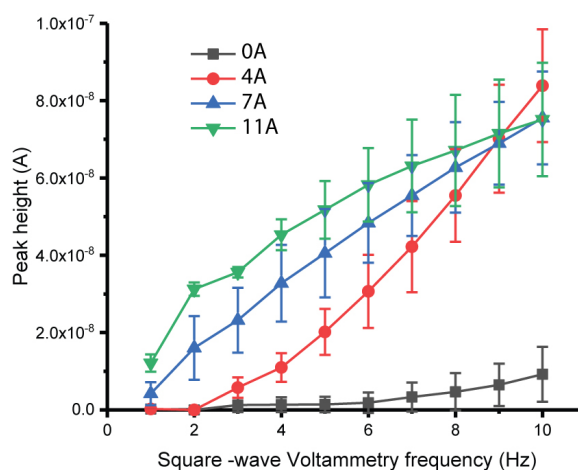


Figure 3.4: Peak height shift at lower frequencies: At lower frequency there is an increase in signal as the redox moiety is moved away from the surface, which is shown in the picture by comparing peak height of 1-10 Hz for four different distance.

shows an increase in peak height with the distance, in agreement with our hypothesis. This signal change due to the distance is conventionally explained as the change in electrochemical kinetics. So, with these data points we calculated the critical frequency by following the method by Lovric et al [89], which could give more insight into the unexpected increase in the signal at higher frequencies from 0A to 4A.

3.4.2 Electrochemical rate change due to distance

From the above experiment the i_p/f_{SWV} was calculated, normalized, and plotted against the $1/f_{SWV}$. In this graph the time at which the highest point corresponds is its critical reaction time. On comparing two different experiments on this graph, the experiment or setup with lower time has the faster kinetics. So, the experiment or setup with faster kinetics have higher peak current in higher SWV frequency measurements and lower peak current with lower SWV frequency measurements. Figure: 3.5 shows the kinetic graph of all twelve experiments. It starts with 0A at the bottom and the other graphs are offset for clarity. The 0A obviously had the longest critical time 0.015 s, as the distance between the surface and the methylene blue increases the rate gets slower making the critical time larger. The lowest frequency we measured is 1 Hz which corresponds to 1 s in the graph. The 14A and 19A are slow enough that the critical time is larger than the range used. Since the graph is a normalized, we can only conclude that the critical time is >1 s. This electrochemical kinetic results fits our expectation of faster reactions at closer distances, even at the lower distances (0A–4A) that had shown discrepancies in the peak height (see above). In other words, the critical time for 0A is smaller than that of 4A, which should theoretically result in higher peak height at higher frequencies. However, as shown in Figure 3.3A–B, the largest currents were observed with the 4A spacer. Although this was initially confusing, we hypothesized that the increasing signal from 0A to 4A is due to some surface-dependent hindrance of DNA hybridization at the electrode. In other words, we believe this is due to double layer on the surface of the electrode,

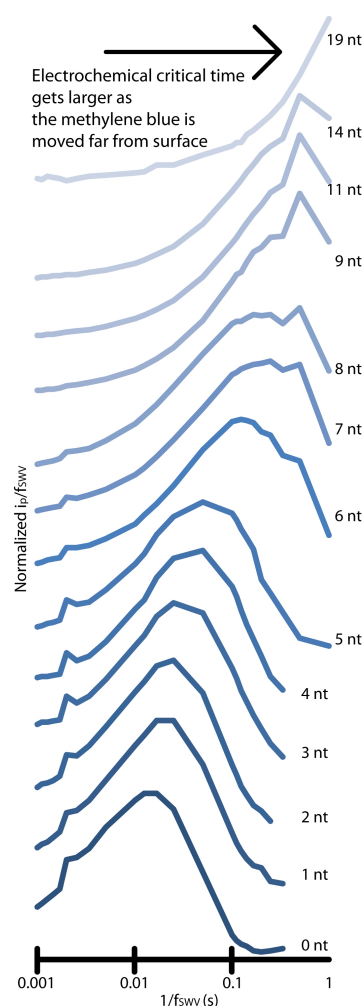


Figure 3.5: Electrochemical kinetics change by distance of methylene blue: At 0 nt the critical time is smaller as we increase the distance the critical time gets larger and 19 nt time is outside the range.

which is explored further in experiments in Section: 3.4.4.

3.4.3 Diffusion layer effect

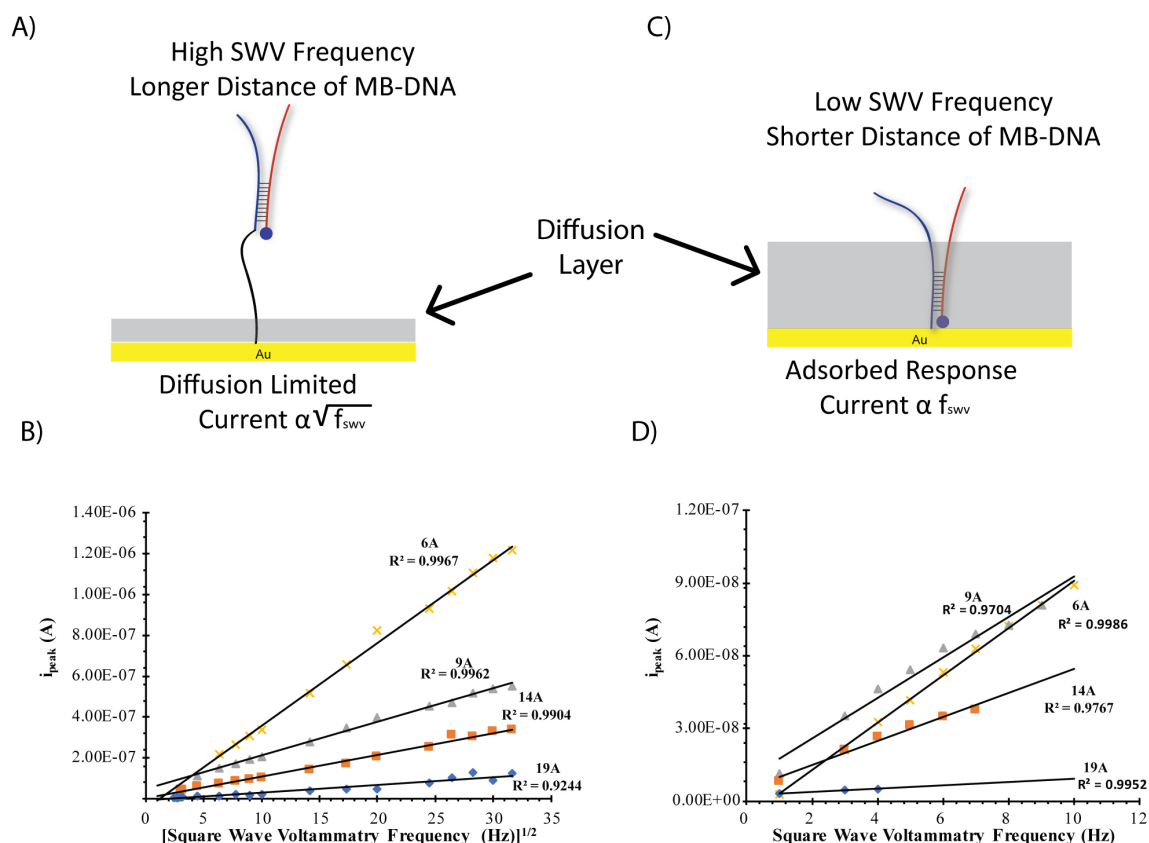


Figure 3.6: Diffusion layer and SWV response :A) Longer linker make the methylene blue far from the diffusion layer at higher frequency, B) the SWV peak height is plotted against the square-root of the frequency for four different length (6A, 9A, 14A and 19A) and the response is fitted with linear equation. This shows that these complex acts as a diffusion limited. C) At lower frequency the diffusion layer is larger which make even the longer tethered molecule act as an adsorbed species, D) shows the response of SWV peak height plotted against the SWV frequency for the sample length, the fitting with linear equation proves that these molecules act as adsorbed species.

A) and C) are not drawn in scale, R2 value based of the average of the three independent electrodes. Error bars are not shown for clarity.

A redox molecule present in the electrochemical diffusion layer acts as an adsorbed molecule, where the current increases linearly with the scan rate (mV s^{-1}). A redox molecule which is far from the diffusion layer needs to diffuse from the bulk solution to get oxidized or reduced, therefore this molecule will give diffusion limited signal where current increases linearly with

square root of scan rate. Huang and White [86] observed that a molecule acts as an adsorbed species until the diffusion layer is about 10 times larger than tethered length. In longer tether lengths, the molecules acts as diffusion limited.

The parameter of SWV frequency is not only responsible for the measuring time but also the scan rate. So instead of cyclic voltammetry scan rate, we used SWV frequency as scan rate and compared our peak height response of different lengths. We observed a similar result to the random walk model. Figure 3.6A portrays the electrochemical diffusion layer thickness at higher frequency with long distance MB-DNA, and this complex should respond like diffusion limited species. Figure 3.6B shows the plot of peak height versus square root of square wave voltammetry frequency for four different long lengths of DNA. As expected, in all the four cases the signal is linear at higher frequency with square root of frequency. Similarly, the low square wave frequency data with shorter distance of MB-DNA are shown in Figure 3.6C. The plot in Figure 3.6D shows that at lower frequency even the longer lengths of DNA can act as a surface bound species, as the electrochemical diffusion layer is larger at low SWV frequencies.

3.4.4 Double layer effect and hybridization Kinetics

To elucidate the initial increase in the signal as we placed the redox-moiety far away from the surface of the electrode, here we have attempted to explain these results with hybridization kinetics. For this, we chose eight thiolated-DNAs (0A to 7A), which places the methylene blue at varying distances (unit in nt) mentioned in the name of the nucleotide. Earlier, for the electrochemical kinetics experiments, we measured signal after reaching hybridization equilibrium (overnight incubation) to avoid discrepancies from any slow (few hours) hybridization kinetics. However, in this experiment, the measurement was done every six minutes once the MB-DNA was added. As mentioned earlier the hybridization energy in all the cases is same since it is the same sequence. As MB-DNA hybridizes to the surface, confined thio-DNA SWV signal will increase as this process brings the redox-moiety to the surface. The peak height is similar and follows the same pattern (increases through 4A then decreases) as we observed in Section

3.4.1. Our hypothesis is that double layer repulsion effects at the electrode surface will hinder hybridization of short DNA sequences at locations very close to the electrode. This hypothesis is described conceptually in Figure 3.7. To test our hypothesis we employed two strategies, 1) change the electric double layer thickness by changing the salt concentration; 2) Evaluate toehold-mediated strand displacement of DNA where the toehold regions are inside and outside the double layer.

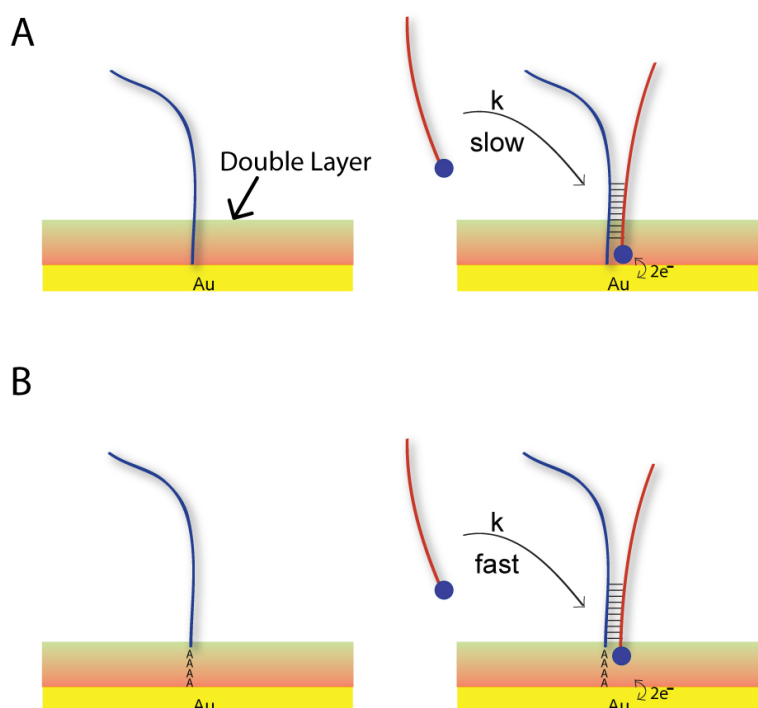


Figure 3.7: **Hybridization on the surface of electrode** : A) the complimentary sequence for of the MB-DNA is in the double layer region which make the hybridization kinetics slower. B) Since the complimentary sequence is out the double layer the hybridization is faster compared to A.

A and B are not in scale.

The double layer, or electrical double layer, is the layer of charge that appears on a surface when it is exposed to fluids. The thickness of the double layer depends on the electrolyte concentration and approximately $1.5 \kappa^{-1}$, where κ^{-1} is the Debye-Huckel length [90]. Figure: 3.7 shows a graphical representation of double layer and hybridization kinetics effect.

$$\kappa^{-1} = \left(\frac{\epsilon \epsilon_0 k T}{2 c^0 z_i^2 e_0^2} \right) \quad (3.1)$$

Here ϵ is relative permittivity of the solvent, ϵ_0 is the vacuum permittivity, k is the Boltzmann constant, T is the temperature, c^0 is the bulk electrolyte concentration, z_i is the ion charge and e_0 is the elementary charge. We used three different salt concentrations to gradually increase the double layer thickness. The approximate double layer thickness calculated for NaClO₄ concentration of 1.0 M, 0.5 M, 0.25 M and 0.125 M is 0.46 nm, 0.65 nm, 0.91 nm, and 1.29 nm respectively.

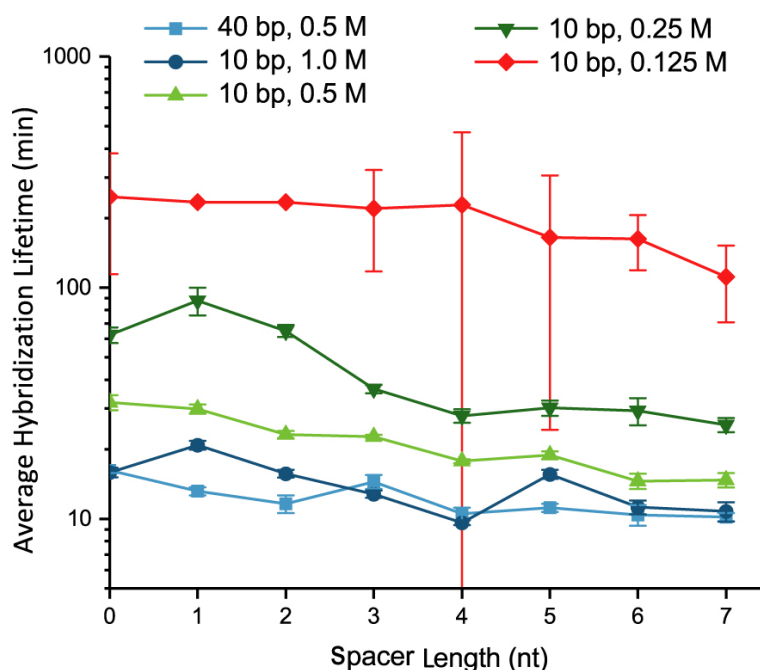


Figure 3.8: Double layer effect on average hybridization lifetime: The increase in lifetime is observed as the double layer increased by the decreasing salt concentration. Using a strong binding energy can overcome the double layer effect which is shown by 40 bp lifetime.

In our typical experiments (above), we used 0.5 M NaClO₄. Comparing this with salt concentrations of 0.125 M, 0.25 M, and 1 M NaClO₄, the double layer thickness will be increased by ~ 2 -, ~ 1.4 -, and decreased ~ 1.4 -fold respectively. So, we expected the hybridization kinetics to decrease for longer poly-A-DNAs in case of 0.125 M and 0.25 M and increase for shorter poly-A-DNAs for 1 M. In addition to this, we have also compared hybridization kinetics of 40 bp MB-DNA in 0.5 M NaClO₄ to understand the effect of higher hybridization energy.

From triplicate experiments we then calculated the average hybridization lifetime. Figure 3.8 shows the average hybridization lifetime of all the above-mentioned conditions plotted against the distance in nucleotide (nt) unit. As we expected, at higher salt concentration (1 M) all poly-A-DNAs have shorter hybridization lifetimes, and at lower salt concentration (0.125 M) all the poly-A-DNAs have very long hybridization lifetimes. The 40 bp hybridization lifetime at typical salt concentrations (0.5 M) is similar to the 10 bp at higher salt concentration, which shows as that for effective surface hybridization, either the double layer thickness should be minimized by adjusting the electrolyte concentration, or the hybridization energy should be made stronger to counteract the double layer effect.

Toe hold strand displacement on surface

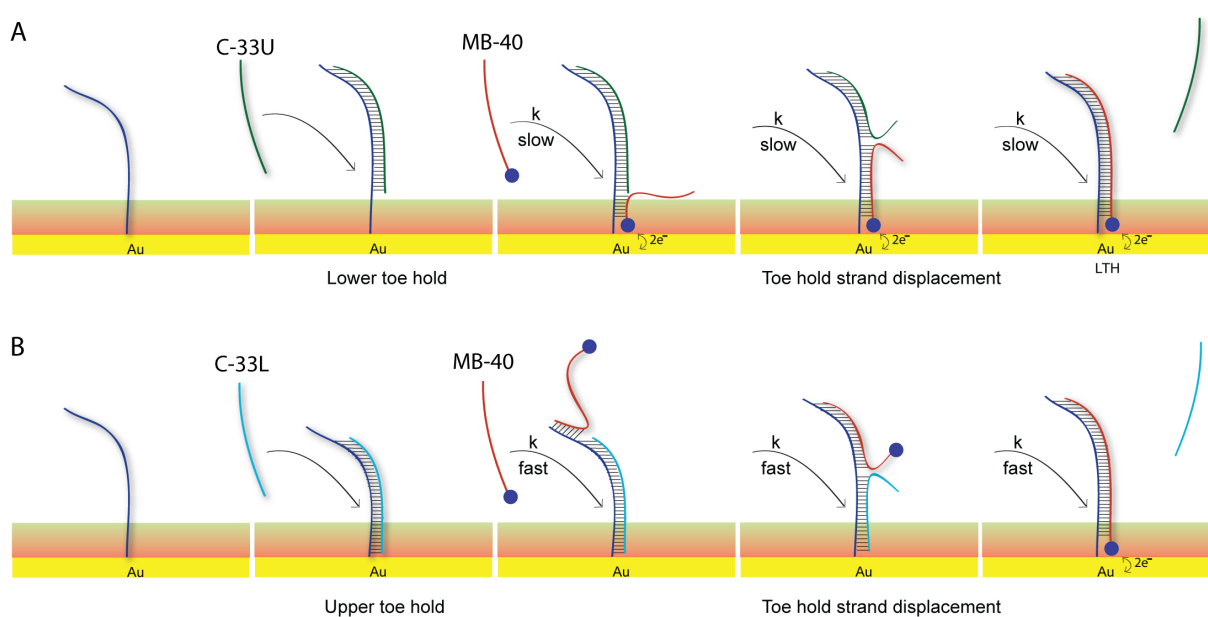


Figure 3.9: Toe hold strand displacement on surface: A) The 33 bp competitor binds to the top part of the thiolated-DNA leaving the 7 bp toehold in the double layer region, The MB-DNA faces the hindrance of the double layer which make the toehold binding slower. B) Competitor binds to the bottom and the toehold is far away from double layer which make the displacement reaction faster without any hindrance.

A and B are not drawn in scale.

To further test our hypothesis of double layer repulsion on DNA hybridization, we came up with a second strategy where we investigated the kinetics of toehold-mediated strand displacement reactions. Here, we utilized 40 bp MB-DNA, which displaces a 33 bp competitor hybridized with 0A-DNA and 4A-DNA. We used two competitors, C-33U and C-33L. C-33U (U stands for upper) binds with the top part of thiolated-DNA, leaving room for a 7 nt toehold closer to the surface. In case of C-33L (L stands for lower), the 7 nt toehold is left on the other side of the strand, away from the surface. Figure: 3.9 shows the representation of our model. In both the cases the DNA binding energies are similar, where the seven nucleotide toehold will be formed first and push the competitor away due to the higher stability of that complex compared to the competitor.

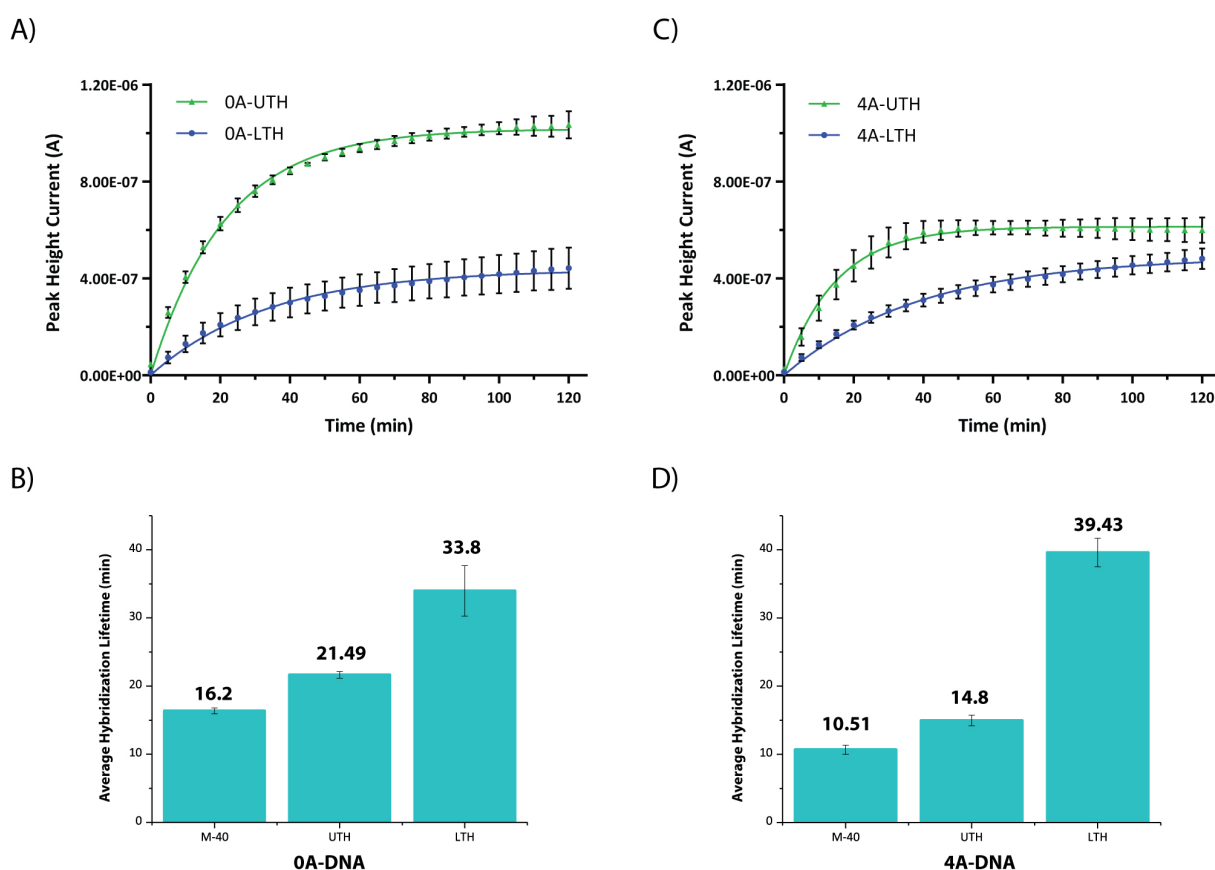


Figure 3.10: **Upper toe hold and lower toe hold strand displacement kinetics:** Peak Height vs Time plot to shows the kinetics of the toe hold strand displacement of the 33-bp competitor by 40 bp MB-DNA A) at 0A and at C) 4A. In 4A the upper toe hold and lower toe hold experiment reaches the same peak height range, but with 0A there is a huge discrepancy in peak height (the LTH replaces very slowly). Average hybridization lifetime of 40 bp and 33 base pair toe hold displacement B) at 0A and D) at 4A.

Figure: 3.10 A and C shows the peak height response with respect to the time for these systems. In 0A-DNA, obviously the upper toehold (0A-UTH) promotes much faster and higher yield of hybridization compared to the lower toehold (0A-LTH) displacement reaction (Figure 3.10A). The displacement with lower toehold will not reach equivalent peak height compared to the upper toehold, and these results confirm our hypothesis. In the case of the 4A-DNA (Figure 3.10C), in which the lower toehold is spaced further from the double layer effects, both the displacement reactions reach a similar peak height, even though the lower toehold reaction is still slower. This supports our hypothesis that the effect of the double layer is less prominent at longer distance. Note that 0A-DNA generally has higher peak heights than 4A-DNA due to the distance dependence which we saw in the previous section, 3.4.2. In Figure: 3.10 B and D, we compare the average hybridization lifetimes of the 40 bp MB-DNA hybridization with 0A and 4A-DNA, in presence of competitor strands leaving upper and lower toeholds; data without competitor is also shown. 4A-DNA has shorter hybridization lifetimes (faster hybridization kinetics) without the competitor (M-40) and with the upper toehold competitor (UTH), which supports our hypothesis. With 0A-DNA and the lower toehold, the reaction seemed to be similar speed to that of 4A-DNA, but the overall peak height did not reach that of the upper toehold displacement reaction.

3.5 Conclusion

In this chapter, we have studied the effect of diffusion layer and double layer. We observed the electrochemical kinetic rate is faster if the redox moiety is present in the diffusion layer, which acts as an adsorbed species. This is shown by placing the redox molecule precisely at various distance from electrode surface and comparing its kinetics. We have also altered the double layer thickness and studied its hindering effect on the surface hybridization. Toehold strand displacement by the DNA within and outside the double layer were done to explore the hybridization kinetic change. These understandings are very valuable in DNA-sensor development and optimization. With this we developed a bistable-switch DNA sensor, which is

potential POC for short oligonucleotide quantification explained in Chapter 6.

Chapter 4

Temperature Dependence of SWV Signal and Branched Assay for ssDNA Quantification

4.1 Introduction

In the diagnosis and treatment of genetic diseases, detection of oligonucleotides with high sensitivity and specificity is of central importance [11]. Conventionally this has been accomplished through optical measurements during melting curve analysis of a polymerase-chain reaction (PCR) amplified oligonucleotide, where single-base mismatches can be resolved [91]. While a number of other specialized techniques exist, electrochemical measurement is an appealing alternative due to its small instrument size, low cost, and ease of handling [11,91]. In one common format for electrochemical oligonucleotide detection, a DNA/RNA capture probe which has a redox moiety like ferrocene or methylene blue (MB) is immobilized onto an electrode surface. Introducing the target, which has complimentary sequence to the capture DNA, results in a conformational change that affects the distance between the redox moiety and the surface and effectively alters the electron transfer rate to the electrode [44, 62, 92–96]. In these protocols the percentage change in the signal is proportional to the target concentration. Similarly, there are methods in which the target brings a redox moiety to the surface from bulk solution [76,97], which makes the signal proportional to the target concentration.

White and coworkers have outlined a theory behind the change in electron-transfer rate by target-induced conformational change [49, 65, 86, 98]. The change in the distance between the redox moiety and the surface should either change the redox moiety from diffusion-limited to adsorbed behavior, or vice-versa [86]. In the absence of conformational changes, the rate of collisions of the redox moiety with the electrode surface is changed [49]. Under this mechanism,

some real-time electrochemical aptamer sensors have been developed using structure switching aptamers [3, 60, 68]. The Plaxco group has effectively discriminated single-nucleotide polymorphisms using electrochemical melt curve analysis [99]. Kelly et al. used a masking DNA template to remove false positives and effectively quantify mutated circulating nucleic acids [76, 97]. A limitation of these mechanisms is that the target should result in effective change in the electron-transfer rate, or an effective masking method of false positive DNA should be used.

In this work, we have amended methodology used in our prior studies of signal and background in homogeneous fluorescence assays [100] and adapted the approach to study DNA-driven electrochemical assays. A customized system is designed to allow precise control of both temperature and square-wave voltammetry (SWV) frequency while experimentally varying DNA hybridization energies at the electrode surface. We demonstrate that high temperature not only weakens the background complexes in target-induced DNA hybridization on surface, but it also contributes to the appreciation of the analytical signal by increasing electron-transfer rates. This approach at amplifying electrochemical signal while reducing target-independent DNA hybridization using temperature control should be applicable to a variety of other systems utilizing electrochemical-DNA (E-DNA) or aptamer sensors (aptasensors). The study also highlights a key role for assay temperature and suggests that it should not be overlooked when designing such systems.

4.2 Reagents and materials

All solutions were prepared with deionized, ultra-filtered water (Fisher Scientific). The following reagents were used as received: 4-(2-hydroxyethyl)-1-piperazineethanesulfonic acid (HEPES) and Sodium perchlorate from Alfa Aesar. tris-(2-carboxyethyl) phosphine hydrochloride (TCEP), mercapto hexanol, gold etchant, and chromium etchant from Sigma-Aldrich. Gold-sputtered on glass (GoG) (Au 100 nm with Cr adhesion layer 5 nm) from Deposition Research Lab, Inc (St. Charles, MO) with dimension 1 inch x 3 inch x 1.1 mm. AZ 40XT

(positive thick photoresist) and AZ 300 MIF developer from Microchemicals, polydimethylsiloxane (PDMS) from Dow Corning Corp. and dimethyl sulfoxide (DMSO) from anachemia. Methylene blue-conjugated DNA was purchased from Biosearch Technologies (Novato, CA), purified by RP-HPLC. Thiolated DNAs were obtained from Integrated DNA Technologies (IDT; Coralville, Iowa), with purity confirmed by mass spectroscopy. DNAs are listed in Table: 4.1.

Strand Names	DNA Sequences
MB- DNA	CCA CCC TCC TCC TTT TCC TAT CTC TCC CTC GTC ACC ATG C /C7-MB/
n=7 thio	/5ThioMC6-D/ AAA AGC ATG GTA TTT TTC GTT CGT TAG GGT TCA AAT CCG CG
Sample n=7,m=6	TAA CGA ACG AAA AAT GAC GAG
Sample n=7,m=7	AAC GAA CGA AAA ATG ACG AGG
Sample n=7,m=8	ACG AAC GAA AAA TGA CGA GGG
Sample n=7,m=9	CGA ACG AAA AAT GAC GAG GGA
Sample n=7,m=10	GAA CGA AAA ATG ACG AGG GAG
n =9 thio	/5ThioMC6-D/ AAA AGC ATG GTG ATT TTT CGT TCG TTA GGG TTC AAA TCC GCG
Sample n=9,m=6	CTA ACG AAC GAA AAA CGA GGG
Sample n=9,m=7	TAA CGA ACG AAA AAC GAG GGA
Sample n=9,m=8	AAC GAA CGA AAA ACG AGG GAG
Sample n=9,m=9	ACG AAC GAA AAA CGA GGG AGA
Sample n=9,m=10	CGA ACG AAA AAC GAG GGA GAT
n =10 thio	/5ThioMC6-D/ AAA AGC ATG GTG ACA TTT TTC GTT CGT TAG GGT TCA AAT CCG CG
Sample n=10,m=6	TAA CGA ACG AAA AAT GAG GGA

Sample n=10,m=7	AAC GAA CGA AAA ATG AGG GAG
Sample n=10,m=8	ACG AAC GAA AAA TGA GGG AGA
Sample n=10,m=9	CGA ACG AAA AAT GAG GGA GAG
Sample n=10,m=10	GAA CGA AAA ATG AGG GAG AGA
n =12 thio	/5ThioMC6-D/ AAA AGC ATG GTG ACG ATT TTC GTT CGT TAG GGT TCA AAT CCG CG
Sample n=12,m=6	CCT AAC GAA CGA AAA GGG AGA
Sample n=12,m=7	CTA ACG AAC GAA AAG GGA GAG
Sample n=12,m=8	TAA CGA ACG AAA AGG GAG AGA
Sample n=12,m=9	AAC GAA CGA AAA GGG AGA GAT
Sample n=12,m=10	ACG AAC GAA AAG GGA GAG ATA
n= 14 thio	/5ThioMC6-D/ AAA AGC ATG GTG ACG AGG TTC GTT CGT TAG GGT TCA AAT CCG CG
Sample n=14,m=6	ACC CTA ACG AAC GAA GAG AGA
Sample n=14,m=7	CCC TAA CGA ACG AAG AGA GAT
Sample n=14,m=8	CCT AAC GAA CGA AGA GAG ATA
Sample n=14,m=9	CTA ACG AAC GAA GAG AGA TAG
Sample n=14,m=10	TAA CGA ACG AAG AGA GAT AGG

Table 4.1: Sequences of DNAs used in single-branched electrochemical oligonucleotide quantification study

/5ThioMC6-D/ = Dithiol attachment (IDT), /MB-C7/= Methylene Blue (Biosearch)

4.3 Experimental methods

4.3.1 Preparation of gold electrode and PDMS electrochemical cell

Electrode masks were designed in Adobe Illustrator, and files were sent to Fineline Imaging (Colorado Springs, Colorado) for printing of positive photomasks. The mask design is shown in Figure: 4.1, where in one glass slide three chips can be made from 1 in² (645 mm²). Using AZ 40XT photoresist, standard photolithographic procedure was followed to make the photoresist pattern on the gold on glass slide (GoG). Then the GoG was introduced into gold etchant followed by chromium etchant for 30 s and 15 s, respectively. In this way, gold and chromium which was not blocked by AZ photoresist was removed, resulting in gold electrodes defined by the mask design. Heating this electrode patterned GoG in DMSO at 110 °C for 30 min removes the positive photoresist from above the gold. The GoG electrodes were rinsed with deionized water followed by ethanol and dried with nitrogen.

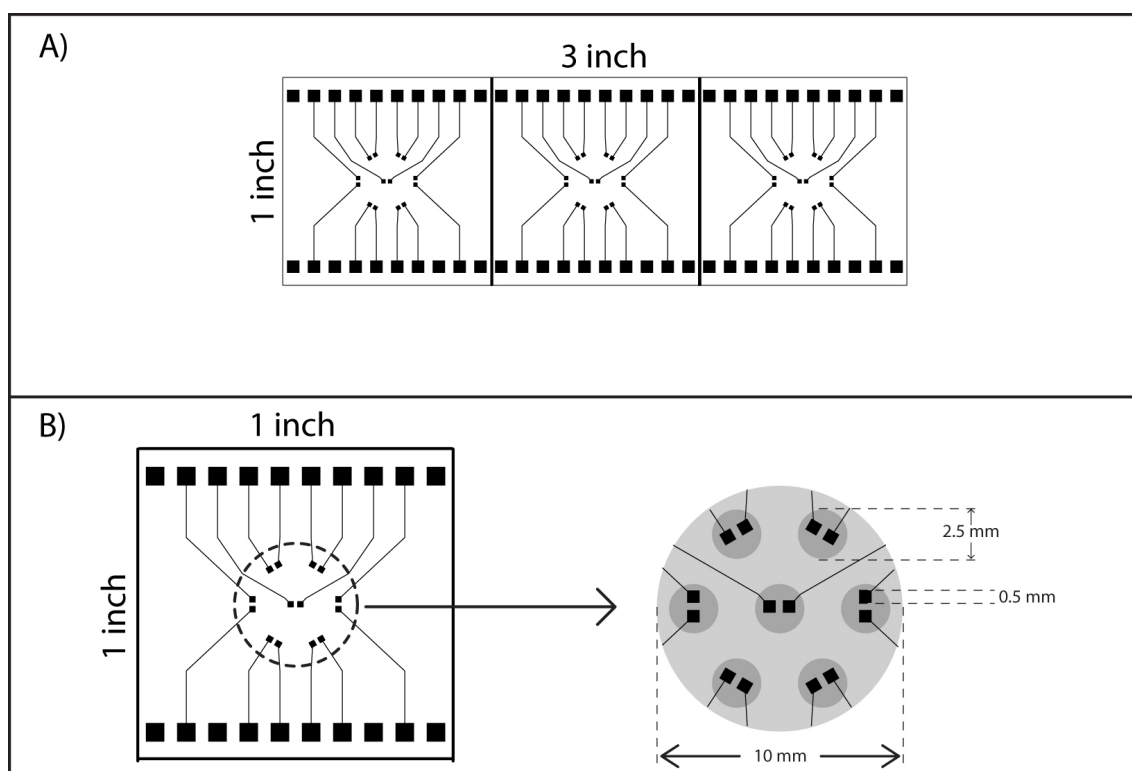


Figure 4.1: AZ photomask model used for GoG preparation: A) shows the mask of one microscopic slide, in which three chips can be made. B) is the enlarged picture of one chip, the right side picture shows the placement of small reservoir and large reservoir.

4.3.2 PDMS electrochemical cell

To form the electrochemical cell, custom PDMS reservoirs were bonded to the GoG slide, and we follow a similar protocol from our previous work [101]. Briefly, a 3D computer animated design (CAD) file was designed in Sketchup (Trimble Navigation Limited), and 3D printing of the mold was performed with a Makerbot Replicator 2 (200 μm layer resolution in the z-direction) and using Makerbots polylactic acid filament (PLA, 1.75 mm diameter). The 3D CAD depiction and an example of a printed mold is shown in Figure: 4.2. The PDMS and curing agent was mixed in the standard 10:1 ratio and poured onto a silicon wafer, and this assembly was placed on flat surface for overnight curing with the 3D-printed PLA mold at 60 $^{\circ}\text{C}$ (care must be taken to keep below the glass transition temperature of PLA, which is 60–65 $^{\circ}\text{C}$). With one mold, nine electrochemical cells can be made in one cycle, and a single mold can be used multiple times. Once the curing process was complete, the PLA mold was removed followed by slicing it to the desired shape and sonicating in methanol for 20 min to quench any leftover curing agent, then it was placed in 100 $^{\circ}\text{C}$ for a minimum of two hours. This PDMS was irreversibly bonded by plasma oxidation to the GoG slide to form an electrochemical cell. The GoG slides and the 3D-CAD templates were modeled to give seven small reservoirs of 2.5 mm diameter and 4 mm height, which were placed below a larger reservoir of 10 mm diameter. Within each small reservoir were two duplicated working electrodes. In these small reservoirs, various samples could be incubated simultaneously under similar conditions, and measurements of all fourteen electrodes could be made in the same buffer through the larger reservoir.

4.3.3 DNA monolayer assembly

Prior to plasma oxidation of the PDMS electrochemical cell, the electrodes were cleaned with piranha solution. The piranha solution ($\text{H}_2\text{SO}_4:\text{H}_2\text{O}_2$, 3:1) was freshly prepared and dropped on the surface of the electrode for 1 minute, and the electrode was rinsed with deionized water. In the meantime, the thiolated DNA was prepared. The thiolated-DNA contained a dithiol group at its 5 terminus. To effectively form the self-assembled monolayer (SAM), first the dithiol

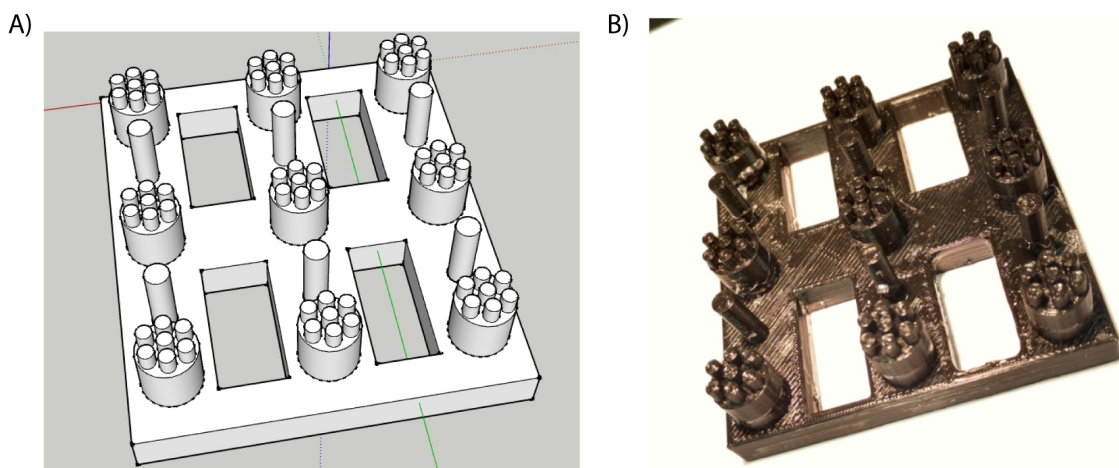


Figure 4.2: 3D-CAD and PLA mold for electrochemical cell: A) the 3D-CAD drawn in SketchUp software. B) Picture of PLA mold printed in Makerbot 3D-printer.

was reduced to a monothiol with TCEP. To reduce 1 μL of 200 μM thio-DNA, 3 μL of 10 mM TCEP as mixed and placed in the dark for 1 hour. The solution was diluted with HEPES buffer (pH 7.4) to form 1.25 μM thio-DNA, and once the PDMS was plasma oxidized, 300 μL of this solution was introduced into the electrochemical cell, then it was placed in the dark for 1 hour. Following this, the electrodes were rinsed with HEPES buffer, then 3 mM mercaptohexanol was incubated on the electrode for 1 hour in dark. After rinsing, the modified electrodes were placed in the refrigerator with buffer and were stable for up to one week.

4.3.4 Square-wave voltammetry frequency study of DNA melting

Electrochemical measurements were performed using a Gamry Reference 600 potentiostat. Once the electrode was immobilized with the thiolated-DNA by the above mentioned procedure, 100 nM of the target and 100 nM of MB-DNA in 10 mM HEPES/0.5 M NaClO_4 (pH 7.4) buffer was introduced and incubated overnight at 4 $^\circ\text{C}$. For background measurement, only 100 nM MB-DNA was introduced. The overnight incubation ensured that hybridization reached equilibrium, and the low temperature minimized evaporation. Following incubation, the chip was placed on our in-house built custom temperature control system with a Peltier device held at 4 $^\circ\text{C}$, and the temperature was slowly increased to 15 $^\circ\text{C}$. Once the system reached 15 $^\circ\text{C}$, the platinum counter electrode (CH instruments) and silver/silver chloride (3 M KCl)

reference electrode (BAS1) were introduced into the reservoir, and the SWV experiment with eighteen different frequencies (4 Hz 900 Hz), was carried out at every 5 °C temperature interval until 70 °C was reached. The SWV parameter were given in Table: 4.2

Parameter Name	Symbol	Values Used
Initial voltage	V_i	-0.425 V
Final voltage	V_f	-0.05 V
Step size	E_s	1 mV
Pulse height	E_p	50 mV
Frequency	SWV-Hz	4 to 900 Hz

Table 4.2: SWV parameters for single branched DNA quantification study

4.3.5 Single branched DNA model

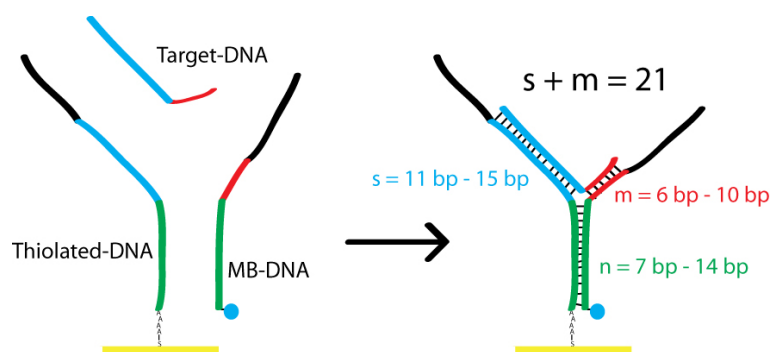


Figure 4.3: **Single branched DNA quantification structure:** To elucidate the sensitive hybridization complex, six different thiolated-DNA is used ($n = 7, 9, 10, 12, 14$) and for each thiolated-DNA five different sample is tested, which differ in binding with both thio-DNA and MB-DNA shown in red and blue.

Our previous work on development of protein quantification by the electrochemical proximity assay [36] (ECPA) used target induced DNA-DNA binding stabilization on the surface of the electrode. In this work, we modified the ECPA model system and extended it to DNA quantification, in which the target DNA (21 nucleotide) binds with a thiolated-DNA and methylene blue-DNA (MB-DNA) to form a single-branched DNA hybridization structure (Figure: 4.3). The stability of the thiolated-DNA and MB-DNA hybridization (green region) was increased

by the presence of target due to the proximity effect. We have used five different thiolated-DNA strands (green region; $n = 7, 9, 10, 12, \text{ or } 14$) which hybridized at different affinities with MB-DNA. For each n , five different oligonucleotide target stabilities was studied (red region; $m = 6, 7, 8, 9, 10$). In all complexes, the target was maintained as a 21-nt DNA strand by varying the length of the thiolated-DNA binding region (blue region, s) such that $s + m = 21$.

4.3.6 DNA quantification

Single step calibration

For the single step calibration, once the electrode was ready, all seven wells and the reservoir were filled with a single concentration of target-DNA and 100 nM MB-DNA in HEPES buffer. This complex was incubated overnight at 4 °C. The chip was then placed on the peltier at 4 °C, and the temperature was increased slowly to the measurement temperature. Finally, the counter and reference electrodes were introduced, and SWV measurement was done. In total, seven different concentrations between 0 to 50 nM sample were measured.

Two step calibration

In the two step calibration, once the electrode was ready, each well was filled with 10 μ l of a single concentration of target-DNA and 100 nM MB-DNA in HEPES buffer, and the system was incubated overnight at 4 °C. After incubation, the chip was placed on the peltier at 4 °C. The sample solutions were removed, and 100 nM MB-DNA was introduced into all of the wells and the larger reservoir. Then measurement is carried out as in the single step calibration above. In one chip, seven concentrations could be measured.

4.3.7 Data analysis

Peak Height

Each set of raw data from square-wave voltametry (including V_{step} and I_{diff}) was transferred to Microsoft Excel, and a nineteen-point moving average was applied to reduce environmental noise. Following this, a third-order polynomial baseline was calculated near the redox potential of MB-DNA. To do this, the Linest equation in Excel was used, and data points from -0.400 V to -0.370 V and -0.15 V to -0.09 V were selected for baseline fitting. The resultant baseline function was subtracted from the 19-point averaged data to get a baseline corrected SWV voltammogram. The maximum current from this graph was used as the peak height of each particular run. Signal-to-background differences and ratios were also calculated using peak heights obtained in this way. An example of 19-point averaged data and the calculated baseline is shown in Figure: 4.4.

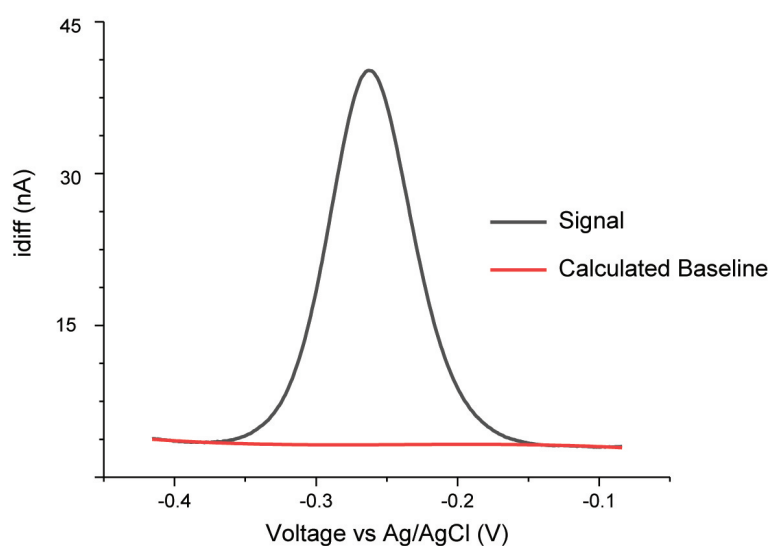


Figure 4.4: *Third order polynomial calculated baseline subtraction:*

Electrochemical Kinetics calculation

The critical time data analysis was done as mentioned in Chapter 3, Section: 3.3.3.

Signal to background difference and ratio

To get the signal to background difference, the peak height value of the background was subtracted from the signal of same n , temperature, and frequency. In a similar way to get the signal to background ratio, the background was divided.

Heat maps

To compare sets of data over a wide range of conditions, two dimensional heat maps were generated from the data using ImageJ. The "fire" look-up table was used to display data, and heat map color legends were included in each figure.

Assay calibrations

Assay responses were fit to a five-point logistic regression shown in equation below.

$$H = \left(\frac{a - d}{1 + \left(\frac{C}{c}\right)^b} \right) + d \quad (4.1)$$

where H was the peak height; C was the concentration of the target; and a , b , c , and d were fitting constants. The curve fitting was done in Excel using the solver function. To calculate a statistically robust lower detection limit (LOD), we followed the method described by Holstein et al [102]. By this method, the LOD with 95% confidence interval was obtained. This was achieved by not only considering the standard deviation of the blank but also the deviation of all the sample concentrations

4.4 Result and discussion

4.4.1 Signal comparisons with varying complex stability

It is known that for an adsorbed redox reporter, an increase in SWV frequency results in an increase in peak height of SWV current [42]. For fixed positions, this effect was observed in our nanostructure as well. An example where $n = 14$, $m = 10$, and $T=25\text{ }^{\circ}\text{C}$ is shown in Figure: 4.5. This effect was observed in all cases where complex stability was expected, confirming that the labeled DNA strands were being held at the electrode surface. This effect was also observed in the heat maps of peak height (Figure: 4.6). Furthermore from these heat maps we observed that signal increased with increasing numbers of base pairs between MB-DNA and thio-DNA (right to left, $n= 7\text{-}14$) and with increasing pairs between MB-DNA and the target DNA (bottom to top, no sample and $m= 6\text{-}10$), as expected. This increase in stability was also witnessed from the melting temperature (T_m) changes. For $n = 9$ with no target, the DNA dissociated/melted and signal was lost above $30\text{ }^{\circ}\text{C}$, whereas for $n = 9$ and $m = 10$ the structure was stable through $50\text{ }^{\circ}\text{C}$. The $n = 14$ system, even with no target, was stable up to $70\text{ }^{\circ}\text{C}$.

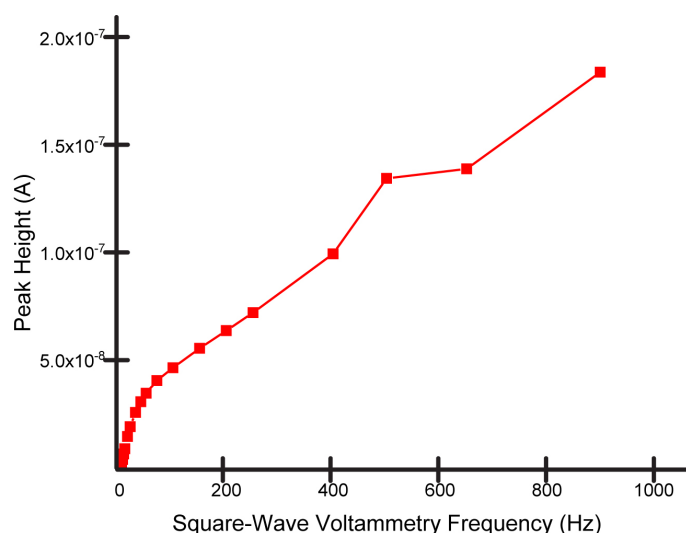


Figure 4.5: Peak height as a function of SWV frequency increase is shown with $n = 14$, $m = 10$, $25\text{ }^{\circ}\text{C}$ as an example

The heat maps of peak height in Figure: 4.6 highlight the importance of fine tuning the DNA binding energies in such assays, particularly when developing a system to quantify small

oligonucleotide targets. For example, signal was significantly lower in the $n = 7$ case compared to the $n = 14$ case, however, there was essentially no difference between the background (no target) and the signal traces in the $n = 14$ case. The complex with $n = 7$, while non-optimal, would function as a sensor, while the complex with $n = 14$ would not be useful. These concepts are explored further in the signal-to-background difference and ratio studies that follow. Moreover, the heat maps illustrate the importance of controlling not only SWV frequency, an easily controlled but sometimes overlooked parameter, but also assay temperature, an often overlooked parameter that requires special control systems.

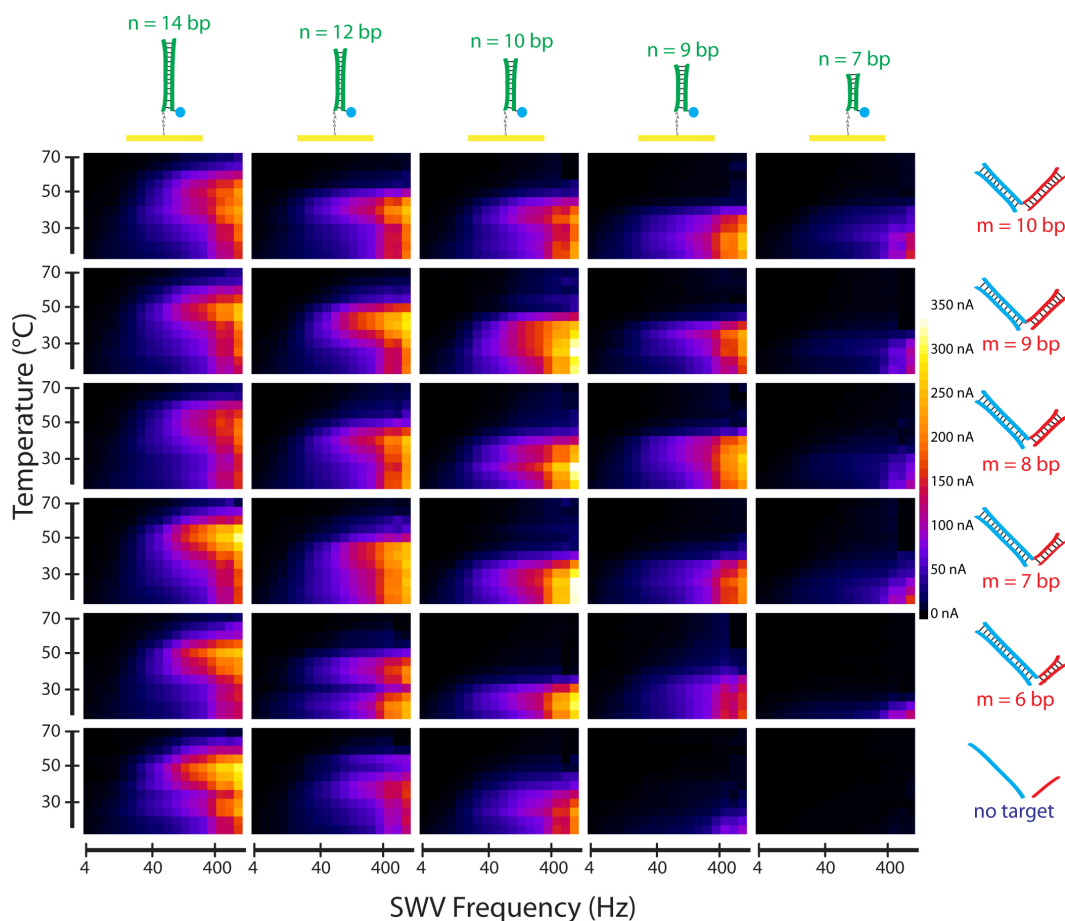


Figure 4.6: Heat map comparing peak height, temperature and SWV frequency of signal and background of all 25 complex: This shows as the binding energy n and m increases the overall signal increases. In the absence of target the DNA melting can be observed especially in the case of $n = 7$ and 9 . Presence of target makes the thiolated-DNA and MB-DNA binding stronger, so the melt temperature is increased. In addition to that effect of temperature in electrochemical signal is also seen, which is seen in $n = 14$ where the complex is stable, the temperature increase results in increasing signal.

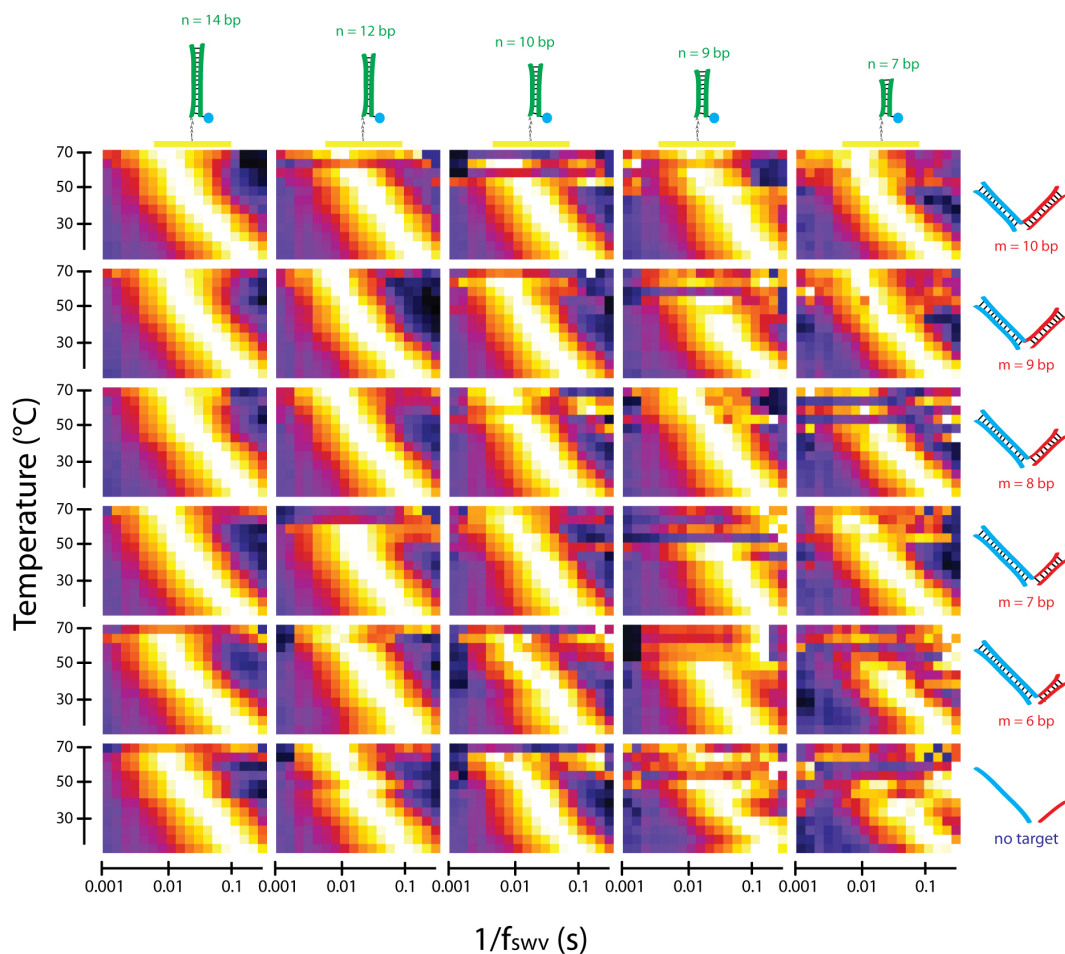


Figure 4.7: Heat map showing the shift in electrochemical critical time with temperature: For all the complex the critical time at 15 °C is 0.1 s (orange spot is the critical time), which shows the stability of the complex does not contribute for the electrochemical kinetics. And as temperature increase all complex undergoes similar decrease in critical time, with weaker complex facing the melting.

4.4.2 Temperature dependence of electrochemical kinetics

As noted above, electrochemical kinetics of the complex at a particular temperature was determined following Sebojka et al. [89], namely by plotting normalized peak height over frequency (I_p/f_{swv}) versus inverse frequency ($1/f_{swv}$), giving the critical electrochemical reaction time from the plot maximum. A heat map using the 25 different complex structures is shown in Figure: 4.7. It is instructive to note that the critical times (brightest points) were approximately 0.1 s at 15 °C for all complexes, showing that complex stability has negligible influence over the electron transfer kinetics between MB-DNA and the electrode. Furthermore, as the temperature was increased, all complexes underwent an increase in kinetics (decrease in critical time), observed as an left-upward diagonal shift in the heat maps (Figure: 4.7). The weakest

complexes lost signal at higher temperatures due to melting from the surface.

Figure: 4.8 shows snapshots of these effects for four different complexes. The most stable complex is shown in the top set of curves ($n = 14$, $m = 10$; with target DNA). As the temperature was increased from 15 to 70 °C, the critical electrochemical reaction time shifted (toward the left) by nearly two orders of magnitude, from 0.1 to 0.008 s. Thus, as temperature was increased, the electrochemical reaction was enhanced. A similar effect was observed in the absence of target DNA ($n = 14$, no target), except that partial complex melting made the kinetics measurement difficult at 70 °C. Although overall SWV currents were certainly lower for less stable complexes, the electrochemical reaction kinetics followed essentially the same trend with $n = 7$, $m = 10$ (with target DNA). However, in the absence of target ($n = 7$, no target), the complex melting prevented the reaction kinetics measurements from being made. These results again confirmed that the complex stability had negligible effect on electron transfer kinetics, which is instead defined largely by the positioning of the MB-DNA with respect to the electrode surface.

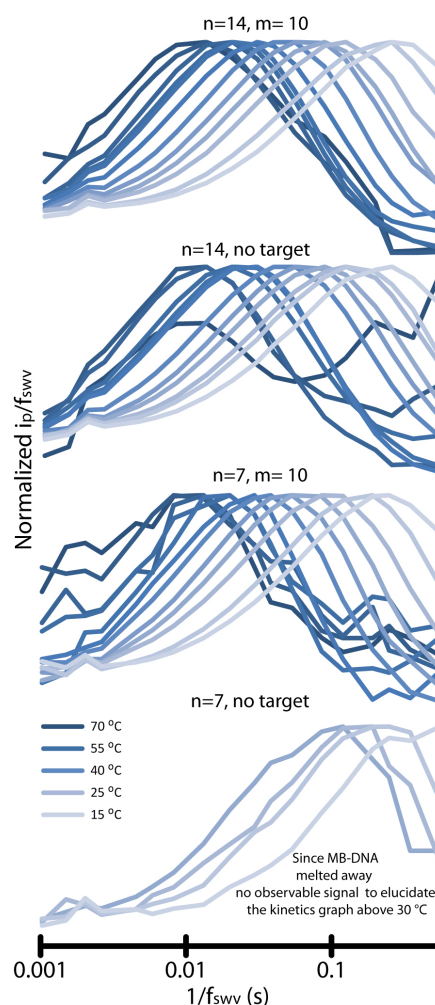


Figure 4.8: I_p/f_{swv} vs $1/f_{swv}$ of temperature: 15 to 70 °C for $n = 14, m = 10$; $n = 14$, no target; $n = 7, m = 10$; $n = 7$, no target; is shown top to bottom. Stability increase by n can be observed by comparing no target graph of $n = 14$ and 7 . Similar change in rate by temperature is elucidated by comparing all the four graph.

This temperature enhancement of the electrochemical kinetics can be understood by considering the diffusion layer thickness [86]. Figure: 4.9 compares the peak height versus scan

rate of a stable complex ($n = 14$, $m = 10$) at 15 °C and 40 °C, in which the increase in diffusion layer thickness with temperature is obvious. The linear dependence on scan rate was observed at higher scan rates at 40 °C compared to 15 °C, indicating behavior that more closely resembled an adsorbed molecule, i.e. a molecule confined within the electrochemical diffusion layer. Thus, the increased temperature extended the diffusion layer further from the electrode, permitting higher electrochemical reaction rates to be observed. These results imply that careful tuning of the complex stabilities and the temperature could give significant enhancements to signal in surface-confined, DNA driven assays with SWV readout.

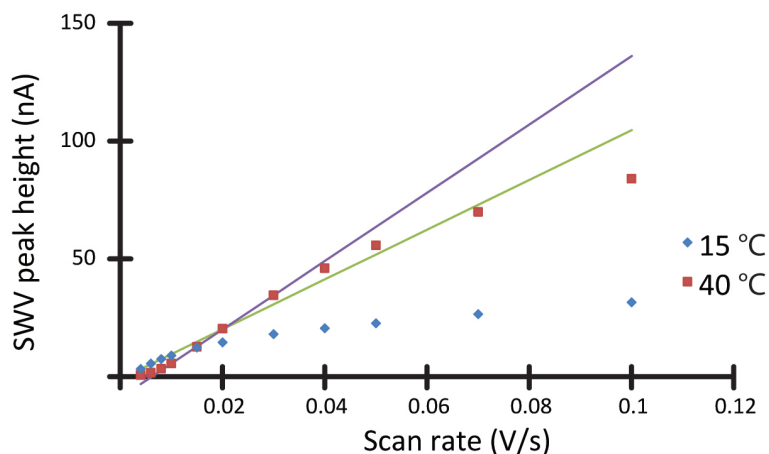


Figure 4.9: Shift in the diffusion layer shown by peak height response: $n = 14$, $m = 10$ signal response, the non-diffusion limited redox molecules have linear increase in peak height with respect to scan rate. The linear response of the peak height vs scan rate is broaden for 40 °C when compared to 15 °C, which shows the increase in diffusion layer with temperature.

4.4.3 Characterizing signal and background

In this work, we have developed a direct-readout (amplification free) DNA quantification method. Using a novel single-branched hybridization structure that exploits the proximity effect, we compared signal and background in twenty-five different complexes in different hybridization arrangements. Below, we present studies of these complexes from two different perspectives: 1) signal-to-background difference, and 2) signal-to-background ratio.

Signal-to-background difference

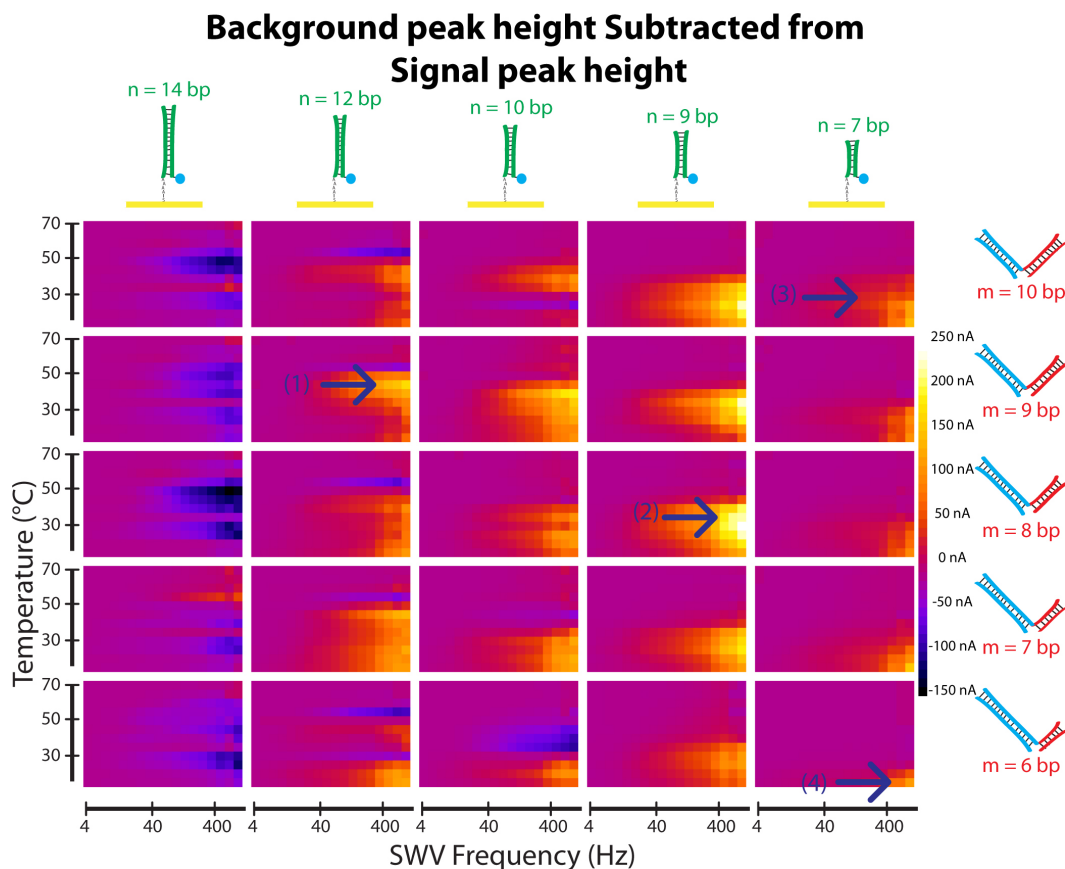


Figure 4.10: Heat map of background signal subtracted from signal: As m increase the difference increases in all the case except $n = 14$. $n = 12$, $m = 9$ has larger signal difference at 45°C which is marked as (1). (2) $n = 9$, $m = 8$, 35°C (also has appreciable difference), (3) $n = 7$, $m = 10$, 30°C and (4) $n = 7$, $m = 6$, 15°C are the other conditions selected for quantification.

Heat maps of signal-to-background differences of all 25 complexes are shown in Figure: 4.10. On studying overall signal to background difference, the insertion of target into the complex elevates the peak height (yellow/orange/red pixels depict positive changes in heat maps) in all cases except where $n = 14$ (blue or black pixels denote negative changes). We believe this is due to the effect of both steric hindrance, which was explained by Mahshid et al. [73, 79], and the increased stability of background when $n = 14$. Since the system was designed for signal-on readout, we ignore $n = 14$ from this point on. Examining other complexes, we observed an increase in n to result in increased signal-to-background differences, as expected from the model since this region does not interact with MB-DNA. However, based on our single-branched design, an increase in m strengthens the binding between MB-DNA

and target, but it weakens the target and thiolated-DNA binding. With this in mind, one would expect to observe one or more optimal arrangements with respect to n , where signal stability, background stability, and electrochemical reaction rates balance to give the highest signal-to-background differences. Indeed, upon observing the heat maps meticulously, it was concluded that optimal temperatures for the various complexes are different and that there may be several optimal arrangements overall. From Figure: 4.10, high differences were observed when $n = 9-12$, and two optimal sets of parameters appeared to stand out as having the highest differences (yellow/white spots). The region labeled (1) in the figure has $n = 12$, $m = 8$, $f_{\text{SWV}} \geq 400$ Hz, and $T=45$ °C. The second region, labeled (2) is the case where $n = 9$, $m = 8$, $f_{\text{SWV}} < 400$ Hz, and $T=35$ °C. This region is labeled as (2) in the figure. Other labeled regions are discussed below.

Signal-to-background ratio

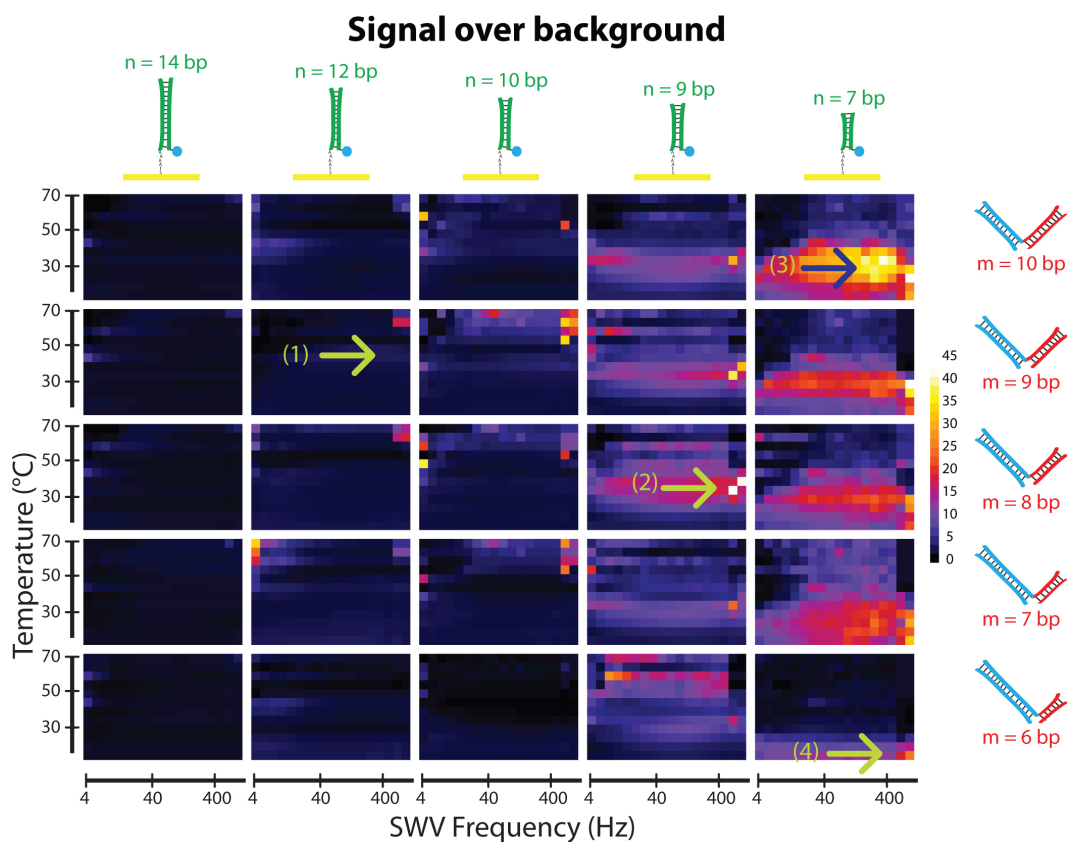


Figure 4.11: Heat map of signal over background of all complexes: $n = 7$ and 9 have very large signal to noise ratio compared to very stable complex due to very low background. $n = 7$, $m = 10$ at 30 °C (3) has very high ratio. $n = 7$, $m = 6$ at 15 °C have larger ratio at lower temperature.

Viewing these data through a second perspective, signal-to-background ratio, we attain a heat map with a different optimal regions (Figure: 4.11). The introduction of sample results in the best ratios where background complexes are the weakest, i.e. when $n = 7$. While the case of $n = 12$ exhibited high signal-to-background differences (Figure: 4.10), this complex showed very low ratios (Figure: 4.11). For $n = 7$, which has the best ratios, as m increases the ratio increases, giving the optimal parameters as $n = 7$, $m = 10$, $f_{\text{SWV}}=100$ Hz, and $T=30$ °C. This region is marked as (3) in Figure: 4.11.

Difference and Ratio Comparisons

On a composite view of signal-to-background differences and ratios, the $n = 9$ complex is unique by being moderate in both cases. Specifically, region (2) in Figure: 4.10 ($n = 9$, $m = 8$, $f_{\text{SWV}} \geq 400$ Hz, and $T=35$ °C) can be selected as a best complex for DNA quantification considering the joint viewpoint. On the other hand, all of these conclusions are based on mix-and-read workflow quantification, or a single-step method. If we consider that a heterogeneous workflow can be used for step wise introduction of target, the binding between target and thiolated-DNA can be stronger without worrying about excessive background formation. In addition to this it would be better if it is moderate in both signal to background difference and ratio. Obviously, (2) is expected to be good with ($n = 7$, $m = 6$, 400 Hz, 15 °C (4) in Figure: 4.11, which has good signal to background ratio at lower temperature.

Data of the selected four set of conditions were extracted and overlapped in Figure: 4.12 in two dimensions. Figure 4.12A and 4.12B compare the signal-to-background differences and ratios, respectively, while the top figures are plotted versus frequency and the bottom as a function of temperature. The four selected set of conditions are highlighted with asterisks. This demonstrates our previous conclusions that (1) gave the maximum difference, (2) showed good signal and a moderate ratio, (3) showed a very high ratio, and (4) is optimal for low-temperature detection.

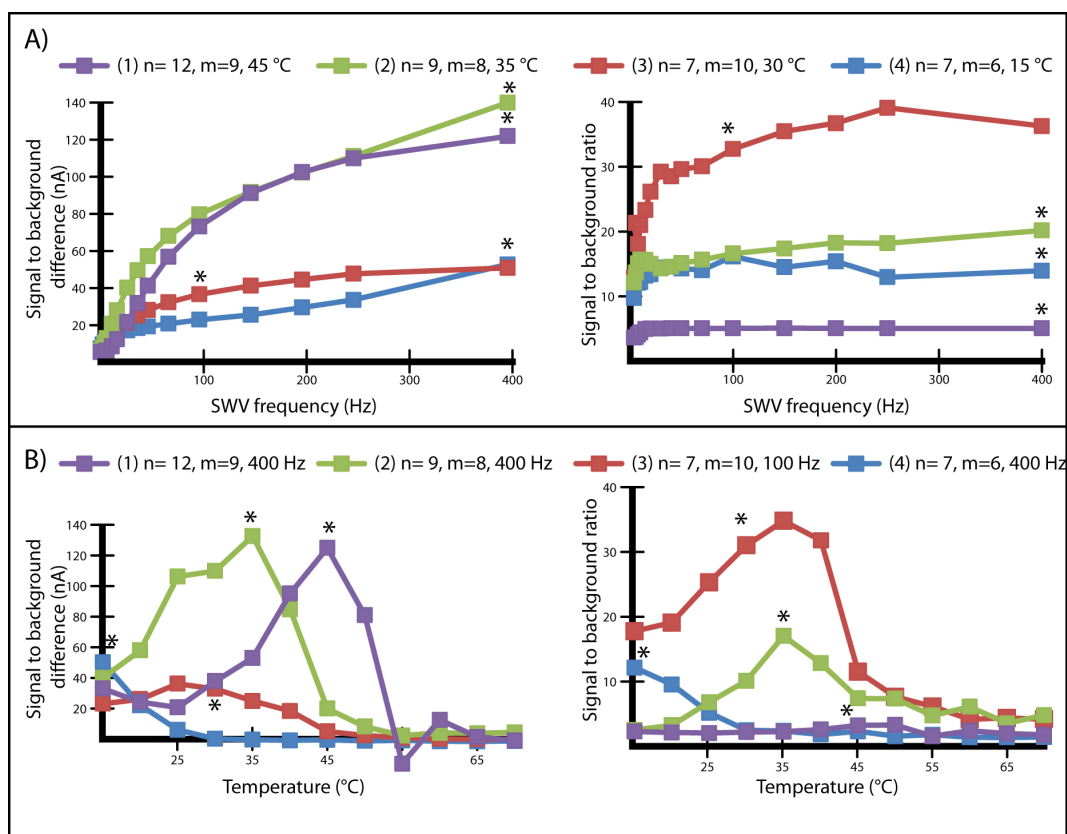


Figure 4.12: SWV frequency and temperature response of selected complexes: (1) $n = 12$, $m = 9$, $45\text{ }^{\circ}\text{C}$, (2) $n = 9$, $m = 8$, $35\text{ }^{\circ}\text{C}$, (3) $n = 7$, $m = 10$, $30\text{ }^{\circ}\text{C}$, and (4) $n = 7$, $m = 6$, $15\text{ }^{\circ}\text{C}$ are plotted against the (A) square-wave voltammetry frequency, (B) Signal to background difference and ratio of the same conditions is plotted against the temperature.

4.4.4 Oligonucleotide quantification

With this information in hand, assay calibration experiments were carried out under all conditions, with results shown in Figure: 4.13. These data compare the calibration curves of single and two-step workflows for all conditions. Condition (1) did not show an appreciable increase in peak height induced by target until 50 nM concentration, in both the single and two step workflows. This is likely due to the very strong binding between MB-DNA and thio-DNA. We observed a similar response with $n = 14$ in our previous experiments. The other three conditions showed a sigmoidal relationship between the SWV peak height and sample DNA concentrations. These curves were fitted with the four-point logistic equation, shown as red curves in the figures. In condition (2) high signal and an increasing response was observed in the low nanomolar region, and the single-step workflow exhibited higher sensitivity and dynamic range compared to the two-step workflow. Similar trends were observed in condition (3),

with slightly improved sensitivity at low concentration but lower overall signal. In contrast, the low temperature assay condition (4) exhibited better results with the two-step workflow.

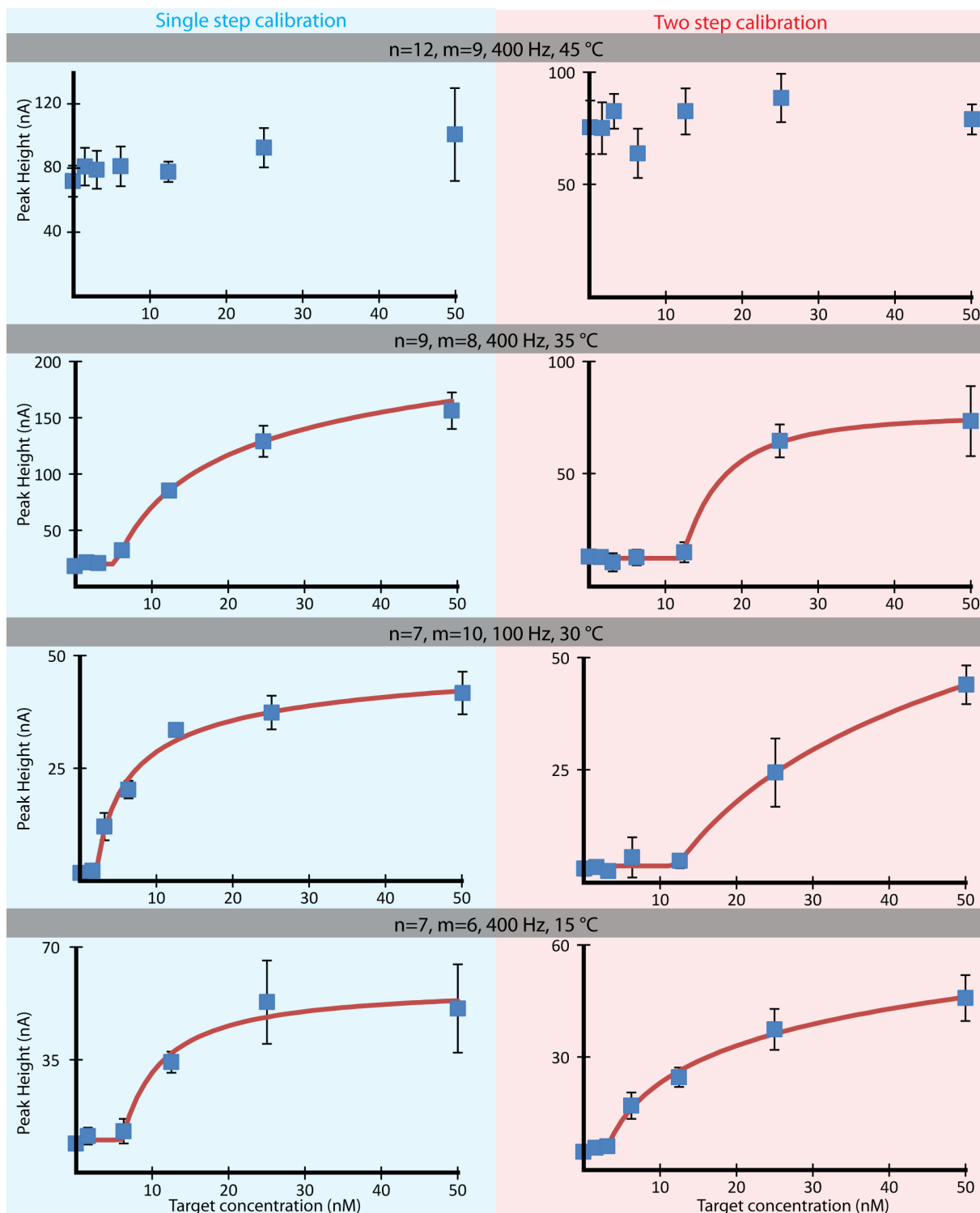


Figure 4.13: **Single and two step quantification of the selected complexes:** (1) $n = 12$, $m = 9$, 400 Hz, 45 °C, (2) $n = 9$, $m = 8$, 400 Hz, 35 °C, (3) $n = 7$, $m = 10$, 100 Hz, 30 °C, and (4) $n = 7$, $m = 6$, 400 Hz, 15 °C are shown from top to bottom respectively. The left side with blue background is for single step calibration, whereas the right side with red background is for two step calibration. The red curve fitted in the curve is four-point logistic curve fit. The standard deviation in all cases is $n=6$.

The limits of detection (LOD) of these assay formats were all between 2 and 20 nM. Under all conditions, LODs were calculated and compared in Figure: 4.14, where red and blue bars represent the one-step and two-step workflows, respectively. It was observed that condition (2) was moderate in both the cases, while having two- to three-fold more sensitivity (see Figure: 4.13) in comparison to the other two conditions. Condition (3) had lower LOD with the one-step workflow yet showed the worst LOD in the two-step method. By contrast, condition (4) had a smaller LOD using a twostep protocol compared to the single-step. Thus,

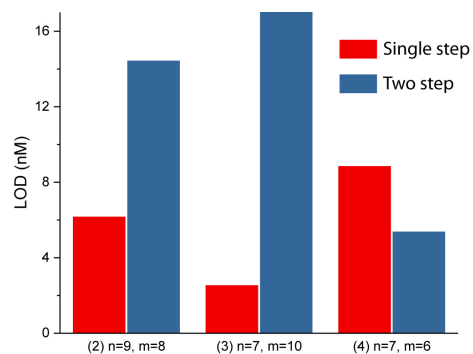


Figure 4.14: Lower detection limit comparison: It show the effect of binding energy, temperature of the assay, and procedure on LOD. For single step (3) $n = 7$, $m = 6$ at $35\text{ }^{\circ}\text{C}$ has low LOD of 2 nM, for two step (4) $n = 7$, $m = 6$ at $15\text{ }^{\circ}\text{C}$ has low LOD of 5 nM.

for a two-step workflow, one should chose condition (4); for a single-step workflow, condition (3) is optimal; and the highest sensitivity and wide range can be achieved with condition (2). Stated differently, for single-step workflows, a balanced increase in both m and n can provide high sensitivity, while maximizing m and minimizing n can result in lower assay LOD. For two-step workflows, one should increase the stability between the sample and capture probe on the surface. More generally, this study has shown that careful control over surface hybridization energies, temperature, and SWV frequency can provide significant flexibility in operating this single-branched electrochemical DNA assay platform.

4.5 Conclusion

In this work, we have presented a new assay design and have developed a system for fine tuning or optimizing electrochemical DNA sensors. Namely, we carefully controlled hybridization energies, square-wave voltammetry frequency, and temperature. Notably, we demonstrate that temperature is indeed a very important factor in optimizing such assays. In homogeneous, DNA-driven assays with optical readout, such as pincer assays [33] or proximity ligation assays [31], our group and others have shown that precise temperature control can serve to reduce

background hybridizations or ligations, yet fluorescence quantum yield tends to decrease as temperature is increased. By contrast, we show here that with precise temperature control in DNA-driven electrochemical assays, electron transfer rates can be increased while background hybridizations are simultaneously minimized. This work highlights the importance of understanding such effects in our novel single-branched DNA assay, and similar trends will likely be observed in many electrochemical DNA assays and aptasensors.

With regard to our single-branched proximity assay developed here, the precise control of the stated parameters revealed an inherent flexibility in the assay. Various formats of the assay could be chosen for low temperature (15 °C) readout, higher temperature (45 °C) readout, minimized LOD, or maximized sensitivity and range. While many reported DNA- or aptamer-driven electrochemical assays have optimized SWV frequency, very few have simultaneously studied the temperature-dependent effects as shown here. Hence, an obvious future direction is to employ a temperature-controlled system as shown here to more carefully optimize the temperature and frequency dependences of these assays.

Chapter 5

DNA Nanostructure for Electrochemical Detection of Broad Range of Analytes

5.1 Introduction

This chapter focuses on development of a versatile electrochemical quantification method for wide range of targets, from small molecules to large proteins, which can be extended to drop-and-read diagnoses and real time measurements. A wide range of analytes have been successfully quantified by conformation switching electrochemical aptasensors. However, hindrances in developing a sensitive structure switching aptamer and the inability to use high performing antibodies as a recognition unit limits these electrochemical aptamer sensors from being generalizable. The Plaxco group has conducted a wide range of in-depth studies and development of many such electrochemical sensors [49]. Among those some study are done with double stranded DNA scaffold for large antibody and protein detection [103, 104]. Figure: 5.1 shows the model, the anchoring-strand with redox moiety tag is immobilized on the electrode surface and hybridized with recognition strand, which is tagged with small molecule recognizing unit. Upon interaction with a large molecule such as an antibody, this rigid double-stranded (ds-DNA) structure showed a decreased faradic current, which could be used for quantification. In another study from this group, using the same model, the interaction between a small molecule and a protein was studied [105]. With this system, dsDNA is used to position the sensing and recognition portions, and the sensing structure is made of two separate DNA molecules, one of which is bound non-covalently.

From our understanding about the DNA hybridization on the surface and the distance dependence of SWV signal, we designed a novel sensing nanostructure (Figure: 5.2) which has

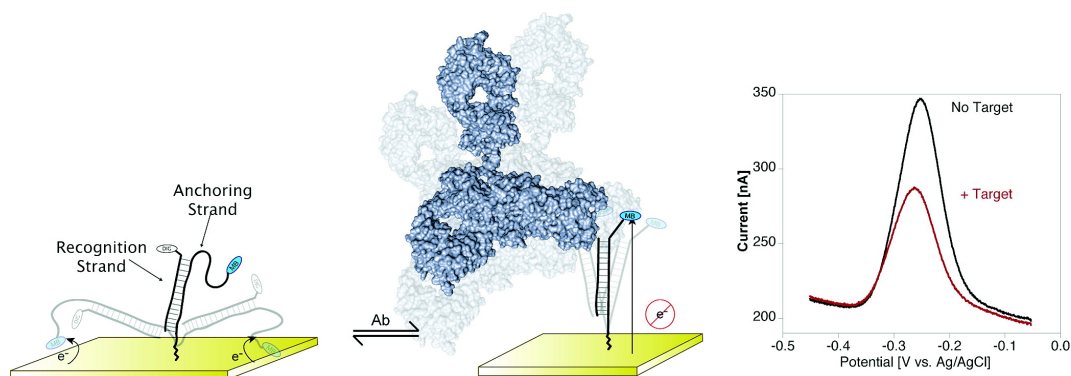


Figure 5.1: DNA scaffold architecture for electrochemical detection of protein-small molecule interaction: Double-stranded DNA forms a rigid-but-dynamic scaffold, in that anchoring strand is attached to the surface and has redox moiety, recognition strand with covalent bound small molecule is hybridized with anchor strand. When a large protein binds to the small molecule signal suppression is observed [105].

Reprinted with permission Copyright ©(2009) American Chemical Society

the redox moiety and anchor recognition in close proximity, more flexible ssDNA between the surface and the redox moiety, and where each sensing nanostructure is a single molecule covalently attached to the electrode. Our hypothesis is that when a large anchor molecule is introduced there will be a change in the tethered diffusion rate which slows the complex mobility to the surface, leading to signal suppression. It should also be possible to introduce a competitor, where the anchor molecule is displaced resulting in increased mobility, observed as a signal increase. By this strategy, both anchor (large protein) molecules and small molecule competitors can be quantified. The anchor molecule quantification will be a direct signal-OFF method (signal suppression), and small molecule detection approach will be an indirect signal-ON (signal appreciation) assay. As we know, the SWV frequency can be tuned to change the current response direction of the assay (signal-OFF to signal-ON or vice versa). This type of change could also give ratiometric or calibration free results.

5.2 Reagents and materials

All solutions were prepared with deionized, ultra-filtered water (Fisher Scientific). The following reagents were used as received: 4-(2-hydroxyethyl)-1-piperazineethanesulfonic acid

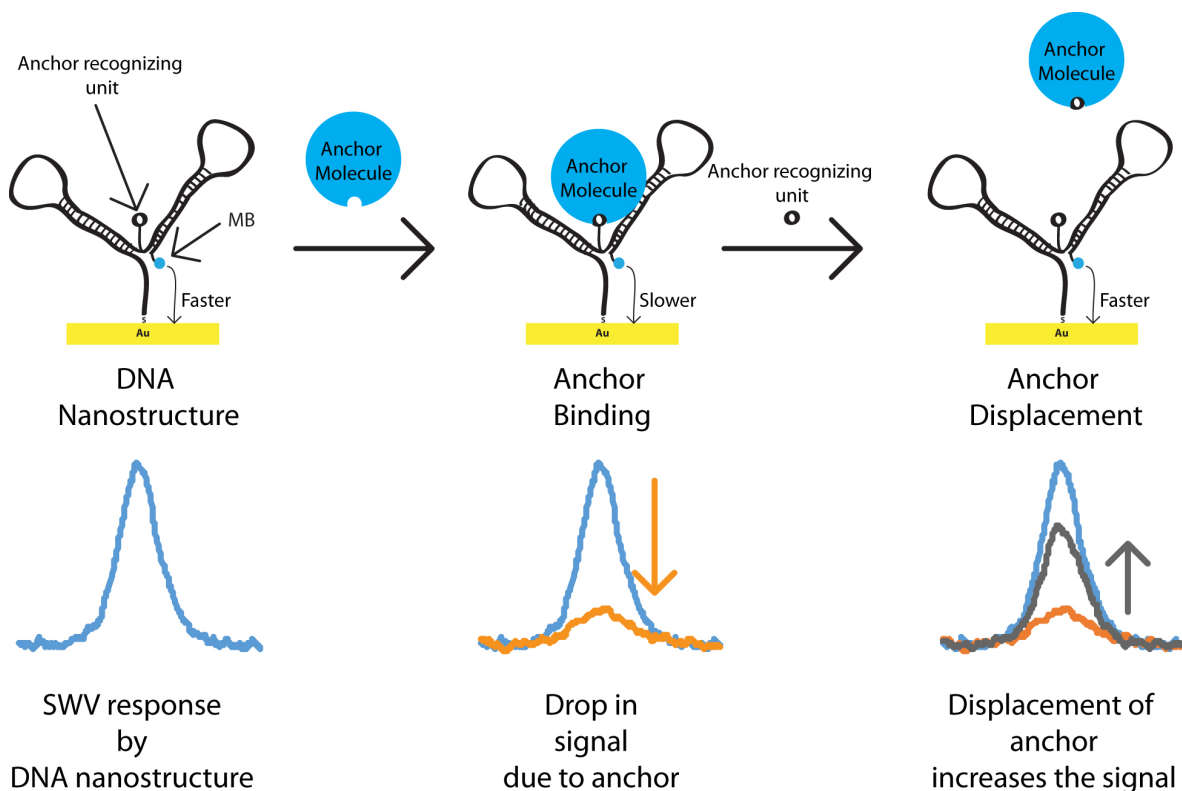


Figure 5.2: Schematic view of DNA nanostructure anchor model for quantification of small molecule and large protein: DNA nanostructure is designed in a way the redox moiety (methylene blue) and the anchor recognition unit are in close proximity, so any interaction in anchor recognition unit will affect the diffusion of the redox moiety to the surface. Initially we expect the diffusion is faster resulting in high SWV current output. When anchor binds with its recognition units the diffusion is hindered suppressing the SWV signal. This attached anchor can be displaced when recognition unit or its competitor comes in contact, due to the thermodynamic stability of the anchor binding with free molecule compared to the constrained one. This increases the signal. By this strategy both anchor and anchor recognition unit can be quantified as signal-OFF direct and signal-ON indirect assay respectively, with anchor being large protein and small molecule as recognition unit.

(HEPES) and Sodium perchlorate from Alfa Aesar. Anti-digoxigenin, digoxigenin, tris-(2-carboxyethyl) phosphine hydrochloride (TCEP), mercapto hexanol, gold etchant, and chromium etchant from Sigma-Aldrich. Gold-sputtered on glass (GoG) (Au 100 nm with Cr adhesion layer 5 nm) from Deposition Research Lab, Inc (St. Charles, MO) with dimension 1 x 3 x 1.1 mm. AZ 40XT (positive thick photoresist) and AZ 300 MIF developer from Microchemicals, polydimethylsiloxane (PDMS) from Dow Corning Corp. and dimethyl sulfoxide (DMSO) from anachemia. Methylene blue-conjugated DNA was purchased from Biosearch Technologies (Novato, CA), purified by RP-HPLC. Thiolated DNAs were obtained from Integrated DNA Technologies (IDT; Coralville, Iowa), with purity confirmed by mass spectroscopy, T4 DNA ligase (400000 units) and adenosine triphosphate (ATP, 10 mM) are bought from New England

Bio, DNAs are listed in Table: 5.1.

Sequence Name	Abbreviation	DNA Sequence listed 5'-3'
Anchor 4A thio-lated DNA	anc4A-DNA	/5Phos/ CTG TGC AAG AAC TCA CAG CCT CAC CTC TTC CTA AAA A /3ThioMC3-D/
Anchor 6A thio-lated DNA	anc6A-DNA	/5Phos/ CTG TGC AAG AAC TCA CAG CCT CAC CTC TTC CTA AAA AAA /3ThioMC3-D/
Anchor 8A thio-lated DNA	anc8A-DNA	/5Phos/ CTG TGC AAG AAC TCA CAG CCT CAC CTC TTC CTA AAA AAA AA /3ThioMC3-D/
Anchor 10A thio-lated DNA	anc10A-DNA	/5Phos/ CTG TGC AAG AAC TCA CAG CCT CAC CTC TTC CTA AAA AAA AAA A /3ThioMC3-D/
Anchor connector desthiobiotin	conn-biotin	/5Phos/ GAG ACA CTG TGT CGT CTC CGG TTG AAG TGG AGA /ideSBioTEG/ TAG GAA GAG GTG AGG
Anchor connector digoxigenin	conn-digoxi	/5Phos/ GGG CGA CTG TGT CCG CCC CGG TTG AAG TGG AGA /iDigN/ TAG GAA GAG GTG AGG
Anchor Methylene Blue DNA	MB-DNA	/dT MB/ CTC CAC TTC AAC CG

Table 5.1: Sequence of DNAs used in anchor model quantification

/5phos/ = Phosphorylation (IDT), /3ThioMC3-D/ = Dithiol attachment (IDT), /ideSBioTEG/ = Intermediate Desthiobiotin-TEG (IDT), /iDigN/ = Intermediate Digoxigenin (IDT), /dT MB/ = Methylene Blue on T-C3 (Biosearch)

5.3 Experimental methods

5.4 Electrode preparation and DNA SAM

Figure: 5.3 shows the photomask of electrode design used in the experiment. Each electrode was 2 mm diameter and it was designed in a way that each electrochemical cell will have single electrode. The geometrical surface area of the electrode was increased to have a high initial signal. Same photolithography protocol explained in Chapter 4, Section: 4.3.1 was followed to prepare GoG. As explained in Section: 4.3.2 the PDMS electrochemical cell was prepared with

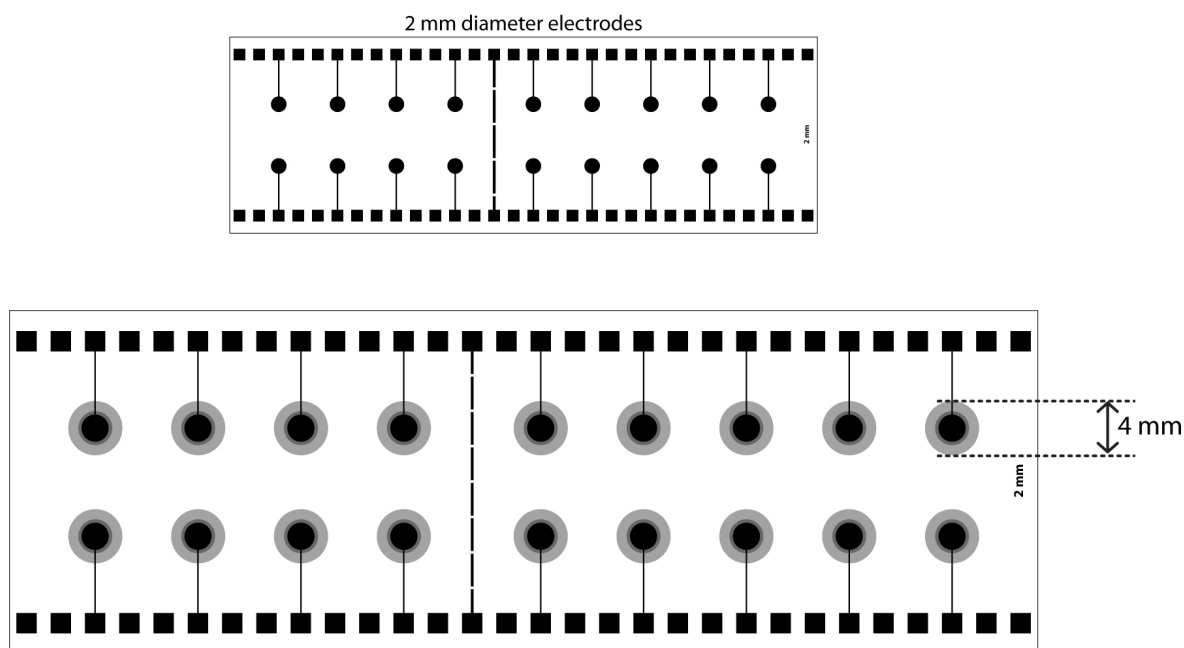


Figure 5.3: *Electrode photomask used for DNA nanostructure quantification: In one microscopic slide eighteen individual 2 mm diameter electrodes.*

3D-CAD and PLA mold shown in Figure: 5.4. Following this thiolated SAM was prepared following the protocol in Section: 2.3.1, with HEPES buffer (10 mM with MgCl_2 10 mM, pH 7).

5.4.1 On-electrode DNA nanostructure assembly using through T4 DNA ligase

Since the efficiency of the T4 DNA ligase enzyme is hindered by sodium ion concentration, ligation reactions at our electrode surfaces were carried out in HEPES buffer with no sodium salt added. To improve the DNA binding energy, 10 mM MgCl_2 was used. After ligation, the typical HEPES buffer (10 mM HEPES, 0.5 M NaClO_4) was used. Once the electrode was ready, 500 nM of anchor connector DNA and anchor MB-DNA was prepared in HEPES buffer (10 mM HEPES, 10 mM MgCl_2 , 1 mM ATP, pH 7). In each well, 200 μL of this mix was introduced into the electrode, following this 0.5 μL of 400,000 Units T4 DNA ligase was dropped into the electrochemical cell, wrapped in Parafilm and incubated overnight at room temperature. Then the electrode was briefly rinsed with water (deionized water drop was pipetted up and down twice and removed), HEPES (10 mM HEPES and 0.5 M NaClO_4) was introduced,

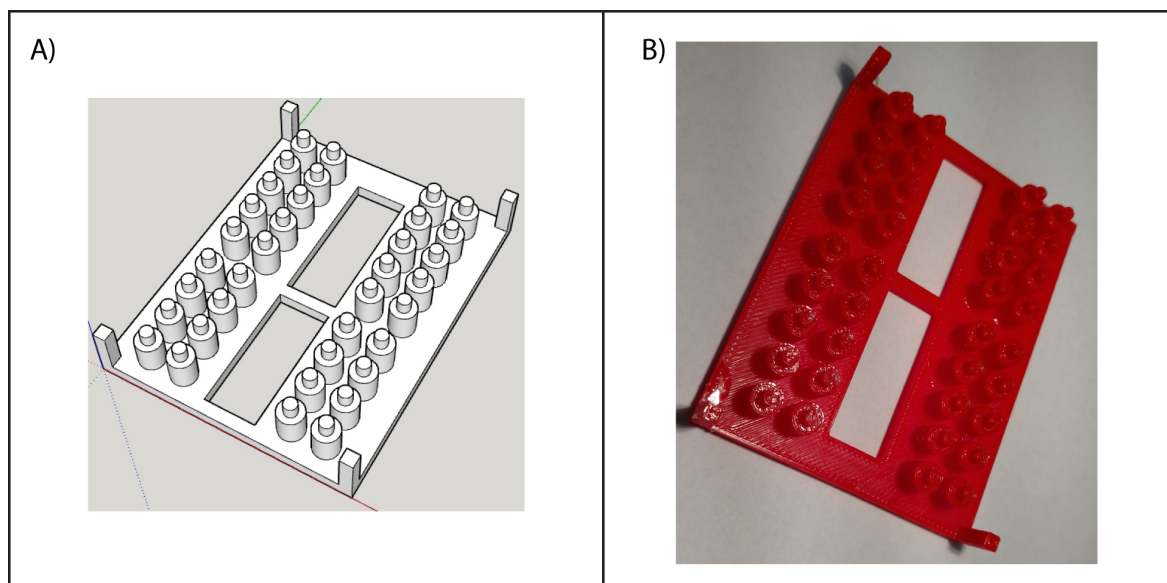


Figure 5.4: 3D-CAD and PLA mold for 2 mm diameter electrode: The small reservoir in the model is help reducing the volume used and helps for effective plasma bonding.

and the electrode was ready to use.

5.4.2 Electrochemical measurement

Electrochemical measurements were performed using a Gamry Reference 600 potentiostat, in a three electrode system setup with the platinum counter electrode (CH instruments) and silver/silver chloride (3 M KCl) reference electrode (BASi). Table: 5.2 gives the SWV parameters used.

Parameter Name	Symbol	Values Used
Initial voltage	V_i	-0.425 V
Final voltage	V_f	-0.05 V
Step size	E_s	1 mV
Pulse height	E_p	50 mV
Frequency	SWV-Hz	4 to 900 Hz

Table 5.2: SWV parameters for single branched DNA quantification study

5.4.3 Data analysis

Baseline correction and peak height

The procedure followed in Section: 4.3.7 was used for subtraction of baseline and peak height measurement.

Signal change percentage

For signal off quantification signal percentage change was used. This was the percentage of signal depressed by the target. Following was the formula used for calculation.

$$\%change = \left(\frac{i_p signal - i_p background}{i_p background} \right) \times 100 \quad (5.1)$$

Where $i_p signal$ and $i_p background$ were peak height after and before target incubation respectively.

5.4.4 Quantification protocol

Streptavidin Quantification

For streptavidin quantification, the DNA nanostructure was made by anc4A-DNA, conn-biotin, and MB-DNA. Once the electrodes were ready background measurement were done by SWV with 100 Hz frequency in 100 μ l of HEPES (10 mM HEPES, 0.5 M NaClO₄, pH 7). Followed by target was incubated for 2 hours, then the same electrochemical measurement was done.

5.4.5 Biotin quantification

Once the nanostructured is formed on the electrode anc4A-DNA, conn-biotin, and MB-DNA, the electrode was introduced to 100 μ L of 2 μ M streptavidin in HEPES buffer and incubated for 2 hours at room temperature. Then the electrodes were rinsed with buffer and background

measurements were done by SWV with 100 Hz frequency. Finally, 100 μ l of target was incubated for 2 hours, then the same electrochemical measurement was done.

5.5 Result and discussion

5.5.1 DNA monolayer formation and its stability

The goal of our experiment was to determine whether the diffusional change by the molecular weight of our nanostructures binding partner could be exploited for quantification. To achieve this, three moieties are needed to be attached to the DNA nanostructure: 1) the thiolated tag for attaching the DNA to the gold electrode, 2) redox moiety for electrochemical signal and 3) anchor recognizing moiety. In addition to this, for an effective signal change, the redox moiety should be in close proximity to the anchor recognizing moiety. Instead of purchasing custom made DNA with three tags, which would be very expensive even with low reaction yield. Instead, utilizing T4 DNA ligase enzyme, we ligated these three single-strand DNA sequences to form a DNA nanostructure on the surface. T4 DNA ligase can only ligate phosphorylated 5' double stranded DNA with 3'. To avoid more complexity, instead of using connectors for making double stranded DNA, we used hairpin structures to form suitable ligation structures. In our previous work, the dithiol tag for thiolated DNA were done at the 5' end. For ligation reaction, in this work we used thiolated-DNA with 3' dithiol tags.

Figure: 5.5 shows the pictorial description of the DNA nanostructure. On addition of anchor-connector and MB-DNA to the SAM electrode, hybridization occurs as shown in Figure: 5.5B. The anchor connector binds with thiolated-DNA, and MB-DNA binds with anchor connector; both bind with 15 bp, which is a strong binding energy at room temperature. There is no hybridization reaction between MB-DNA and thiolated DNA, which eliminates the false signal in the background, methylene blue with anchor recognizing unit. When T4 DNA ligase is added with ATP, the enzyme effectively ligates the two positions on the surface and makes it a single DNA complex with three tags. One other advantage is that the method can be quickly

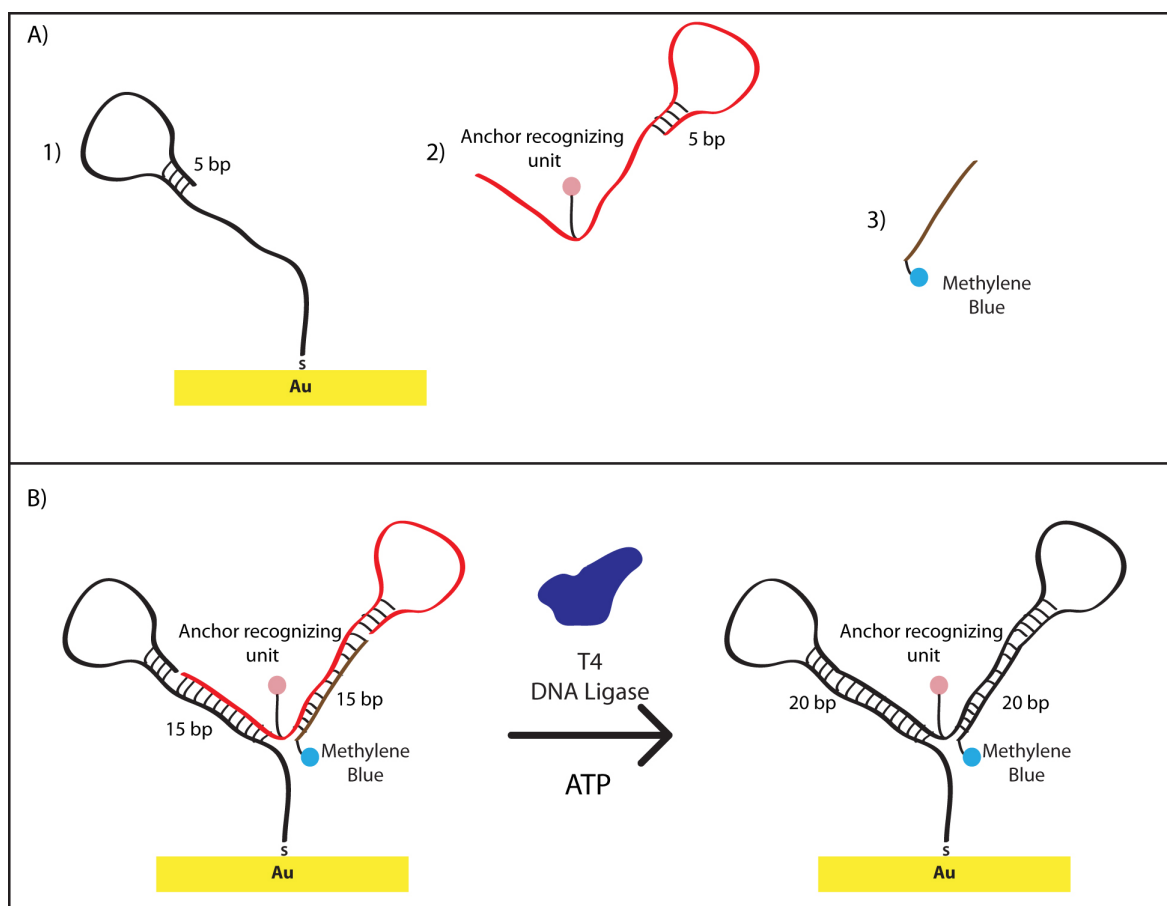


Figure 5.5: DNA nanostructure formation on gold electrode: Instead of buying a DNA with three different tag, which is expensive and lower yield, we bought three individual DNA with single tag and ligated on the surface by T4 DNA ligase. The thiolated-DNA and the connector DNA has 5 bp hairpin loop, with on hybridization places the phosphorylated end and 3 prime end in close proximity in double stranded mode for ligation. On ligation the three DNA becomes a long single DNA.

extended to other target just by changing the DNA with anchor recognizing unit.

To support our assumption that by ligation single DNA is formed, we compared the ligated and non-ligated complex signal. First the electrodes are rinsed with buffer (HEPES 10 mM, with 0.5 M NaClO₄, pH 7). On comparison the signal between the ligated and non-ligated are similar (Figure: 5.6). The hybridization energy with 0.5 M NaClO₄ is very stable, which results in similar signal. Then the electrodes were rinsed with deionized water. On measurement after this rinse shows that the non-ligated complex is almost fully removed in just one water rinse cycle. On cycling this process for two more time, we see that ligated DNA is stable on the surface, which shows that is a single DNA covalently bound on the surface of the gold electrode. As an

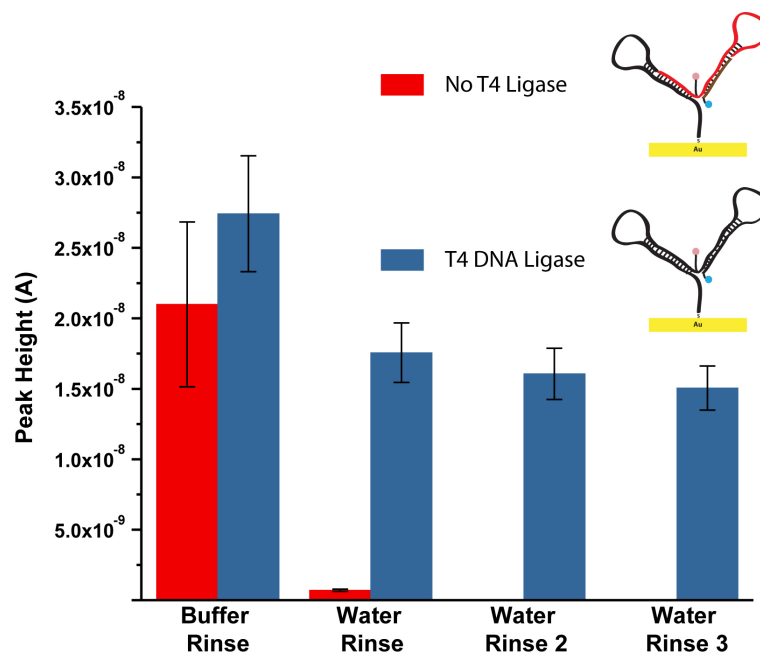


Figure 5.6: DNA nanostructure stability: To prove T4 DNA ligation is successful we compared the electrochemical response of ligated and non-ligated complex after buffer rinse followed by water rinse. After buffer rinse both ligated and non-ligated has observable signal, but on rinsing with water the non-ligated complex is removed. On other hand the ligated complex is even after two more rinse.

additional confirmation of DNA nanostructure stability and effective DNA ligation, DNA melt study is done, with sybr-green florescent intercalation dye. Figure: 5.7 compares derivative curve of non-ligated and ligated DNA. The peak temperature represents the melt-temperature. The T_m temperature of non-ligated is around 55 °C, whereas the ligated complex is stable until 75 °C.

5.5.2 Proof of concept for DNA nanostructure signal suppression by high molecular weight anchor

Once we confirmed the formation of DNA nanostructure by T4 DNA ligation on the electrode surface and proved its stability, we tested our hypothesis of signal suppression by molecular anchor. Our understanding is that signal suppression should be due to the slowing down of the complex diffusion. So, the complex, specifically the redox moiety, should be diffusion limited and devoid of other interactions (double layer) which hinders hybridization. This led us to design a thiolated-DNA which placed the redox moiety at a distance of 4 to 10 (4A, 6A,

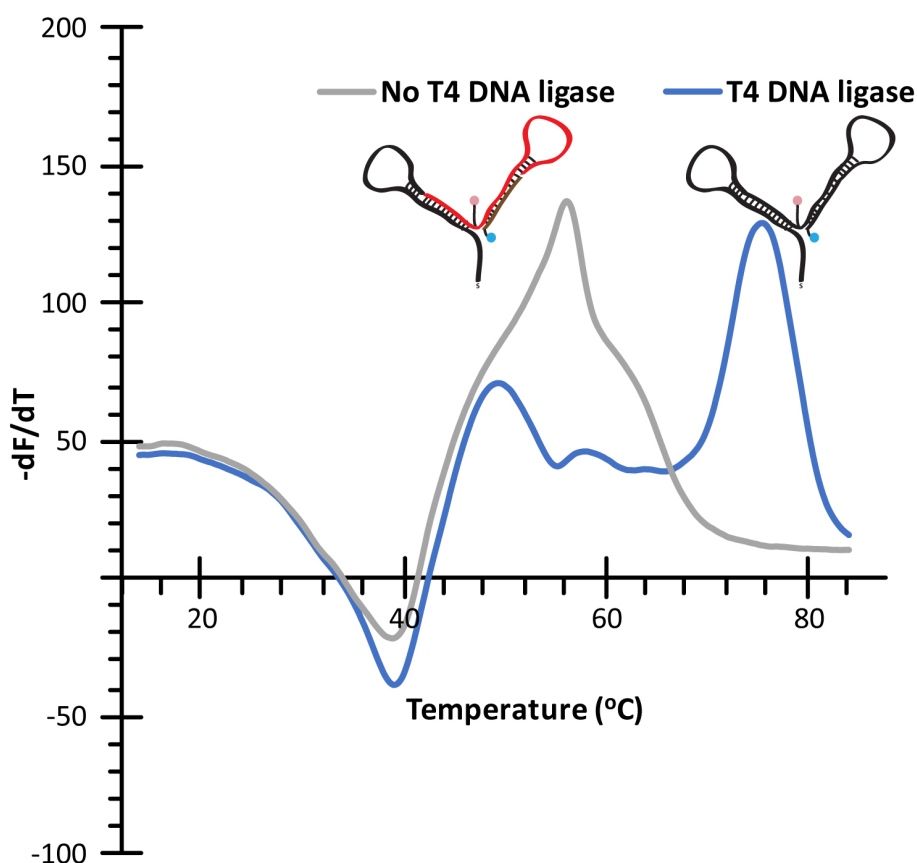


Figure 5.7: DNA nanostructure formation and stability by DNA melting analysis: To support the T4 DNA ligation formation the thermal fluometric analysis of ligated and non-ligated complex is compared. We observe the non-ligated complex melts at 60 °C, whereas ligated product is stable till 80 °C. This supports that T4 ligase is successful in ligation.

8A, and 10A) nucleotides from the surface. We did not use longer distances as we knew the signal would be minimal due to distance dependence. Figure: 5.8 shows the comparison of signal suppression by binding streptavidin (1 μM) to the nanostructure with 4A, 6A, 8A, and 10A spacers. As expected, the DNA nanostructure signal dropped as the redox moiety was placed far from the surface due to distance dependence. But the signal comparison between the four complexes after streptavidin was attached showed a similar response. We assume that the effects of distance were less pronounced due to the large protein attachment. To select the optimal complex for quantification, we compared the signal suppression. Obviously, the 4A complex underwent a larger signal suppression by streptavidin (or generally larger molecule), which will be sensitive among the four complex. For a small molecule competitor assay, a complex which can result in more signal gain is the suitable one. From the comparison, since

4A undergoes a large signal suppression, it can result in higher signal gain in displacement of an anchor molecule.

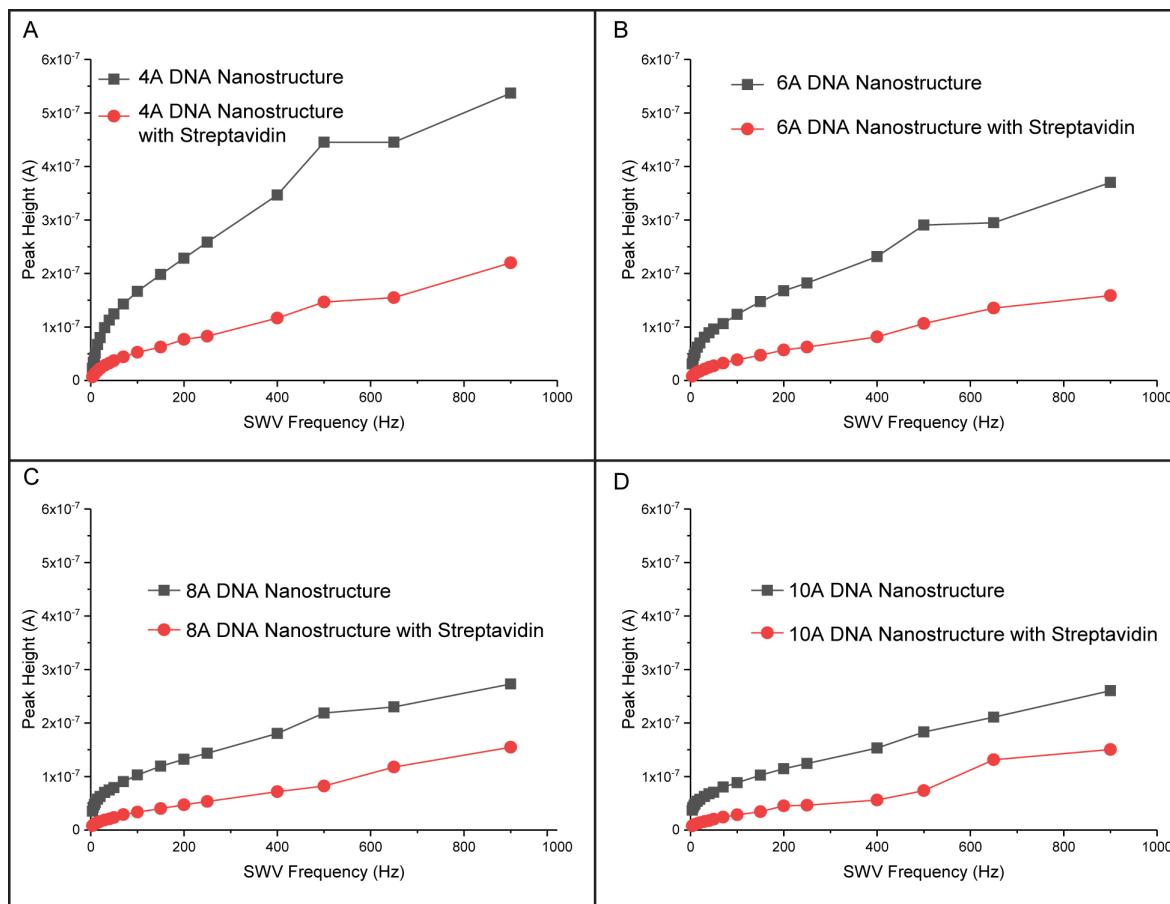


Figure 5.8: Proof-of-concept of signal suppression and comparison of various distance: Comparison of signal from four different complex, which places the redox moiety at a distance of 4A, 6A, 8A, and 10A. The result correlates our earlier distance dependence study. On comparison 4A undergoes large percentage of signal suppression.

We were expecting to use the SWV frequency to tune the signaling dimension of the assay. Even though the signal for 4A complex was larger, the critical time was lower than the window used (0.001 to 1000 ms), which is an important factor for SWV tuning. This also explains the reason for similar response for all SWV frequency used. In Chapter 6 (future work) we have discussed some strategies to make the critical time in the chosen frame usable to exploit the SWV frequency.

5.5.3 Streptavidin and biotin

Streptavidin and biotin were chosen to confirm our system for the following reasons: 1) They have the strongest known non-covalent binding ($K_d = 10^{-15}$ M), 2) streptavidin is a large protein molecule with 52.8 kDa, and biotin is a small molecule with 244.3 Da, which makes a good combination for our assay. We employed desthiobiotin as an anchor recognition unit in the connector DNA. Desthiobiotin is a biotin analogue which can bind with biotin-binding protein with lower affinity, i.e. higher K_d (10^{-12} M), compared to biotin, so the protein can be displaced by biotin effectively [106]. Figure: 5.9 shows the sensor response to different concentration of streptavidin, where we observed a dynamic range of 5 to 500 nM. By this data, streptavidin protein is directly measured by a signal-OFF amplification free electrochemical assay. Other than quantification of streptavidin, two more things are to be closely noted: 1) Higher concentration of streptavidin suppressed about 80 % of the signal, 2) the signal alteration by blank is very minimal. Together, this shows that the DNA nanostructure with the streptavidin can be used as a sensor for quantification of biotin. Figure: fig:strpmodel shows the biotin quantification model and sensor response with different concentration of biotin. We observed a good but narrow response to biotin (dynamic range is 5 to 50 μ M). This work shows our anchor model can also be used for quantification of small molecules by an indirect, signal-ON assay. In comparison, we observe streptavidin assay to be very sensitive. This is due to the four binding sites available in streptavidin. This multivalence nature helps streptavidin to bind effectively to the surface. In addition to this there is a need for excess biotin to compete and displace the streptavidin. In this work, we showed the same DNA nanostructure to be useful for detecting both larger proteins and small molecules.

5.5.4 Anti-digoxigenin and digoxigenin

To further test the generalizability of our approach, we have confirmed the assay with anti-digoxigenin antibodies and digoxigenin. The digoxigenin is used as an anchor recognition unit in connector-DNA. The same thiolated-DNA (anc4A-DNA) and MB-DNA were used, result of DNA nanostructure formation by T4 ligation enzyme. Figure: 5.10 shows the signal response

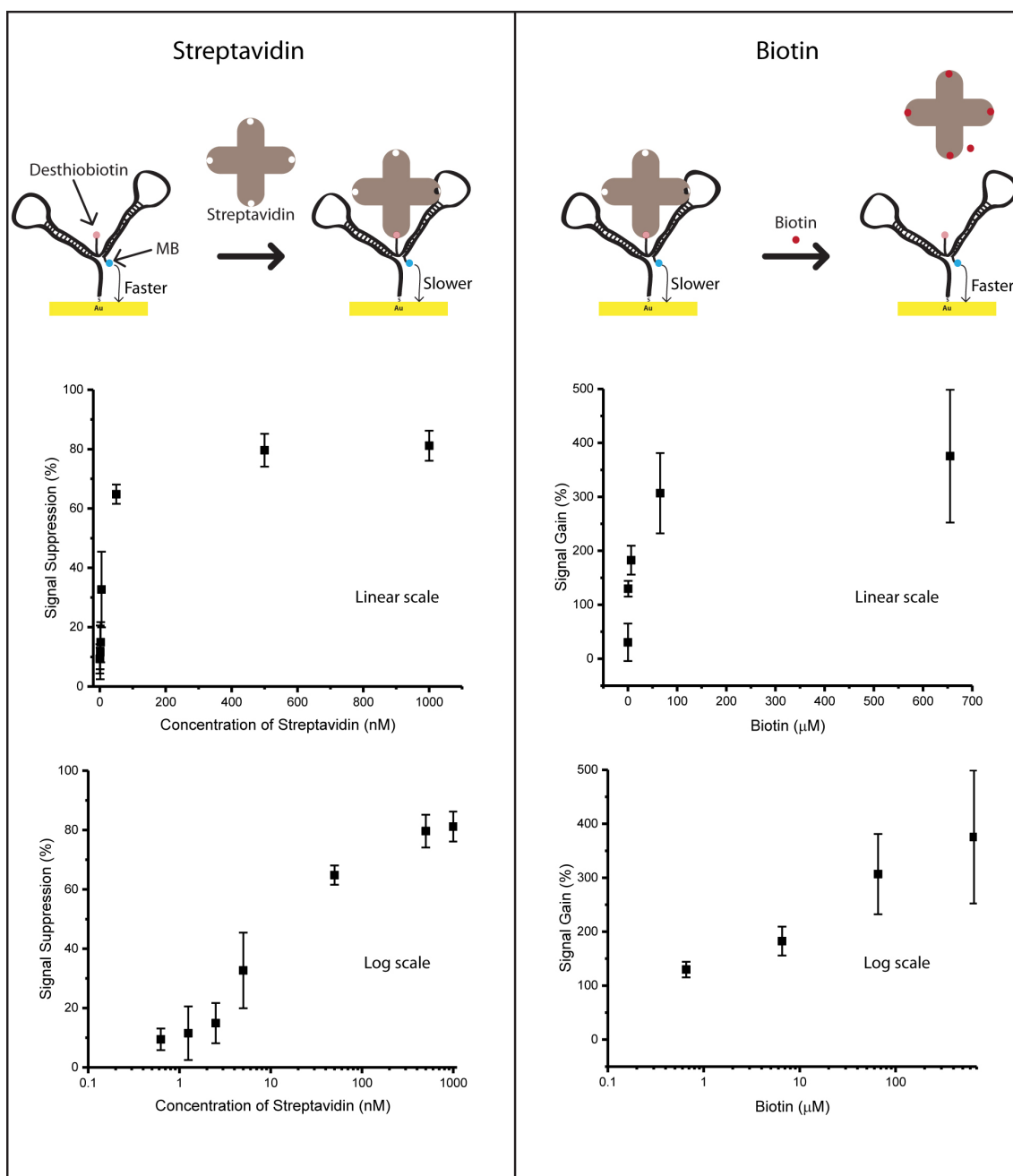


Figure 5.9: Streptavidin and biotin detection: Streptavidin is used as an anchor. Streptavidin is quantified as direct signal-OFF assay and biotin as indirect signal-ON assay. The dynamic range is 5 nM to 500 nM and 5 to 50 μM for streptavidin and biotin respectively. **Figures are not drawn in scale.**

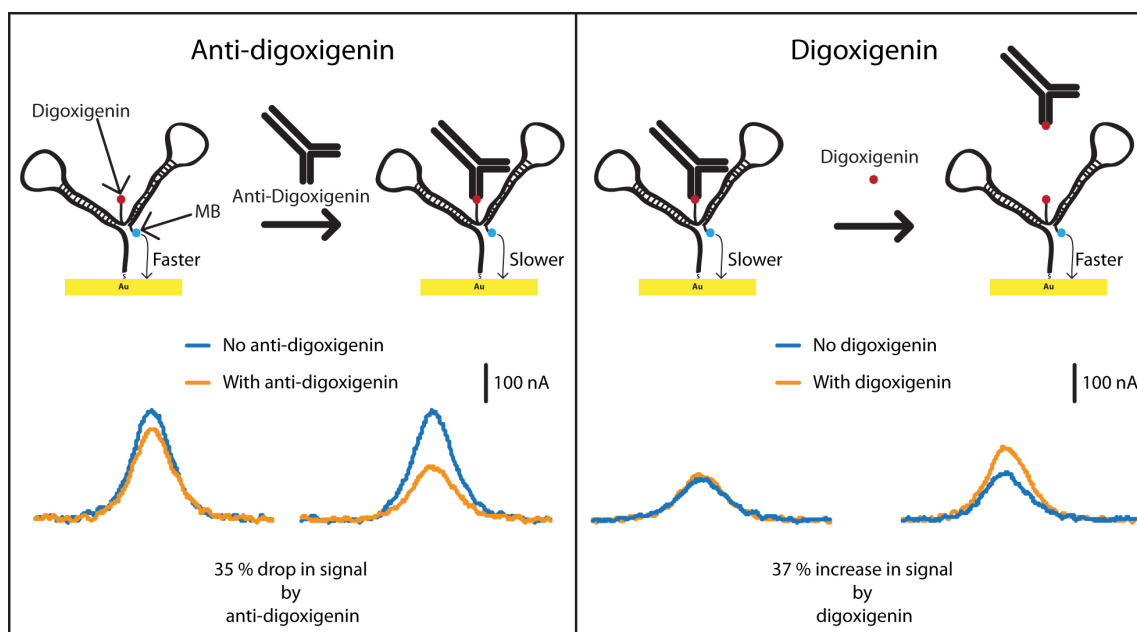


Figure 5.10: Anti-digoxigenin and digoxigenin detection: As a proof of concept for quantification of antibody and small molecule and to support generalizability of the sensor anti-digoxigenin and digoxigenin is detected. The sensor shows a good response to the target with 35% signal suppression by anti-digoxigenin anchor and 37% signal appreciation by digoxigenin.

for both anti-digoxigenin antibody and digoxigenin. On introduction of anti-digoxigenin antibody to the DNA nanostructure, we observed a 35% signal suppression. This is not seen in the absence of target. Similar results were observed with digoxigenin, where the digoxigenin displaces the antibody resulting in a 37% signal increase. This proves that the DNA nanostructure anchor model can be extended for quantification of both small molecules and large protein binding partners such as antibodies. As a development in this quantification, we assume that the binding energy of the anti-digoxigenin is lower, resulting in lower signal suppression. This affected the sensitivity in digoxigenin quantification. Multiple antibodies should be compared, and we expect that a more sensitive assay could be devised.

5.6 Conclusion

In this chapter, we have developed a versatile quantification strategy for both large proteins and small molecules. As a proof of concept, we successfully quantified streptavidin and biotin, as

a direct and indirect assay. The gold standard method like ELISA needs dual antibody system for effective quantification, and at present electrochemical sensors require conformational changing aptamers. We have shown a sensor which uses a single antibody and ignores conformational change of binding partners such as aptamers. This is supported by our results with digoxigenin, in which the sensor responded to both antibody and small molecule. Perhaps the most exciting feature is that the sensor is drop-and-read, and no reagents or enzymes are used for amplification, which simplifies the advancement of this method for a possible POC assay.

Chapter 6

Summary and future work

6.1 Summary

This dissertation work focused on the development and optimization of DNA-based electrochemical assays. The importance of temperature management, double layer effects, and the impact of the diffusion layer in these assays are explained. The results shown in the development of a single-branched oligonucleotide assay give promise for the application of quantifying microRNA. We also introduced new assay formats, structure-switching and steric hindrance assays, which exploit the molecular weight of the protein as an anchor for diffusion to quantify proteins and small molecules. For this reason, we made a DNA nanostructure on the surface of the electrode with the assistance of T4 DNA ligase. This novel method is generalizable, shown by detection of streptavidin, biotin, anti-digoxigenin, and digoxigenin. In addition to that, this is a drop-and-read method, which eliminates sample preparation steps, signaling substrate additions, or enzyme additions for amplification, giving the method great potential as a point-of-care (POC) system.

6.2 Future directions

6.2.1 Bistable switch DNA quantification model

With the understanding of diffusion layer effect from Chapter 3, we developed a quantification method for short length oligonucleotide. This exploits the bistable DNA strand displacement,

used as a noncovalent catalyst in Winfree lab [107]. Figure: 6.1 shows the electrochemical bistable switch model for DNA quantification. On addition of target DNA, undergoes an allosteric strand displacement placing the redox moiety into the diffusion layer, which is otherwise far. This results in increase in SWV signal, leading to a novel drop-and-read DNA quantification method.

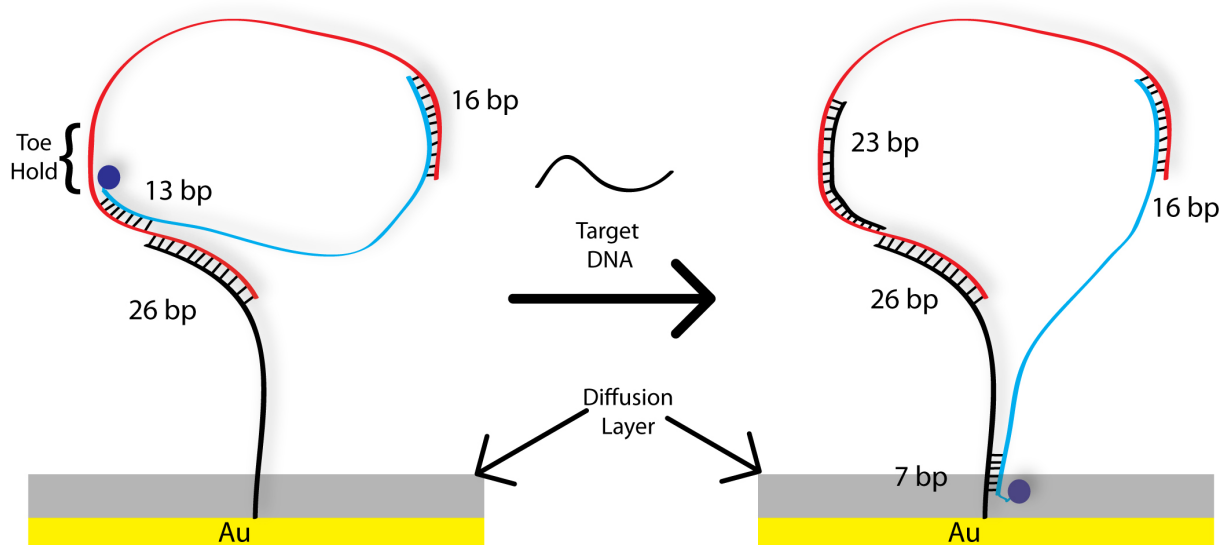


Figure 6.1: **Bistable switch DNA quantification model:**The target binds to the toe hold region and displaces the MB-DNA, which binds with thiolated-DNA closer to the surface placing the methylene blue in the diffusion layer.

Figure is not drawn in scale

6.2.2 Insulin Quantification

In Chapter 5, we showed that small molecules can be quantified indirectly with the DNA-nanostructure. In our perspective, the term “small molecule” is not limited to clinically relevant molecules less than 500 Da, but it also includes peptides and small proteins. To supports this, in our single-branched oligonucleotide quantification, target addition (21 nt) resulted in negligible signal loss (in the case of $n=14$, $m=10$), where the molecular weight of 21 nt is ~ 6825 Da. So, the next application of this method will be to quantify peptides and small proteins below 10 kDa. Insulin (~ 5.8 kDa) will be the first choice, since Dr. Easley's research work focuses on proteins involved in diabeties. Figure: Fig:insulinanchor shows a conceptual cartoon of the

design and expected SWV outcome on the assay.

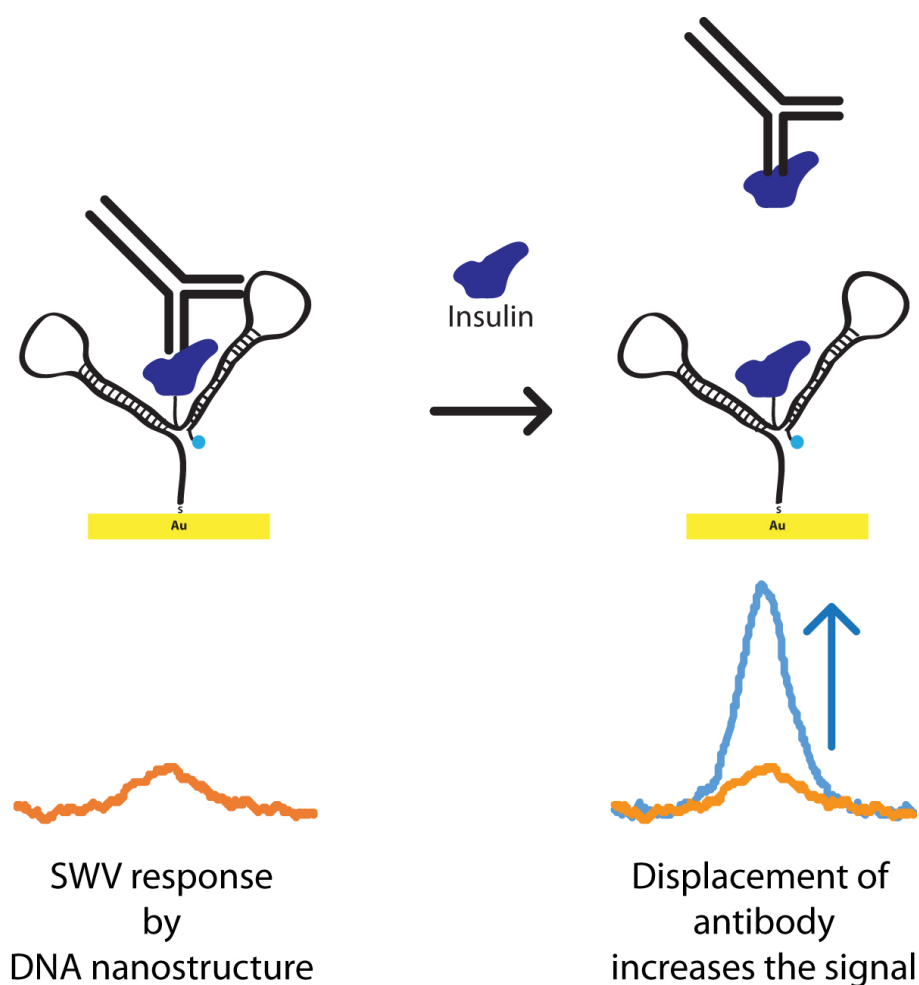


Figure 6.2: DNA nanostructure for insulin quantification

6.2.3 Optimizing the DNA nanostructure

In Chapter 5, we also observed that even though the DNA nanostructure gave good signal, the electrochemical kinetics were out of the practically observable window (0.001 to 1 s). The assay could be ratiometric or signal dimensions could be changed if the critical time was in our working window. To achieve this, the molecular weight of the DNA nanostructure should be reduced. Figure: 6.3 shows an example for reducing the molecular weight. PEG can be used as an alternative to DNA in the hairpin portion. Decreasing the binding energy also helps in decreasing in molecular weight (number of nucleotides reduced), and this does not largely affect the DNA nanostructure formation since the enzyme reaction is a non-equilibrium process that

is efficient at temperatures >20 deg C.

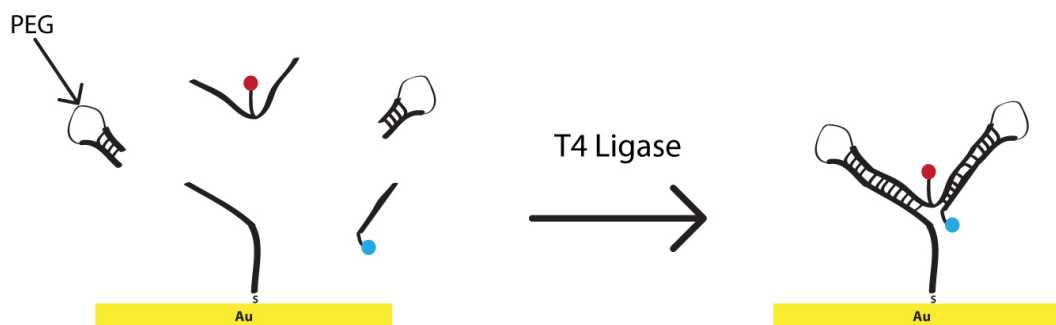


Figure 6.3: Optimizing the DNA nanostructure : Reducing the molecular weight of the DNA nanostructure is one way of improving the sensitivity. The figure shows a way to reduce the molecular weight by using PEG connector.

6.2.4 Real time measurement

Real-time measurements of clinically relevant molecules will be helpful in gaining a better understanding of physiological systems and useful in elucidating pharmacology of drugs. In most sensitive quantification methods, the usage of multiple substrates or enzymes limits them from having a real-time workflow. Electrochemical DNA-based sensors have the potential for real time measurement, proved by E-aptamer sensors developed by the Plaxco and Soh laboratories, which measured drug concentrations in serum of live animals [67]. We believe that the DNA nanostructure for small molecules can be applied for real time measurements. Figure: 6.4 shows the cartoon for a proposed method of making the nanostructure capable of realtime quantification. In this case the anchor is attached to the surface with a long thiolated-DNA as shown in the figure, and T4 DNA ligase can be used to achieve this. Initially the antibody will be anchoring the DNA nanostructure, resulting in lower signal. When the sample is introduced, the antibody will be displaced, which increases the signal. When there is a drop in the concentration of the target in bulk solution, due to the equilibrium nature of the binding, the target will be lost by the antibody, resulting in anchoring the nanostructure once more. Of course, it will be important to characterize and perhaps control binding constants for this purpose.

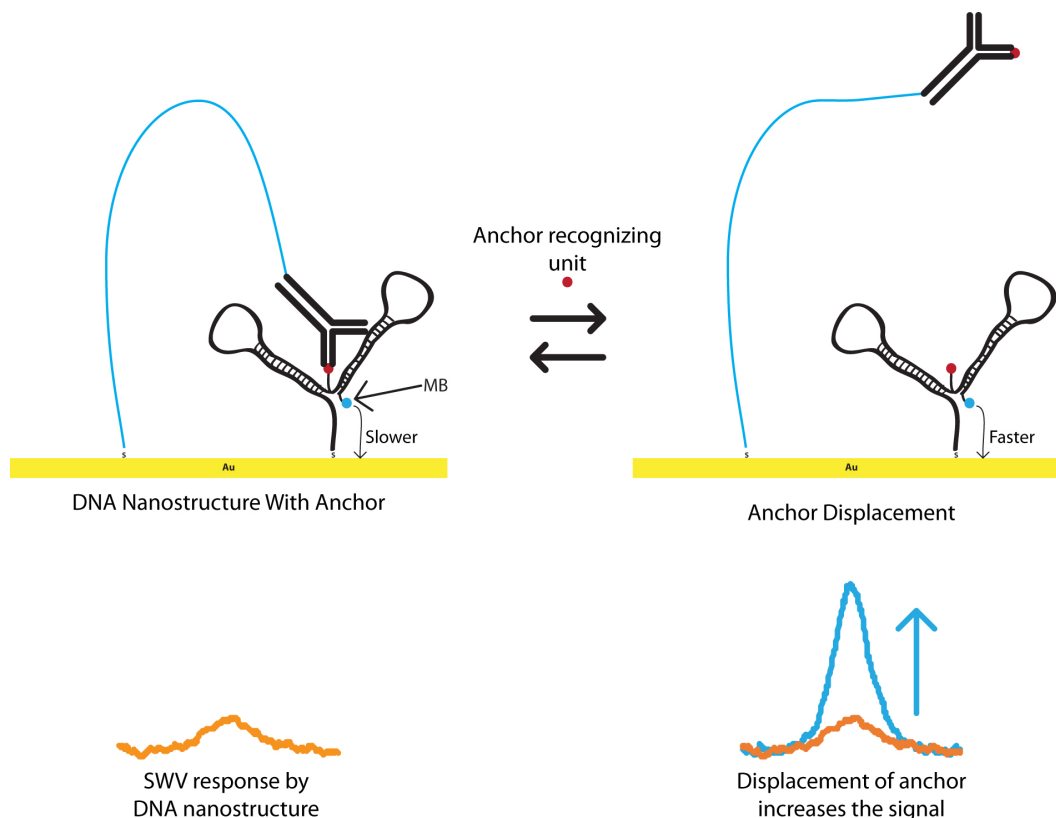


Figure 6.4: Real time measurement of small molecules using DNA nanostructure model: DNA nanostructure is formed on the surface, simultaneously antibody tagged with the long DNA (~100 nt) is attached to the surface. This antibody binds with the anchor recognition unit in the DNA nanostructure. When the target is introduced the antibody binds with target in the bulk solution resulting in increase in the signal. We also believe that reverse process also possible.

6.2.5 Impact of this work on future systems

Overall this work gives a better understanding of SWV signal in DNA-based sensor, which help in developing and optimizing real-time electrochemical sensor for small molecule, protein, and oligonucleotide. This will be helpful in Dr. Easley lab's goal of understanding the dynamic function of endocrine tissues.

References

- [1] Leroy Hood, James R. Heath, Michael E. Phelps, and Biaoyang Lin. Systems Biology and New Technologies Enable Predictive and Preventative Medicine. Science, 306(5696):640–643, 2004.
- [2] Mahmoud Labib, Edward H. Sargent, and Shana O. Kelley. Electrochemical Methods for the Analysis of Clinically Relevant Biomolecules. Chemical Reviews, 116(16):9001–9090, aug 2016.
- [3] P. L. Mage, B. S. Ferguson, D. Maliniak, K. L. Ploense, T. E. Kippin, and H. T. Soh. Closed-loop control of circulating drug levels in live animals. Nature Biomedical Engineering, 1(5):0070, may 2017.
- [4] Y M Lo, T H Rainer, L Y Chan, N M Hjelm, and R A Cocks. Plasma DNA as a prognostic marker in trauma patients. Clinical chemistry, 46(3):319–323, mar 2000.
- [5] Christine P-Y Chang, Rhu-Hsin Chia, Tsu-Lan Wu, Kuo-Chien Tsao, Chien-Feng Sun, and James T Wu. Elevated cell-free serum DNA detected in patients with myocardial infarction. Clinica chimica acta; international journal of clinical chemistry, 327(1-2):95–101, jan 2003.
- [6] Catherine Alix-Panabières and Klaus Pantel. Challenges in circulating tumour cell research. Nature Reviews Cancer, 14(9):623–631, jul 2014.
- [7] N Leigh Anderson and Norman G Anderson. The human plasma proteome: history, character, and diagnostic prospects. Molecular & cellular proteomics : MCP, 1(11):845–867, nov 2002.

- [8] Hoon Young Kong and Jonghoe Byun. Nucleic Acid aptamers: new methods for selection, stabilization, and application in biomedical science. Biomolecules & therapeutics, 21(6):423–434, nov 2013.
- [9] Andrew D. Ellington and Jack W. Szostak. In vitro selection of RNA molecules that bind specific ligands. Nature, 346(6287):818–822, aug 1990.
- [10] Tao Bing, Hongcheng Mei, Nan Zhang, Cui Qi, Xiangjun Liu, and Dihua Shangguan. Exact tailoring of an ATP controlled streptavidin binding aptamer. RSC Advances, 4(29):15111, mar 2014.
- [11] Gerd-Uwe Flechsig, Jörg Peter, Gerhard Hartwich, , § Joseph Wang, and Peter Gründler. DNA Hybridization Detection at Heated Electrodes. Langmuir, 21(17):7848–7853, 2005.
- [12] Eva Engvall and Peter Perlmann. Enzyme-linked immunosorbent assay (ELISA) quantitative assay of immunoglobulin G. Immunochemistry, 8(9):871–874, sep 1971.
- [13] B K. Van Weemen and A H.W.M. Schuurs. Immunoassay using antigen-enzyme conjugates. FEBS letters, 15(3):232–236, jun 1971.
- [14] Eva Engvall. The ELISA, Enzyme-Linked Immunosorbent Assay. Clinical Chemistry, 56(2):319–320, 2010.
- [15] Rudolf M Lequin. Enzyme immunoassay (EIA)/enzyme-linked immunosorbent assay (ELISA). Clinical chemistry, 51(12):2415–8, dec 2005.
- [16] T Porstmann and S T Kiessig. Enzyme immunoassay techniques. An overview. Journal of immunological methods, 150(1-2):5–21, jun 1992.
- [17] David A. Giljohann and Chad A. Mirkin. Drivers of biodiagnostic development. Nature, 462(7272):461–464, nov 2009.

- [18] Balenahalli N Ramesh, T S Sathyanarayana Rao, Annamalai Prakasam, Kumar Sambamurti, and K S Jagannatha Rao. Neuronutrition and Alzheimer's disease. Journal of Alzheimer's disease : JAD, 19(4):1123–39, 2010.
- [19] Pothur R Srinivas, Barnett S Kramer, and Sudhir Srivastava. Trends in biomarker research for cancer detection. The Lancet Oncology, 2(11):698–704, nov 2001.
- [20] David M Rissin, Cheuk W Kan, Todd G Campbell, Stuart C Howes, David R Fournier, Linan Song, Tomasz Piech, Purvish P Patel, Lei Chang, Andrew J Rivnak, Evan P Ferrell, Jeffrey D Randall, Gail K Provuncher, David R Walt, and David C Duffy. Single-molecule enzyme-linked immunosorbent assay detects serum proteins at subfemtomolar concentrations. Nature Biotechnology, 28(6):595–599, jun 2010.
- [21] David M. Rissin, Hans H. Gorris, and David R. Walt. Distinct and Long-Lived Activity States of Single Enzyme Molecules. Journal of the American Chemical Society, 130(15):5349–5353, apr 2008.
- [22] David M. Rissin and David R. Walt. Digital Concentration Readout of Single Enzyme Molecules Using Femtoliter Arrays and Poisson Statistics. Nano Letters, 6(3):520–523, 2006.
- [23] David M. Rissin and David R. Walt. Digital Readout of Target Binding with Attomole Detection Limits via Enzyme Amplification in Femtoliter Arrays. Journal of the American Chemical Society, 128(19):6286–6287, 2006.
- [24] Lucille Beaudet, Roberto Rodriguez-Suarez, Marie-Hélène Venne, Mireille Caron, Julie Bédard, Véronique Brechler, Stéphane Parent, and Martina Bielefeld-Sévigny. AlphaLISA immunoassays: the no-wash alternative to ELISAs for research and drug discovery. Nature Methods, 5, 2008.
- [25] E F Ullman, H Kirakossian, S Singh, Z P Wu, B R Irvin, J S Pease, A C Switchenko, J D Irvine, A Dafforn, and C N Skold. Luminescent oxygen channeling immunoassay: measurement of particle binding kinetics by chemiluminescence. Proceedings of the

- National Academy of Sciences of the United States of America, 91(12):5426–5430, jun 1994.
- [26] E F Ullman, H Kirakossian, A C Switchenko, J Ishkanian, M Ericson, C A Wartchow, M Pirio, J Pease, B R Irvin, S Singh, R Singh, R Patel, A Dafforn, D Davalian, C Skold, N Kurn, and D B Wagner. Luminescent oxygen channeling assay (LOCI): sensitive, broadly applicable homogeneous immunoassay method. Clinical chemistry, 42(9):1518–1526, sep 1996.
- [27] Tomasz Heyduk. Practical biophysics: Sensors for rapid detection of biological targets utilizing target-induced oligonucleotide annealing. Biophysical Chemistry, 151(3):91–95, oct 2010.
- [28] Feng Li, Hongquan Zhang, Zhixin Wang, Xukun Li, Xing-Fang Li, and X. Chris Le. Dynamic DNA Assemblies Mediated by Binding-Induced DNA Strand Displacement. Journal of the American Chemical Society, 135(7):2443–2446, feb 2013.
- [29] Hongquan Zhang, Xing-Fang Li, and X. Chris Le. Binding-Induced DNA Assembly and Its Application to Yoctomole Detection of Proteins. Analytical Chemistry, 84(2):877–884, jan 2012.
- [30] Hongquan Zhang, Feng Li, Brittany Dever, Chuan Wang, Xing-Fang Li, and X. Chris Le. Assembling DNA through Affinity Binding to Achieve Ultrasensitive Protein Detection. Angewandte Chemie International Edition, 52(41):10698–10705, oct 2013.
- [31] Simon Fredriksson, Mats Gullberg, Jonas Jarvius, Charlotta Olsson, Kristian Pietras, Sigrún Margrét Gústafsdóttir, Arne Östman, and Ulf Landegren. Protein detection using proximity-dependent DNA ligation assays. Nature Biotechnology, 20(5):473–477, may 2002.

- [32] Mats Gullberg, Sigrún M Gústafsdóttir, Edith Schallmeiner, Jonas Jarvius, Mattias Bjarnegård, Christer Betsholtz, Ulf Landegren, and Simon Fredriksson. Cytokine detection by antibody-based proximity ligation. Proceedings of the National Academy of Sciences of the United States of America, 101(22):8420–8424, jun 2004.
- [33] Ewa Heyduk and Tomasz Heyduk. Nucleic acid-based fluorescence sensors for detecting proteins. Analytical chemistry, 77(4):1147–1156, feb 2005.
- [34] Ewa Heyduk, Benjamin Dummit, Yie-Hwa Chang, and Tomasz Heyduk. Molecular Pincers: Antibody-Based Homogeneous Protein Sensors. Analytical Chemistry, 80(13):5152–5159, jul 2008.
- [35] Jiaming Hu, Tanyu Wang, Joonyul Kim, Curtis Shannon, and Christopher J. Easley. Quantitation of Femtomolar Protein Levels via Direct Readout with the Electrochemical Proximity Assay. Journal of the American Chemical Society, 134(16):7066–7072, apr 2012.
- [36] Jiaming Hu, Yajiao Yu, Jessica C. Brooks, Leah A. Godwin, Subramaniam Somasundaram, Ferdous Torabinejad, Joonyul Kim, Curtis Shannon, and Christopher J. Easley. A Reusable Electrochemical Proximity Assay for Highly Selective, Real-Time Protein Quantitation in Biological Matrices. Journal of the American Chemical Society, 136(23):8467–8474, jun 2014.
- [37] Kewei Ren, Jie Wu, Feng Yan, and Huangxian Ju. Ratiometric electrochemical proximity assay for sensitive one-step protein detection. Scientific Reports, 4(1):4360, may 2014.
- [38] Yan-Li Zhang, Yong Huang, Jian-Hui Jiang, Guo-Li Shen, and Ru-Qin Yu. Electrochemical Aptasensor Based on Proximity-Dependent Surface Hybridization Assay for Single-Step, Reusable, Sensitive Protein Detection. J. AM. CHEM. SOC., 129:15448–15449, 2007.

- [39] Yan-Li Zhang, Peng-Fei Pang, Jian-Hui Jiang, Guo-Li Shen, and Ru-Qin Yu. Electrochemical Aptasensor Based on Proximity-Dependent Surface Hybridization Assay for Protein Detection. Electroanalysis, 21(11):1327–1333, jun 2009.
- [40] Lauren R. Schoukroun-Barnes, Florika C. Macazo, Brenda Gutierrez, Justine Lottermoser, Juan Liu, and Ryan J. White. Reagentless, Structure-Switching, Electrochemical Aptamer-Based Sensors. Annual Review of Analytical Chemistry, 9(1):163–181, jun 2016.
- [41] Andreas C. Schmidt, Xin Wang, Yuntian Zhu, and Leslie A. Sombers. Carbon Nanotube Yarn Electrodes for Enhanced Detection of Neurotransmitter Dynamics in Live Brain Tissue. ACS Nano, 7(9):7864–7873, sep 2013.
- [42] Janet G. Osteryoung and Robert A. Osteryoung. Square wave voltammetry. Analytical Chemistry, 57(1):101A–110A, 1985.
- [43] Janet Osteryoung. Pulse voltammetry. Journal of Chemical Education, 60(4):296, apr 1983.
- [44] Chunhai Fan, Kevin W Plaxco, and Alan J Heeger. Electrochemical interrogation of conformational changes as a reagentless method for the sequence-specific detection of DNA. Proceedings of the National Academy of Sciences of the United States of America, 100(16):9134–9137, aug 2003.
- [45] Yi Xiao, Arica A. Lubin, Alan J. Heeger, and Kevin W. Plaxco. Label-Free Electronic Detection of Thrombin in Blood Serum by Using an Aptamer-Based Sensor. Angewandte Chemie International Edition, 44(34):5456–5459, aug 2005.
- [46] Jianwei J Li, Xiaohong Fang, and Weihong Tan. Molecular aptamer beacons for real-time protein recognition. Biochemical and biophysical research communications, 292(1):31–40, mar 2002.

- [47] Francesco Ricci, Rebecca Y. Lai, and Kevin W. Plaxco. Linear, redox modified DNA probes as electrochemical DNA sensors. Chemical Communications, 0(36):3768, sep 2007.
- [48] Lauren R. Schoukroun-Barnes, Ethan P. Glaser, and Ryan J. White. Heterogeneous Electrochemical Aptamer-Based Sensor Surfaces for Controlled Sensor Response. Langmuir, 31(23):6563–6569, jun 2015.
- [49] Ryan J. White and Kevin W. Plaxco. Exploiting Binding-Induced Changes in Probe Flexibility for the Optimization of Electrochemical Biosensors. Analytical Chemistry, 82(1):73–76, jan 2010.
- [50] Abd-Elgawad Radi and Ciara K. O’Sullivan. Aptamer conformational switch as sensitive electrochemical biosensor for potassium ion recognition. Chemical Communications, 0(32):3432, aug 2006.
- [51] Brian R. Baker, Rebecca Y. Lai, McCall S. Wood, Elaine H. Doctor, Alan J. Heeger, and Kevin W. Plaxco. An Electronic, Aptamer-Based Small-Molecule Sensor for the Rapid, Label-Free Detection of Cocaine in Adulterated Samples and Biological Fluids. J. AM. CHEM. SOC., 128:3138–3139, 2006.
- [52] Xiaolei Zuo, Shiping Song, Jiong Zhang, Dun Pan, Lihua Wang, and Chunhai Fan. A Target-Responsive Electrochemical Aptamer Switch (TREAS) for Reagentless Detection of Nanomolar ATP. J. AM. CHEM. SOC., 129:1042–1043, 2007.
- [53] Elena E. Ferapontova, Eva M. Olsen, , and Kurt V. Gothelf. An RNA Aptamer-Based Electrochemical Biosensor for Detection of Theophylline in Serum. J. AM. CHEM. SOC., 130:4256–4258, 2008.
- [54] Rebecca Y. Lai, Kevin W. Plaxco, and Alan J. Heeger. Aptamer-Based Electrochemical Detection of Picomolar Platelet-Derived Growth Factor Directly in Blood Serum. Anal. Chem., 79:229–233, 2006.

- [55] Alexis Vallée-Bélisle, Francesco Ricci, Takanori Uzawa, Fan Xia, and Kevin W. Plaxco. Bioelectrochemical Switches for the Quantitative Detection of Antibodies Directly in Whole Blood. Journal of the American Chemical Society, 134(37):15197–15200, sep 2012.
- [56] Ryan J. White, Hannah M. Kallewaard, Wen Hsieh, Adriana S. Patterson, Jesse B. Kasehagen, Kevin J. Cash, Takanori Uzawa, H. Tom Soh, and Kevin W. Plaxco. Wash-free, Electrochemical Platform for the Quantitative, Multiplexed Detection of Specific Antibodies. Analytical Chemistry, 84(2):1098–1103, jan 2012.
- [57] Di Kang, Sheng Sun, Martin Kurnik, Demosthenes Morales, Frederick W. Dahlquist, and Kevin W. Plaxco. New Architecture for Reagentless, Protein-Based Electrochemical Biosensors. Journal of the American Chemical Society, 139(35):12113–12116, sep 2017.
- [58] Ying Liu, Timothy Kwa, and Alexander Revzin. Simultaneous detection of cell-secreted TNF- α and IFN- γ using micropatterned aptamer-modified electrodes. Biomaterials, 33(30):7347–7355, oct 2012.
- [59] Ying Liu, Ying Liu, Zimple Matharu, Ali Rahimian, and Alexander Revzin. Detecting multiple cell-secreted cytokines from the same aptamer-functionalized electrode. Biosensors and Bioelectronics, 64:43–50, feb 2015.
- [60] Qing Zhou, Timothy Kwa, Yandong Gao, Ying Liu, Ali Rahimian, and Alexander Revzin. On-chip regeneration of aptasensors for monitoring cell secretion. Lab on a chip, 14(2):276–279, jan 2014.
- [61] Agnè S Anne, Agnè S Bouchardon, and Jacques Moiroux. 3-Ferrocene-Labeled Oligonucleotide Chains End-Tethered to Gold Electrode Surfaces: Novel Model Systems for Exploring Flexibility of Short DNA Using Cyclic Voltammetry. J. AM. CHEM. SOC, 125:1112–1113, 2003.

- [62] Andrea Idili, Alessia Amodio, Marco Vidonis, Jacob Feinberg-Somerson, Matteo Castonovo, and Francesco Ricci. Folding-Upon-Binding and Signal-On Electrochemical DNA Sensor with High Affinity and Specificity. Analytical Chemistry, 86(18):9013–9019, sep 2014.
- [63] Tanyu Wang, Emilie Viennois, Didier Merlin, and Gangli Wang. Microelectrode miRNA Sensors Enabled by Enzymeless Electrochemical Signal Amplification. Analytical Chemistry, 87(16):8173–8180, aug 2015.
- [64] Di Kang, Alexis Vallée-Bélisle, Alessandro Porchetta, Kevin W. Plaxco, and Francesco Ricci. Re-engineering Electrochemical Biosensors To Narrow or Extend Their Useful Dynamic Range. Angewandte Chemie International Edition, 51(27):6717–6721, jul 2012.
- [65] Ryan J White, Aaron A Rowe, and Kevin W Plaxco. Re-engineering aptamers to support reagentless, self-reporting electrochemical sensors. The Analyst, 135(3):589–594, mar 2010.
- [66] Ryan J White, Noelle Phares, Arica A Lubin, Yi Xiao, and Kevin W Plaxco. Optimization of electrochemical aptamer-based sensors via optimization of probe packing density and surface chemistry. Langmuir : the ACS journal of surfaces and colloids, 24(18):10513–10518, sep 2008.
- [67] Brian Scott Ferguson, David A Hoggarth, Dan Maliniak, Kyle Ploense, Ryan J White, Nick Woodward, Kuangwen Hsieh, Andrew J Bonham, Michael Eisenstein, Tod E Kippin, Kevin W Plaxco, and Hyongsok Tom Soh. Real-time, aptamer-based tracking of circulating therapeutic agents in living animals. Science translational medicine, 5(213):213ra165, nov 2013.
- [68] Netzahualcóyotl Arroyo-Currás, Jacob Somerson, Philip A Vieira, Kyle L Ploense, Tod E Kippin, and Kevin W Plaxco. Real-time measurement of small molecules directly in awake, ambulatory animals. Proceedings of the National Academy of Sciences of the United States of America, 114(4):645–650, jan 2017.

- [69] Hui Li, Netzahualcóyotl Arroyo-Currás, Di Kang, Francesco Ricci, and Kevin W. Plaxco. Dual-Reporter Drift Correction To Enhance the Performance of Electrochemical Aptamer-Based Sensors in Whole Blood. Journal of the American Chemical Society, 138(49):15809–15812, dec 2016.
- [70] Hui Li, Philippe Dauphin-Ducharme, Gabriel Ortega, and Kevin W. Plaxco. Calibration-Free Electrochemical Biosensors Supporting Accurate Molecular Measurements Directly in Undiluted Whole Blood. Journal of the American Chemical Society, 139(32):11207–11213, aug 2017.
- [71] Ying Lu, Ningning Zhu, Ping Yu, and Lanqun Mao. Aptamer-based electrochemical sensors that are not based on the target binding-induced conformational change of aptamers. The Analyst, 133(9):1256, aug 2008.
- [72] Jagotamoy Das and Shana O. Kelley. Protein Detection Using Arrayed Microsensor Chips: Tuning Sensor Footprint to Achieve Ultrasensitive Readout of CA-125 in Serum and Whole Blood. Analytical Chemistry, 83(4):1167–1172, feb 2011.
- [73] Sahar Sadat Mahshid, Sébastien Camiré, Francesco Ricci, and Alexis Vallée-Bélisle. A Highly Selective Electrochemical DNA-Based Sensor That Employs Steric Hindrance Effects to Detect Proteins Directly in Whole Blood. Journal of the American Chemical Society, 137(50):15596–15599, dec 2015.
- [74] Alan K H Cheng, Bixia Ge, and Hua-Zhong Yu. Aptamer-Based Biosensors for Label-Free Voltammetric Detection of Lysozyme. Anal Chem, 79:5158–5164, 2007.
- [75] Justin D. Besant, Jagotamoy Das, Edward H. Sargent, and Shana O. Kelley. Proximal Bacterial Lysis and Detection in Nanoliter Wells Using Electrochemistry. ACS Nano, 7(9):8183–8189, sep 2013.
- [76] Jagotamoy Das, Ivaylo Ivanov, Edward H. Sargent, and Shana O. Kelley. DNA Clutch Probes for Circulating Tumor DNA Analysis. Journal of the American Chemical Society, 138(34):11009–11016, aug 2016.

- [77] Jagotamoy Das and Shana O. Kelley. Tuning the Bacterial Detection Sensitivity of Nanostructured Microelectrodes. Analytical Chemistry, 85(15):7333–7338, aug 2013.
- [78] Zhichao Fang, Leyla Soleymani, Georgios Pampalakis, Maisa Yoshimoto, Jeremy A. Squire, Edward H. Sargent, and Shana O. Kelley. Direct Profiling of Cancer Biomarkers in Tumor Tissue Using a Multiplexed Nanostructured Microelectrode Integrated Circuit. ACS Nano, 3(10):3207–3213, oct 2009.
- [79] Sahar S. Mahshid, Francesco Ricci, Shana O. Kelley, and Alexis Vallée-Bélisle. Electrochemical DNA-Based Immunoassay That Employs Steric Hindrance To Detect Small Molecules Directly in Whole Blood. ACS Sensors, 2(6):718–723, jun 2017.
- [80] Sahar Sadat Mahshid, Alexis Vallée-Bélisle, and Shana O. Kelley. Biomolecular Steric Hindrance Effects Are Enhanced on Nanostructured Microelectrodes. Analytical Chemistry, 89(18):9751–9757, sep 2017.
- [81] Wendi Zhou, Sahar S. Mahshid, Weijia Wang, Alexis Vallée-Bélisle, Peter W. Zandstra, Edward H. Sargent, and Shana O. Kelley. Steric Hindrance Assay for Secreted Factors in Stem Cell Culture. ACS Sensors, 2(4):495–500, apr 2017.
- [82] Klaus Jung, Jürgen Zachow, Michael Lein, Brigitte Brux, Pranav Sinha, Severin Lenk, Dietmar Schnorr, and Stefan A Loening. Rapid detection of elevated prostate-specific antigen levels in blood: performance of various membrane strip tests compared. Urology, 53(1):155–160, jan 1999.
- [83] Luis Sorell Gómez and Gertrudis Rojas. A simple visual immunoassay (VIA) for rapid identification of high lipoprotein(a) blood levels. Clinica Chimica Acta, 260(1):65–71, apr 1997.
- [84] Megan A. Mann and Lawrence A. Bottomley. Cyclic Square Wave Voltammetry of Surface-Confined Quasireversible Electron Transfer Reactions. Langmuir, 31(34):9511–9520, sep 2015.

- [85] A W Peterson, R J Heaton, and R M Georgiadis. The effect of surface probe density on DNA hybridization. Nucleic acids research, 29(24):5163–5168, dec 2001.
- [86] Kuan-Chun Huang and Ryan J. White. Random Walk on a Leash: A Simple Single-Molecule Diffusion Model for Surface-Tethered Redox Molecules with Flexible Linkers. Journal of the American Chemical Society, 135(34):12808–12817, aug 2013.
- [87] Daniel J Fish, M Todd Horne, Greg P Brewood, Jim P Goodarzi, Saba Alemayehu, Ashwini Bhandiwad, Robert P Searles, and Albert S Benight. DNA multiplex hybridization on microarrays and thermodynamic stability in solution: a direct comparison. Nucleic acids research, 35(21):7197–7208, 2007.
- [88] Arnold Vainrub and B. Montgomery Pettitt. Surface electrostatic effects in oligonucleotide microarrays: Control and optimization of binding thermodynamics. Biopolymers, 68(2):265–270, feb 2003.
- [89] Šebojka Komorsky-Lovrić and Milivoj Lovrić. Kinetic measurements of a surface confined redox reaction. Analytica Chimica Acta, 305(1-3):248–255, apr 1995.
- [90] Zbigniew Stojek. The Electrical Double Layer and Its Structure. In Electroanalytical Methods, pages 3–9. Springer Berlin Heidelberg, Berlin, Heidelberg, 2010.
- [91] Zuliang Shen, Herman O. Sintim, and Steve Semancik. Rapid nucleic acid melting analyses using a microfabricated electrochemical platform. Analytica Chimica Acta, 853:265–270, jan 2015.
- [92] Rebecca Y Lai, Eric T Lagally, Sang-Ho Lee, H T Soh, Kevin W Plaxco, and Alan J Heeger. Rapid, sequence-specific detection of unpurified PCR amplicons via a reusable, electrochemical sensor. Proceedings of the National Academy of Sciences of the United States of America, 103(11):4017–4021, mar 2006.
- [93] Rebecca Y. Lai. Chapter Eight Folding- and Dynamics-Based Electrochemical DNA Sensors. In Methods in Enzymology, volume 589, pages 221–252. 2017.

- [94] Adriana Patterson, Felice Caprio, Alexis Vallee-Belisle, Danila Moscone, Kevin W. Plaxco, Giuseppe Palleschi, and Francesco Ricci. Using Triplex-Forming Oligonucleotide Probes for the Reagentless, Electrochemical Detection of Double-Stranded DNA. Analytical Chemistry, 82(21):9109–9115, nov 2010.
- [95] Kevin A. Peterlinz and Rosina M. Georgiadis. Observation of Hybridization and Dehybridization of Thiol-Tethered DNA Using Two-Color Surface Plasmon Resonance Spectroscopy. J. Am. Chem. Soc., 119(14):3401–3402, 1997.
- [96] Zuliang Shen, Shizuka Nakayama, Steve Semancik, and Herman O. Sintim. Signal-on electrochemical Y or junction probe detection of nucleic acid. Chemical Communications, 48(61):7580, jul 2012.
- [97] Jagotamoy Das, Ivaylo Ivanov, Laura Montermini, Janusz Rak, Edward H. Sargent, and Shana O. Kelley. An electrochemical clamp assay for direct, rapid analysis of circulating nucleic acids in serum. Nature Chemistry, 7(7):569–575, jun 2015.
- [98] Takanori Uzawa, Ryan R. Cheng, Ryan J. White, Dmitrii E. Makarov, and Kevin W. Plaxco. A Mechanistic Study of Electron Transfer from the Distal Termini of Electrode-Bound, Single-Stranded DNAs. Journal of the American Chemical Society, 132(45):16120–16126, nov 2010.
- [99] Allen H. J. Yang, Kuangwen Hsieh, Adriana S. Patterson, B. Scott Ferguson, Michael Eisenstein, Kevin W. Plaxco, and H. Tom Soh. Accurate Zygote-Specific Discrimination of Single-Nucleotide Polymorphisms Using Microfluidic Electrochemical DNA Melting Curves. Angewandte Chemie International Edition, 53(12):3163–3167, mar 2014.
- [100] Joonyul Kim, Juan Hu, Andresa B. Bezerra, Mark D. Holtan, Jessica C. Brooks, and Christopher J. Easley. Protein Quantification Using Controlled DNA Melting Transitions in Bivalent Probe Assemblies. Analytical Chemistry, 87(19):9576–9579, oct 2015.
- [101] Jessica C. Brooks, Katarena I. Ford, Dylan H. Holder, Mark D. Holtan, and Christopher J. Easley. Macro-to-micro interfacing to microfluidic channels using 3D-printed

- templates: application to time-resolved secretion sampling of endocrine tissue. The Analyst, 141(20):5714–5721, 2016.
- [102] Carly A Holstein, Maryclare Griffin, Jing Hong, and Paul D Sampson. Statistical Method for Determining and Comparing Limits of Detection of Bioassays. Analytical Chemistry, 87(19):9795–9801, 2015.
- [103] Andrew J Bonham, Nicole G Paden, Francesco Ricci, and Kevin W Plaxco. Detection of IP-10 protein marker in undiluted blood serum via an electrochemical E-DNA scaffold sensor. Analyst, 138(19):5580–5583, oct 2013.
- [104] Kevin J. Cash, Francesco Ricci, and Kevin W. Plaxco. A general electrochemical method for label-free screening of proteinsmall molecule interactions. Chemical Communications, (41):6222, nov 2009.
- [105] Kevin J. Cash, Francesco Ricci, and Kevin W. Plaxco. An Electrochemical Sensor for the Detection of ProteinSmall Molecule Interactions Directly in Serum and Other Complex Matrices. Journal of the American Chemical Society, 131(20):6955–6957, may 2009.
- [106] James D Hirsch, Leila Eslamizar, Brian J Filanoski, Nabi Malekzadeh, Rosaria P Haugland, Joseph M Beechem, and Richard P Haugland. Easily reversible desthiobiotin binding to streptavidin, avidin, and other biotin-binding proteins: uses for protein labeling, detection, and isolation. Analytical biochemistry, 308(2):343–357, sep 2002.
- [107] David Yu Zhang and Erik Winfree. Dynamic Allosteric Control of Noncovalent DNA Catalysis Reactions. Journal of the American Chemical Society, 130(42):13921–13926, oct 2008.



Title: An Electronic, Aptamer-Based Small-Molecule Sensor for the Rapid, Label-Free Detection of Cocaine in Adulterated Samples and Biological Fluids

Author: Brian R. Baker, Rebecca Y. Lai, McCall S. Wood, et al

Publication: Journal of the American Chemical Society

Publisher: American Chemical Society

Date: Mar 1, 2006

Copyright © 2006, American Chemical Society

Logged in as:
Subramaniam Somasundaram
Auburn University
Account #:
3001219225

[LOGOUT](#)

PERMISSION/LICENSE IS GRANTED FOR YOUR ORDER AT NO CHARGE

This type of permission/license, instead of the standard Terms & Conditions, is sent to you because no fee is being charged for your order. Please note the following:

- Permission is granted for your request in both print and electronic formats, and translations.
- If figures and/or tables were requested, they may be adapted or used in part.
- Please print this page for your records and send a copy of it to your publisher/graduate school.
- Appropriate credit for the requested material should be given as follows: "Reprinted (adapted) with permission from (COMPLETE REFERENCE CITATION). Copyright (YEAR) American Chemical Society." Insert appropriate information in place of the capitalized words.
- One-time permission is granted only for the use specified in your request. No additional uses are granted (such as derivative works or other editions). For any other uses, please submit a new request.

If credit is given to another source for the material you requested, permission must be obtained from that source.

[BACK](#)

[CLOSE WINDOW](#)



RightsLink®

[Home](#) [Create Account](#) [Help](#)



Title: An Electrochemical Sensor for the Detection of Protein–Small Molecule Interactions Directly in Serum and Other Complex Matrices

Author: Kevin J. Cash, Francesco Ricci, Kevin W. Plaxco

Publication: Journal of the American Chemical Society

Publisher: American Chemical Society

Date: May 1, 2009

Copyright © 2009, American Chemical Society

LOGIN
If you're a copyright.com user, you can login to RightsLink using your copyright.com credentials. Already a RightsLink user or want to [learn more?](#)

PERMISSION/LICENSE IS GRANTED FOR YOUR ORDER AT NO CHARGE

This type of permission/license, instead of the standard Terms & Conditions, is sent to you because no fee is being charged for your order. Please note the following:

- Permission is granted for your request in both print and electronic formats, and translations.
- If figures and/or tables were requested, they may be adapted or used in part.
- Please print this page for your records and send a copy of it to your publisher/graduate school.
- Appropriate credit for the requested material should be given as follows: "Reprinted (adapted) with permission from (COMPLETE REFERENCE CITATION). Copyright (YEAR) American Chemical Society." Insert appropriate information in place of the capitalized words.
- One-time permission is granted only for the use specified in your request. No additional uses are granted (such as derivative works or other editions). For any other uses, please submit a new request.

If credit is given to another source for the material you requested, permission must be obtained from that source.

[BACK](#)

[CLOSE WINDOW](#)

Copyright © 2017 Copyright Clearance Center, Inc. All Rights Reserved. [Privacy statement](#). [Terms and Conditions](#). Comments? We would like to hear from you. E-mail us at customer@copyright.com



RightsLink®

[Home](#) [Account Info](#) [Help](#)



Title: Tuning the Bacterial Detection Sensitivity of Nanostructured Microelectrodes

Author: Jagotamoy Das, Shana O. Kelley

Publication: Analytical Chemistry

Publisher: American Chemical Society

Date: Aug 1, 2013

Copyright © 2013, American Chemical Society

Logged in as:
Subramaniam Somasundaram
Auburn University
Account #: 3001219225

[LOGOUT](#)

PERMISSION/LICENSE IS GRANTED FOR YOUR ORDER AT NO CHARGE

This type of permission/license, instead of the standard Terms & Conditions, is sent to you because no fee is being charged for your order. Please note the following:

- Permission is granted for your request in both print and electronic formats, and translations.
- If figures and/or tables were requested, they may be adapted or used in part.
- Please print this page for your records and send a copy of it to your publisher/graduate school.
- Appropriate credit for the requested material should be given as follows: "Reprinted (adapted) with permission from (COMPLETE REFERENCE CITATION). Copyright (YEAR) American Chemical Society." Insert appropriate information in place of the capitalized words.
- One-time permission is granted only for the use specified in your request. No additional uses are granted (such as derivative works or other editions). For any other uses, please submit a new request.

If credit is given to another source for the material you requested, permission must be obtained from that source.

[BACK](#)

[CLOSE WINDOW](#)

Copyright © 2017 Copyright Clearance Center, Inc. All Rights Reserved. [Privacy statement](#). [Terms and Conditions](#). Comments? We would like to hear from you. E-mail us at customer@copyright.com



RightsLink®

Home

Account Info

Help



Title: An RNA Aptamer-Based Electrochemical Biosensor for Detection of Theophylline in Serum

Author: Elena E. Ferapontova, Eva M. Olsen, Kurt V. Gothelf

Publication: Journal of the American Chemical Society

Publisher: American Chemical Society

Date: Apr 1, 2008

Copyright © 2008, American Chemical Society

Logged in as:
Subramaniam Somasundaram
Auburn University
Account #: 3001219225
[LOGOUT](#)

PERMISSION/LICENSE IS GRANTED FOR YOUR ORDER AT NO CHARGE

This type of permission/license, instead of the standard Terms & Conditions, is sent to you because no fee is being charged for your order. Please note the following:

- Permission is granted for your request in both print and electronic formats, and translations.
- If figures and/or tables were requested, they may be adapted or used in part.
- Please print this page for your records and send a copy of it to your publisher/graduate school.
- Appropriate credit for the requested material should be given as follows: "Reprinted (adapted) with permission from (COMPLETE REFERENCE CITATION). Copyright (YEAR) American Chemical Society." Insert appropriate information in place of the capitalized words.
- One-time permission is granted only for the use specified in your request. No additional uses are granted (such as derivative works or other editions). For any other uses, please submit a new request.

If credit is given to another source for the material you requested, permission must be obtained from that source.

[BACK](#)

[CLOSE WINDOW](#)

Copyright © 2017 Copyright Clearance Center, Inc. All Rights Reserved. [Privacy statement](#). [Terms and Conditions](#).
Comments? We would like to hear from you. E-mail us at customer@copyright.com



Title: Real-Time, Aptamer-Based Tracking of Circulating Therapeutic Agents in Living Animals

Author: Brian Scott Ferguson, David A. Hoggarth, Dan Maliniak, Kyle Ploense, Ryan J. White, Nick Woodward, Kuangwen Hsieh, Andrew J. Bonham, Michael Eisenstein, Tod E. Kippin, Kevin W. Plaxco, Hyongsok Tom Soh

Publication: Science Translational Medicine

Publisher: The American Association for the Advancement of Science

Date: Nov 27, 2013
Copyright © 2013, Copyright © 2013, American Association for the Advancement of Science

Logged in as:
Subramaniam Somasundaram
Auburn University
Account #: 3001219225
[Logout](#)

Order Completed

Thank you for your order.

This Agreement between Auburn University -- Subramaniam Somasundaram ("You") and The American Association for the Advancement of Science ("The American Association for the Advancement of Science") consists of your license details and the terms and conditions provided by The American Association for the Advancement of Science and Copyright Clearance Center.

Your confirmation email will contain your order number for future reference.

[printable details](#)

License Number	4236891202212
License date	Nov 27, 2017
Licensed Content Publisher	The American Association for the Advancement of Science
Licensed Content Publication	Science Translational Medicine
Licensed Content Title	Real-Time, Aptamer-Based Tracking of Circulating Therapeutic Agents in Living Animals
Licensed Content Author	Brian Scott Ferguson, David A. Hoggarth, Dan Maliniak, Kyle Ploense, Ryan J. White, Nick Woodward, Kuangwen Hsieh, Andrew J. Bonham, Michael Eisenstein, Tod E. Kippin, Kevin W. Plaxco, Hyongsok Tom Soh
Licensed Content Date	Nov 27, 2013
Licensed Content Volume	5
Licensed Content Issue	213
Volume number	5
Issue number	213
Type of Use	Thesis / Dissertation
Requestor type	Scientist/individual at a research institution
Format	Print and electronic
Portion	Figure
Number of figures/tables	1
Order reference number	
Title of your thesis / dissertation	Development of Oligonucleotide, Small Molecule, and Protein Assays using Square-wave Voltammetry with Electrode-bound Nucleic Acid Nanostructure
Expected completion date	Dec 2017
Estimated size(pages)	100
Requestor Location	Auburn University 179 Chemistry Building AUBURN UNIVERSITY, AL 36849 United States Attn: Auburn University
Billing Type	Invoice
Billing address	Auburn University 179 Chemistry Building AUBURN UNIVERSITY, AL 36849 United States Attn: Auburn University
Total	0.00 USD

[ORDER MORE](#) [CLOSE WINDOW](#)

Copyright © 2017 Copyright Clearance Center, Inc. All Rights Reserved. [Privacy statement](#). [Terms and Conditions](#). Comments? We would like to hear from you. E-mail us at customercare@copyright.com



RightsLink®

Home Account Info Help



Title: Protein detection using proximity-dependent DNA ligation assays
Author: Simon Fredriksson, Mats Gullberg, Jonas Jarvius, Charlotta Olsson, Kristian Pietras et al.
Publication: Nature Biotechnology
Publisher: Nature Publishing Group
Date: May 1, 2002

Logged in as: Subramaniam Somasundaram
Auburn University
Account #: 3001219225
Logout

Copyright © 2002, Rights Managed by Nature Publishing Group

Order Completed

Thank you for your order.

This Agreement between Auburn University -- Subramaniam Somasundaram ("You") and Nature Publishing Group ("Nature Publishing Group") consists of your license details and the terms and conditions provided by Nature Publishing Group and Copyright Clearance Center.

Your confirmation email will contain your order number for future reference.

printable details

Table with license details including License Number (4237351079429), License date (Nov 27, 2017), Licensed Content Publisher (Nature Publishing Group), Licensed Content Publication (Nature Biotechnology), Licensed Content Title (Protein detection using proximity-dependent DNA ligation assays), Licensed Content Author (Simon Fredriksson, Mats Gullberg, Jonas Jarvius, Charlotta Olsson, Kristian Pietras et al.), Licensed Content Date (May 1, 2002), Licensed Content Volume (20), Licensed Content Issue (5), Type of Use (reuse in a dissertation / thesis), Requestor type (academic/educational), Format (print and electronic), Portion (figures/tables/illustrations), Number of figures/tables/illustrations (1), High-res required (no), Figures (Figure 1), Author of this NPG article (no), Your reference number, Title of your thesis / dissertation (Development of Oligonucleotide, Small Molecule, and Protein Assays using Square-wave Voltammetry with Electrode-bound Nucleic Acid Nanostructure), Expected completion date (Dec 2017), Estimated size (number of pages) (100), Requestor Location (Auburn University, 179 Chemistry Building, Auburn University, AL 36849, United States, Attn: Auburn University), Billing Type (Invoice), Billing address (Auburn University, 179 Chemistry Building, Auburn University, AL 36849, United States, Attn: Auburn University), Total (0.00 USD)

ORDER MORE CLOSE WINDOW

Copyright © 2017 Copyright Clearance Center, Inc. All Rights Reserved. Privacy statement, Terms and Conditions. Comments? We would like to hear from you. E-mail us at customercare@copyright.com



RightsLink®

[Home](#)

[Account Info](#)

[Help](#)



ACS Publications
Most Trusted. Most Cited. Most Read.

Title: Molecular Pincers: Antibody-Based Homogeneous Protein Sensors
Author: Ewa Heyduk, Benjamin Dummit, Yie-Hwa Chang, et al
Publication: Analytical Chemistry
Publisher: American Chemical Society
Date: Jul 1, 2008
Copyright © 2008, American Chemical Society

Logged in as:
Subramaniam Somasundaram
Auburn University
Account #:
3001219225
[LOGOUT](#)

PERMISSION/LICENSE IS GRANTED FOR YOUR ORDER AT NO CHARGE

This type of permission/license, instead of the standard Terms & Conditions, is sent to you because no fee is being charged for your order. Please note the following:

- Permission is granted for your request in both print and electronic formats, and translations.
- If figures and/or tables were requested, they may be adapted or used in part.
- Please print this page for your records and send a copy of it to your publisher/graduate school.
- Appropriate credit for the requested material should be given as follows: "Reprinted (adapted) with permission from (COMPLETE REFERENCE CITATION). Copyright (YEAR) American Chemical Society." Insert appropriate information in place of the capitalized words.
- One-time permission is granted only for the use specified in your request. No additional uses are granted (such as derivative works or other editions). For any other uses, please submit a new request.

If credit is given to another source for the material you requested, permission must be obtained from that source.

[BACK](#)

[CLOSE WINDOW](#)

Copyright © 2017 Copyright Clearance Center, Inc. All Rights Reserved. [Privacy statement](#). [Terms and Conditions](#).
Comments? We would like to hear from you. E-mail us at gustomecare@copyright.com



RightsLink®

[Home](#)

[Account Info](#)

[Help](#)



ACS Publications
Most Trusted. Most Cited. Most Read.

Title: Quantitation of Femtomolar Protein Levels via Direct Readout with the Electrochemical Proximity Assay
Author: Jiaming Hu, Tanyu Wang, Joonyul Kim, et al
Publication: Journal of the American Chemical Society
Publisher: American Chemical Society
Date: Apr 1, 2012
Copyright © 2012, American Chemical Society

Logged in as:
Subramaniam Somasundaram
Auburn University
Account #:
3001219225
[LOGOUT](#)

PERMISSION/LICENSE IS GRANTED FOR YOUR ORDER AT NO CHARGE

This type of permission/license, instead of the standard Terms & Conditions, is sent to you because no fee is being charged for your order. Please note the following:

- Permission is granted for your request in both print and electronic formats, and translations.
- If figures and/or tables were requested, they may be adapted or used in part.
- Please print this page for your records and send a copy of it to your publisher/graduate school.
- Appropriate credit for the requested material should be given as follows: "Reprinted (adapted) with permission from (COMPLETE REFERENCE CITATION). Copyright (YEAR) American Chemical Society." Insert appropriate information in place of the capitalized words.
- One-time permission is granted only for the use specified in your request. No additional uses are granted (such as derivative works or other editions). For any other uses, please submit a new request.

If credit is given to another source for the material you requested, permission must be obtained from that source.

[BACK](#)

[CLOSE WINDOW](#)

Copyright © 2017 Copyright Clearance Center, Inc. All Rights Reserved. [Privacy statement](#). [Terms and Conditions](#).
Comments? We would like to hear from you. E-mail us at gustomecare@copyright.com



RightsLink®

Home

Account Info

Help



Title:

A Highly Selective Electrochemical DNA-Based Sensor That Employs Steric Hindrance Effects to Detect Proteins Directly in Whole Blood

Author: Sahar Sadat Mahshid, Sébastien Camiré, Francesco Ricci, et al

Publication: Journal of the American Chemical Society

Publisher: American Chemical Society

Date: Dec 1, 2015

Copyright © 2015, American Chemical Society

Logged in as:
Subramaniam Somasundaram
Auburn University
Account #:
3001219225

LOGOUT

PERMISSION/LICENSE IS GRANTED FOR YOUR ORDER AT NO CHARGE

This type of permission/license, instead of the standard Terms & Conditions, is sent to you because no fee is being charged for your order. Please note the following:

- Permission is granted for your request in both print and electronic formats, and translations.
- If figures and/or tables were requested, they may be adapted or used in part.
- Please print this page for your records and send a copy of it to your publisher/graduate school.
- Appropriate credit for the requested material should be given as follows: "Reprinted (adapted) with permission from (COMPLETE REFERENCE CITATION). Copyright (YEAR) American Chemical Society." Insert appropriate information in place of the capitalized words.
- One-time permission is granted only for the use specified in your request. No additional uses are granted (such as derivative works or other editions). For any other uses, please submit a new request.

If credit is given to another source for the material you requested, permission must be obtained from that source.

BACK

CLOSE WINDOW

Copyright © 2017 Copyright Clearance Center, Inc. All Rights Reserved. [Privacy statement](#). [Terms and Conditions](#).
Comments? We would like to hear from you. E-mail us at customer-care@copyright.com



RightsLink®

Home

Account Info

Help



Title:

Electrochemical DNA-Based Immunoassay That Employs Steric Hindrance To Detect Small Molecules Directly in Whole Blood

Author: Sahar S. Mahshid, Francesco Ricci, Shana O. Kelley, et al

Publication: ACS Sensors

Publisher: American Chemical Society

Date: Jun 1, 2017

Copyright © 2017, American Chemical Society

Logged in as:
Subramaniam Somasundaram
Auburn University
Account #:
3001219225

LOGOUT

PERMISSION/LICENSE IS GRANTED FOR YOUR ORDER AT NO CHARGE

This type of permission/license, instead of the standard Terms & Conditions, is sent to you because no fee is being charged for your order. Please note the following:

- Permission is granted for your request in both print and electronic formats, and translations.
- If figures and/or tables were requested, they may be adapted or used in part.
- Please print this page for your records and send a copy of it to your publisher/graduate school.
- Appropriate credit for the requested material should be given as follows: "Reprinted (adapted) with permission from (COMPLETE REFERENCE CITATION). Copyright (YEAR) American Chemical Society." Insert appropriate information in place of the capitalized words.
- One-time permission is granted only for the use specified in your request. No additional uses are granted (such as derivative works or other editions). For any other uses, please submit a new request.

If credit is given to another source for the material you requested, permission must be obtained from that source.

BACK

CLOSE WINDOW

Copyright © 2017 Copyright Clearance Center, Inc. All Rights Reserved. [Privacy statement](#). [Terms and Conditions](#).
Comments? We would like to hear from you. E-mail us at customer-care@copyright.com



RightsLink®

Home

Account Info

Help



Title: Square Wave Voltammetry
Author: Janet G. Osteryoung, Robert A. Osteryoung
Publication: Analytical Chemistry
Publisher: American Chemical Society
Date: Jan 1, 1985
Copyright © 1985, American Chemical Society

Logged in as:
Subramaniam Somasundaram
Auburn University
Account #:
3001219225
[LOGOUT](#)

PERMISSION/LICENSE IS GRANTED FOR YOUR ORDER AT NO CHARGE

This type of permission/license, instead of the standard Terms & Conditions, is sent to you because no fee is being charged for your order. Please note the following:

- Permission is granted for your request in both print and electronic formats, and translations.
- If figures and/or tables were requested, they may be adapted or used in part.
- Please print this page for your records and send a copy of it to your publisher/graduate school.
- Appropriate credit for the requested material should be given as follows: "Reprinted (adapted) with permission from (COMPLETE REFERENCE CITATION). Copyright (YEAR) American Chemical Society." Insert appropriate information in place of the capitalized words.
- One-time permission is granted only for the use specified in your request. No additional uses are granted (such as derivative works or other editions). For any other uses, please submit a new request.

If credit is given to another source for the material you requested, permission must be obtained from that source.

[BACK](#)

[CLOSE WINDOW](#)

Copyright © 2017 Copyright Clearance Center, Inc. All Rights Reserved. [Privacy statement](#), [Terms and Conditions](#).
Comments? We would like to hear from you. E-mail us at customercare@copyright.com

ROYAL SOCIETY OF CHEMISTRY LICENSE
TERMS AND CONDITIONS

Nov 27, 2017

This Agreement between Auburn University -- Subramaniam Somasundaram ("You") and Royal Society of Chemistry ("Royal Society of Chemistry") consists of your license details and the terms and conditions provided by Royal Society of Chemistry and Copyright Clearance Center.

License Number	4236600342170
License date	Nov 26, 2017
Licensed Content Publisher	Royal Society of Chemistry
Licensed Content Publication	Chemical Communications (Cambridge)
Licensed Content Title	Aptamer conformational switch as sensitive electrochemical biosensor for potassium ion recognition
Licensed Content Author	Abd-Elgawad Radi,Ciara K. O'Sullivan
Licensed Content Date	Jul 6, 2006
Licensed Content Volume	0
Licensed Content Issue	32
Type of Use	Thesis/Dissertation
Requestor type	academic/educational
Portion	figures/tables/images
Number of figures/tables/images	1
Format	print and electronic
Distribution quantity	5
Will you be translating?	no
Order reference number	
Title of the thesis/dissertation	Development of Oligonucleotide, Small Molecule, and Protein Assays using Square-wave Voltammetry with Electrode-bound Nucleic Acid Nanostructure
Expected completion date	Dec 2017
Estimated size	100
Requestor Location	Auburn University 179 Chemistry Building AUBURN UNIVERSITY, AL 36849 United States Attn: Auburn University
Billing Type	Invoice
Billing Address	Auburn University 179 Chemistry Building AUBURN UNIVERSITY, AL 36849 United States Attn: Auburn University
Total	0.00 USD
Terms and Conditions	



RightsLink®

[Home](#) [Account Info](#) [Help](#)

Title: Ratiometric electrochemical proximity assay for sensitive one-step protein detection
Author: Kewei Ren, Jie Wu, Feng Yan, Huangxian Ju
Publication: Scientific Reports
Publisher: Nature Publishing Group
Date: Mar 12, 2014
Copyright © 2014, Rights Managed by Nature Publishing Group

Logged in as:
Subramaniam Somasundaram
Auburn University
Account #: 0001219225
[LOGOUT](#)

Creative Commons

The request you have made is considered to be non-commercial/educational. As the article you have requested has been distributed under a Creative Commons license (Attribution-Noncommercial), you may reuse this material for non-commercial/educational purposes without obtaining additional permission from Nature Publishing Group, providing that the author and the original source of publication are fully acknowledged (please see the article itself for the license version number). You may reuse this material without obtaining permission from Nature Publishing Group, providing that the author and the original source of publication are fully acknowledged, as per the terms of the license. For license terms, please see <http://creativecommons.org/>

[BACK](#)

[CLOSE WINDOW](#)

Copyright © 2017 Copyright Clearance Center, Inc. All Rights Reserved. [Privacy statement](#). [Terms and Conditions](#).
Comments? We would like to hear from you. E-mail us at customercare@copyright.com



RightsLink®

Home Account Info Help



Title: Single-molecule enzyme-linked immunosorbent assay detects serum proteins at subfemtomolar concentrations
Author: David M Rissin, Cheuk W Kan, Todd G Campbell, Stuart C Howes, David R Fournier et al.
Publication: Nature Biotechnology
Publisher: Nature Publishing Group
Date: May 23, 2010
Copyright © 2010, Rights Managed by Nature Publishing Group

Logged in as: Subramaniam Somasundaram Auburn University
Account #: 3001219225
LOGOUT

Order Completed

Thank you for your order.

This Agreement between Auburn University -- Subramaniam Somasundaram ("You") and Nature Publishing Group ("Nature Publishing Group") consists of your license details and the terms and conditions provided by Nature Publishing Group and Copyright Clearance Center.

Your confirmation email will contain your order number for future reference.

printable details

Table with license details including License Number (4237340262055), License date (Nov 27, 2017), Licensed Content (Nature Publishing Group), and Requestor Location (Auburn University).

ORDER MORE CLOSE WINDOW

Copyright © 2017 Copyright Clearance Center, Inc. All Rights Reserved. Privacy Statement Terms and Conditions



RightsLink®

Home Account Info Help



Title: Reagentless, Structure-Switching, Electrochemical Aptamer-Based Sensors
Author: Lauren R. Schoukroun-Barnes, Florika C. Macazo, Brenda Gutierrez, et al
Publication: Annual Review of Analytical Chemistry
Publisher: Annual Reviews
Date: Jun 12, 2016
Copyright © 2016, Annual Reviews

Logged in as: Subramaniam Somasundaram Auburn University
Account #: 3001219225
LOGOUT

Permission Not Required

Material may be republished in a thesis / dissertation without obtaining additional permission from Annual Reviews, providing that the author and the original source of publication are fully acknowledged.

BACK CLOSE WINDOW

Copyright © 2017 Copyright Clearance Center, Inc. All Rights Reserved. Privacy statement. Terms and Conditions. Comment? We would like to hear from you. E-mail us at: customercare@copyright.com



RightsLink®

[Home](#)

[Account Info](#)

[Help](#)



ACS Publications
Most Trusted. Most Cited. Most Read.

Title: Exploiting Binding-Induced Changes in Probe Flexibility for the Optimization of Electrochemical Biosensors
Author: Ryan J. White, Kevin W. Plaxco
Publication: Analytical Chemistry
Publisher: American Chemical Society
Date: Jan 1, 2010

Copyright © 2010, American Chemical Society

Logged in as:
Subramaniam Somasundaram
Auburn University
Account #:
3001219225

[LOGOUT](#)

PERMISSION/LICENSE IS GRANTED FOR YOUR ORDER AT NO CHARGE

This type of permission/license, instead of the standard Terms & Conditions, is sent to you because no fee is being charged for your order. Please note the following:

- Permission is granted for your request in both print and electronic formats, and translations.
- If figures and/or tables were requested, they may be adapted or used in part.
- Please print this page for your records and send a copy of it to your publisher/graduate school.
- Appropriate credit for the requested material should be given as follows: "Reprinted (adapted) with permission from (COMPLETE REFERENCE CITATION). Copyright (YEAR) American Chemical Society." Insert appropriate information in place of the capitalized words.
- One-time permission is granted only for the use specified in your request. No additional uses are granted (such as derivative works or other editions). For any other uses, please submit a new request.

If credit is given to another source for the material you requested, permission must be obtained from that source.

[BACK](#)

[CLOSE WINDOW](#)

Copyright © 2017 Copyright Clearance Center, Inc. All Rights Reserved. [Privacy statement](#). [Terms and Conditions](#).
Comments? We would like to hear from you. E-mail us at customer-care@copyright.com



RightsLink®

[Home](#)

[Account Info](#)

[Help](#)



ACS Publications
Most Trusted. Most Cited. Most Read.

Title: Random Walk on a Leash: A Simple Single-Molecule Diffusion Model for Surface-Tethered Redox Molecules with Flexible Linkers
Author: Kuan-Chun Huang, Ryan J. White
Publication: Journal of the American Chemical Society
Publisher: American Chemical Society
Date: Aug 1, 2013

Copyright © 2013, American Chemical Society

Logged in as:
Subramaniam Somasundaram
Auburn University

[LOGOUT](#)

PERMISSION/LICENSE IS GRANTED FOR YOUR ORDER AT NO CHARGE

This type of permission/license, instead of the standard Terms & Conditions, is sent to you because no fee is being charged for your order. Please note the following:

- Permission is granted for your request in both print and electronic formats, and translations.
- If figures and/or tables were requested, they may be adapted or used in part.
- Please print this page for your records and send a copy of it to your publisher/graduate school.
- Appropriate credit for the requested material should be given as follows: "Reprinted (adapted) with permission from (COMPLETE REFERENCE CITATION). Copyright (YEAR) American Chemical Society." Insert appropriate information in place of the capitalized words.
- One-time permission is granted only for the use specified in your request. No additional uses are granted (such as derivative works or other editions). For any other uses, please submit a new request.

If credit is given to another source for the material you requested, permission must be obtained from that source.

[BACK](#)

[CLOSE WINDOW](#)

JOHN WILEY AND SONS LICENSE
TERMS AND CONDITIONS

Nov 27, 2017

This Agreement between Auburn University -- Subramaniam Somasundaram ("You") and John Wiley and Sons ("John Wiley and Sons") consists of your license details and the terms and conditions provided by John Wiley and Sons and Copyright Clearance Center.

License Number	4233281030789
License date	Nov 20, 2017
Licensed Content Publisher	John Wiley and Sons
Licensed Content Publication	Angewandte Chemie International Edition
Licensed Content Title	Assembling DNA through Affinity Binding to Achieve Ultrasensitive Protein Detection
Licensed Content Author	Hongquan Zhang,Feng Li,Brittany Dever,Chuan Wang,Xing-Fang Li,X. Chris Le
Licensed Content Date	Aug 26, 2013
Licensed Content Pages	8
Type of use	Dissertation/Thesis
Requestor type	University/Academic
Format	Print and electronic
Portion	Figure/table
Number of figures/tables	1
Original Wiley figure/table number(s)	Figure 1
Will you be translating?	No
Title of your thesis / dissertation	Development of Oligonucleotide, Small Molecule, and Protein Assays using Square-wave Voltammetry with Electrode-bound Nucleic Acid Nanostructure
Expected completion date	Dec 2017
Expected size (number of pages)	100
Requestor Location	Auburn University 179 Chemistry Building AUBURN UNIVERSITY, AL 36849 United States Attn: Auburn University
Publisher Tax ID	EU826007151
Billing Type	Invoice
Billing Address	Auburn University 179 Chemistry Building AUBURN UNIVERSITY, AL 36849 United States Attn: Auburn University
Total	0.00 USD
Terms and Conditions	



Copyright
Clearance
Center

RightsLink®

Home

Account
Info

Help



ACS Publications
Most Trusted. Most Cited. Most Read.

Title: A Target-Responsive
Electrochemical Aptamer Switch
(TREAS) for Reagentless
Detection of Nanomolar ATP
Author: Xiaolei Zuo, Shiping Song, Jiong
Zhang, et al
Publication: Journal of the American
Chemical Society
Publisher: American Chemical Society
Date: Feb 1, 2007
Copyright © 2007, American Chemical Society

Logged in as:
Subramaniam Somasundaram
Auburn University
Account #:
3001219225

LOGOUT

PERMISSION/LICENSE IS GRANTED FOR YOUR ORDER AT NO CHARGE

This type of permission/license, instead of the standard Terms & Conditions, is sent to you because no fee is being charged for your order. Please note the following:

- Permission is granted for your request in both print and electronic formats, and translations.
- If figures and/or tables were requested, they may be adapted or used in part.
- Please print this page for your records and send a copy of it to your publisher/graduate school.
- Appropriate credit for the requested material should be given as follows: "Reprinted (adapted) with permission from (COMPLETE REFERENCE CITATION). Copyright (YEAR) American Chemical Society." Insert appropriate information in place of the capitalized words.
- One-time permission is granted only for the use specified in your request. No additional uses are granted (such as derivative works or other editions). For any other uses, please submit a new request.

If credit is given to another source for the material you requested, permission must be obtained from that source.

BACK

CLOSE WINDOW

Copyright © 2017 Copyright Clearance Center, Inc. All Rights Reserved. [Privacy statement](#). [Terms and Conditions](#).
Comments? We would like to hear from you. E-mail us at customercare@copyright.com